

**University of Alberta**

**Targeted delivery of immunoliposomal doxorubicin to B-lymphoid cells via an anti-  
CD19 whole monoclonal antibody or fragments of antibody**

By

**Wilson Wan Kin Cheng**



A thesis submitted to the Faculty of Graduate Studies and Research in partial fulfillment  
of the requirements for the degree of Doctor of Philosophy

Department of Pharmacology

Edmonton, Alberta

Spring 2008



Library and  
Archives Canada

Bibliothèque et  
Archives Canada

Published Heritage  
Branch

Direction du  
Patrimoine de l'édition

395 Wellington Street  
Ottawa ON K1A 0N4  
Canada

395, rue Wellington  
Ottawa ON K1A 0N4  
Canada

*Your file Votre référence*  
*ISBN: 978-0-494-45405-3*  
*Our file Notre référence*  
*ISBN: 978-0-494-45405-3*

**NOTICE:**

The author has granted a non-exclusive license allowing Library and Archives Canada to reproduce, publish, archive, preserve, conserve, communicate to the public by telecommunication or on the Internet, loan, distribute and sell theses worldwide, for commercial or non-commercial purposes, in microform, paper, electronic and/or any other formats.

The author retains copyright ownership and moral rights in this thesis. Neither the thesis nor substantial extracts from it may be printed or otherwise reproduced without the author's permission.

**AVIS:**

L'auteur a accordé une licence non exclusive permettant à la Bibliothèque et Archives Canada de reproduire, publier, archiver, sauvegarder, conserver, transmettre au public par télécommunication ou par l'Internet, prêter, distribuer et vendre des thèses partout dans le monde, à des fins commerciales ou autres, sur support microforme, papier, électronique et/ou autres formats.

L'auteur conserve la propriété du droit d'auteur et des droits moraux qui protègent cette thèse. Ni la thèse ni des extraits substantiels de celle-ci ne doivent être imprimés ou autrement reproduits sans son autorisation.

---

In compliance with the Canadian Privacy Act some supporting forms may have been removed from this thesis.

Conformément à la loi canadienne sur la protection de la vie privée, quelques formulaires secondaires ont été enlevés de cette thèse.

While these forms may be included in the document page count, their removal does not represent any loss of content from the thesis.

Bien que ces formulaires aient inclus dans la pagination, il n'y aura aucun contenu manquant.

  
**Canada**

**Dedicated to my beloved parents, my family and to those who  
have loved and supported me**

## ABSTRACT

Anticancer drug therapy can have significant adverse effects, resulting from non-selective toxicities. Treatment with antibody-targeted liposomes such as Stealth<sup>®</sup> immunoliposomes (SIL) results in improved selectivity of chemotherapeutics for cancer cells that can be easily accessed from the vasculature, e.g., haematological malignancies. This thesis examined, in an animal model of a B-cell malignancy, the activity of doxorubicin (DXR) encapsulated in SIL and targeted via an anti-CD19 whole monoclonal antibody (mAb), its Fab' fragment (Fab') or a single chain Fv fragment (scFv), all directed against the same epitope of CD19. The therapeutic effect of DXR-loaded SIL (SIL-DXR) was hypothesized to be influenced by the differences in the pharmacokinetics (PK) properties of the targeted liposomes.

Various anti-CD19 scFv constructs were compared for their stability, production yield, and affinity. Production yield and activity of native scFv from the periplasmic space of *E. coli* were compared with those of refolded scFv from denatured inclusion bodies. The ability to refold the scFv and the stability of the resulting construct were the major factors in determining its success as a targeting agent. Of the several scFv constructs tested, only one demonstrated suitable properties for targeting SIL. The coupling of scFv to polyethylene glycol-lipid micelles was found to increase their storage stability, making it possible to generate the amounts of scFv required for the *in vivo* experiments.

SIL-DXR targeted via mAb, Fab' or scFv had improved cytotoxicity to B cells, over untargeted liposomal DXR, via CD19-mediated mechanisms. PK studies demonstrated that Fab'-targeted SIL-DXR had long circulation times, similar to

untargeted liposomes, while mAb-targeted SIL-DXR was rapidly cleared by the liver and spleen. The presence of poly-histidine and c-myc tags on the scFv increased their uptake into liver, compared to tagless scFv. However, the differences in PK between the various formulations of SIL-DXR did not result in differences in their therapeutic effects. These results suggested that, in the treatment of haematological malignancies, the choice between mAb, Fab' or scFv as targeting agents for SIL may be dependent on other factors, such as immunogenicity, toxicity, or production cost, rather than the PK properties of the individual construct.

## ACKNOWLEDGEMENTS

I thank Dr. Theresa Allen for giving me the opportunity to study in her laboratory. Her supervision and guidance in the past five years have been invaluable. The completion of this thesis would not be possible without her support. My other supervisory committee members, Dr. Dion Brocks and Dr. David Murray, have also been tremendously supportive in the past years. I am grateful for their insightful suggestions and the assistance they have provided. I would also like to thank Dr. Marcel Bally and Dr. Susan Dunn for their time and contribution to my thesis defense. I am grateful for Dr. Susan Dunn and Dr. Wendy Gati, for their work as graduate student coordinators and the support they have provided. I would also like to thank Dr. Georg Fey and Dr. Sergei Kipriyanov for their insightful discussions and material support. Financial support from the CIHR is greatly appreciated.

It was a memorable experience, and also a privilege to be working with members of the Allen laboratory. I would like to thank Ms. Elaine Moase for her assistance and her supervision of the daily operation of the laboratory. I am also grateful to Ms. Kimberley Laginha and Ms. Jennifer Hare, for their support and companionship. Their friendship has enriched my experience in the Allen laboratory. I have learned a great deal from previous graduate students, post-doctoral fellows and technicians in our laboratory. Specifically, I thank Dr. Gregory Charrois, Dr. Puja Sapra, Dr. Dipankar Das, Dr. Davis Mumbengegwi, Ms. Susan Cubitt, and Ms. Heather Vandertol-Vanier, for their help and guidance. I am grateful to my friends in the Department of Pharmacology, for their friendship. I thank Mr. Ray Kozak, Mr. Darin Brox, Dr. Martin Davies, Mr.

Christian Carter, Dr. Jagdip Jaswal, Mr. Haitao You, and Ms. Isabelle Paulsen for the fun times that we have shared.

All this would not be possible without the love and support of my family and the people that loved me. I am forever indebted to my parents, Peter and Maisie, for their love and encouragement. I thank my brother, Edward, for his support and care during my most difficult time in the past year.

The last five years have been enjoyable and rewarding, but they have also been difficult and challenging at times. I am grateful for my loving family and friends, who have inspired and encouraged me over the years. I feel fortunate to be surrounded by talented colleagues and mentors. I am thankful for the knowledge that they have passed on and instilled in me.

## TABLE OF CONTENT

<b>Chapter 1</b> .....	1
1. Introduction, Hypothesis and Objective .....	2
1.1. Introduction .....	2
1.2. Liposomes as a Nano-particulate Drug Delivery System .....	4
1.2.1. Classical Liposomes.....	10
1.2.2. Sterically Stabilized and Stealth® Liposomes .....	11
1.2.3. Ligand-targeted Liposomes.....	13
1.3. Preparation of Liposomes.....	16
1.4. Drug-loading Methods .....	18
1.4.1. Rate of Drug Release .....	19
1.5. Antibody-coupling Methods .....	23
1.6. Post-insertion Approach.....	25
1.7. Choice of Target.....	27
1.7.1. Targeting to Tumor Antigens or Antigens Against Tumor-associated Cells	28
1.7.2. Internalizing vs. Non-internalizing Antigens.....	29
1.8. Choice of Targeting Ligand .....	31
1.8.1. Monoclonal Antibodies and Fragments of Antibodies .....	32
1.8.2. Affinity, Avidity and Antibody Density .....	34
1.8.3. Pharmacokinetics of Immunoliposomes .....	37
1.8.4. Methods of Producing Whole Antibodies and Fragments of Antibodies .....	38
1.9. Model System.....	41
1.9.1. B-cell Antigen: CD19 .....	43

1.9.2. Doxorubicin .....	45
1.10. Hypothesis.....	48
1.11. Objectives.....	48
<b>Chapter 2</b> .....	<b>49</b>
2. Materials and Methods.....	50
2.1. Materials.....	50
2.2. Cell lines.....	51
2.3. Antibodies .....	51
2.4. Animals .....	52
2.5. Expression and Extraction of ScFv from the Periplasmic Space of <i>E. coli</i> and Inclusion Bodies.....	53
2.6. Western Blot Analysis.....	55
2.7. Preparation of Liposomes and Doxorubicin Loading .....	55
2.8. Preparation of Immunoliposomes .....	56
2.9. Separation of Coupled RGF 4G7-micelles from Free RGF 4G7 and Determination of Free Thiol Groups.....	59
2.10. Flow Cytometry Studies.....	60
2.11. <i>In vitro</i> Cell Binding Studies Using Tritium-labeled Liposomes .....	61
2.12. <i>In vitro</i> Cytotoxicity Studies .....	62
2.13. Pharmacokinetics and Biodistribution Studies.....	63
2.14. Therapeutic Studies .....	64
2.15. Statistical Analysis .....	64

<b>Chapter 3</b> .....	66
3. Expression, Purification and Screening of Various Constructs of Single Chain Fv Fragments .....	67
3.1. Abstract .....	67
3.2. Introduction .....	67
3.3. Antibodies and ScFv Constructs Used .....	69
3.4. Results .....	69
3.4.1. Screening of B-cell Lines.....	69
3.4.2. Binding of the HD37-CHC and FMC63-CHC constructs to B cell lines .....	71
3.4.3. Extraction, Production Yield, Concentration and Stability .....	71
3.4.4. Generation of Tagless Constructs, Production Yield, Refolding and Stability.....	75
3.4.5. Binding Activity of Tagless Constructs .....	75
3.4.6. Yield, Purification, Stability and Binding of HD37-CCH Purified from the Periplasmic Space .....	76
3.4.7. Coupling and Binding of RGF 4G7 scFv .....	79
3.4.8. Trouble-shooting the Low Binding of SIL[RGF 4G7] to Raji Cells.....	79
3.5. Discussion and Conclusions.....	86
<b>Chapter 4</b> .....	91
4. Expression and Purification of an Anti-CD19 Single Chain Fv Fragment for Targeting Liposomes to CD19-expressing Cells.....	92
4.1. Abstract .....	92
4.2. Introduction .....	92

4.3. Antibodies and ScFv Constructs Used .....	95
4.4. Results .....	95
4.5. Discussion and Conclusions.....	103
<b>Chapter 5</b> .....	107
5. Targeted Delivery of Anti-CD19 Liposomal Doxorubicin in B-cell Lymphoma: A Comparison of Whole Monoclonal Antibody, Fab' and Single Chain Fv Fragments .....	108
5.1. Abstract .....	108
5.2. Introduction .....	109
5.3. Whole Monoclonal Antibody and Fragments of Antibody Used .....	111
5.4. Results .....	111
5.5. Discussion and Conclusions.....	125
<b>Chapter 6</b> .....	133
6. General Discussion and Future Directions .....	134
6.1. Discussion .....	134
6.1.1. Stability of ScFv Constructs .....	134
6.1.2. Refolding of ScFv .....	137
6.1.3. Effect of ScFv Tags. ....	137
6.1.4. Targeting of Immunoliposomes Using MAb, Fab' or ScFv.....	138
6.1.5. Single Chain Fv in the Clinic as Anticancer Therapy.....	139
6.1.6. Failure to Respond and Resistance to Antibody-targeted Immunoliposomal Drugs.....	140
6.2. Future Directions.....	141

6.2.1. Combination of Immunoliposomal Drugs .....	141
6.2.2. Triggered Release Systems .....	142
6.2.3. Novel Antibody Constructs: Bispecific Antibodies.....	143
6.2.4. Innovative Approaches to Production of Antibody Fragments .....	144
6.3. Conclusions .....	145
<b>References</b> .....	<b>146</b>

## LIST OF TABLES

Table 1.1. Currently marketed liposomal drugs.....	5
Table 1.2. Comparison of PK parameters for free DXR and liposomal DXR in human...	9
Table 1.3. Partial list of currently marketed monoclonal antibodies. ....	33
Table 3.1. Production yields, concentration and stability of scFv constructs.....	73
Table 3.2. Post-insertion and coupling conditions used for RGF 4G7 scFv.....	81
Table 5.1. Cytotoxicity of free and liposomal DXR against Raji and Molt4 cells. ....	115
Table 5.2. Comparison of the pharmacokinetic parameters of targeted and untargeted liposomal DXR in Raji-bearing SCID mice. ....	121
Table 5.3A. Survival times of SCID mice after tumor cells implantation and DXR treatment. ....	127
Table 5.3B. Statistical comparisons of mean survival times.....	128

## LIST OF FIGURES

Figure 1.1. Structures of some common liposome-forming lipids. ....	8
Figure 1.2. Schematic representation of Stealth <sup>®</sup> and immunoliposomes coupled to various antibody constructs.....	12
Figure 1.3. Schematic representation of various antibody constructs. ....	14
Figure 1.4. Classification of liposomes based on size and lamellarity. ....	17
Figure 1.5. Schematic presentation of remote loading of DXR using the ammonium sulfate gradient.....	20
Figure 1.6. Theoretical relationship between the rate of drug release and therapeutic activity.....	22
Figure 1.7. Schematic representation of the post-insertion method.....	26
Figure 1.8. Structure of doxorubicin.....	46
Figure 3.1. Screening of various B-cell lines for expression of CD19, CD20, and CD22. ....	70
Figure 3.2. FACS of all scFv constructs.....	72
Figure 3.3. Western blot of HD37-CHC scFv extracted from inclusion bodies.....	74
Figure 3.4. Binding of immunoliposomes to B-lymphoid cells. ....	77
Figure 3.5. Binding study of SIL[HD37-CCH] and SL to CD19 <sup>+</sup> Raji cells.....	78
Figure 3.6. Mean fluorescence intensity (MFI) as a function of concentration of RGF 4G7.....	80
Figure 3.7. Elution profile of a 1 mL G-100 column.....	83
Figure 3.8. Binding study of SIL[RGF 4G7] and SL to CD19 <sup>+</sup> Raji cells.. ....	85

Figure 3.9. Binding study of conventionally coupled SIL[RGF 4G7] and SL to CD19 <sup>+</sup> Raji cells.....	87
Figure 4.1. Flow cytometry analysis.....	96
Figure 4.2. Mean fluorescence intensity (MFI) as a function of concentration of FMC63 mAb.....	97
Figure 4.3. Mean fluorescence intensity (MFI) as a function of concentration of HD37 mAb.....	98
Figure 4.4. Mean fluorescence intensity (MFI) as a function of concentration of HD37-CCH. ....	100
Figure 4.5. Purification of HD37-CCH after periplasmic extraction.....	101
Figure 4.6. Binding of SIL[HD37-CCH] to Raji Cells.....	102
Figure 5.1. Binding of HD37-CCH and HD37-CCH Mal-PEG <sub>2000</sub> -DSPE micelles to Raji cells.....	112
Figure 5.2. Specific binding of SIL[HD37-CCH], SIL[HD37 Fab'] and SIL[HD37 mAb] to Raji cells.....	113
Figure 5.3. Pharmacokinetics and bio-distribution study of SIL-DXR in naïve mice.	117
Figure 5.4. Pharmacokinetics and bio-distribution study of SIL-DXR in Raji-bearing mice.....	120
Figure 5.5. Pharmacokinetics and bio-distribution study of SIL-DXR targeted via tagged or non-tagged scFv constructs.....	124
Figure 5.6. Kaplan-Meier plot for Raji-bearing SCID mice treated with various formulations of DXR.....	126

## LIST OF ABBREVIATIONS

2-MEA	2-mercaptoethanol
<sup>3</sup> H-CHE	Chol-[1,2- <sup>3</sup> H-( <i>N</i> )]hexadecyl ether
<sup>14</sup> C-DXR	<sup>14</sup> C-labeled doxorubicin
β-ME	β-mercaptoethanol
ABVD	Drug combination of doxorubicin, bleomycin, vinblastine, and dacarbazine
ACS	Aqueous Counting Scintillant
ADCC	Antibody-dependent cellular cytotoxicity
ADEPT	Antibody-directed enzyme pro-drug therapy
Ara-C	Cytarabine
AUC	Area under the concentration vs. time curve
BD	Biodistribution
bs	Bispecific
CDC	Complement-dependent cytotoxicity
CDR	Complementarity determining region
CEA	Carcinogenic embryonic antigen
Chol	Cholesterol
CHOP	Drug combination of cyclophosphamide, doxorubicin, vincristine, and prednisone
CL	Clearance
CR	Complete response

Cys	Cysteine
DDS	Drug delivery system
DLBCL	Diffuse large B-cell lymphoma
DNP	2, 4-Dinitrophenol
DOPE	Dioleolyphosphatidylethanolamine
DSPE	Distearoylphosphatidylethanolamine
DTNB	5,5'-Dithiobis(2-nitrobenzoic acid)
DTT	1,4-dithiothreitol
DXR	Doxorubicin
EDTA	Ethylenediamine tetraacetic acid
EGFR	Epidermal growth factor receptor
EPR	Enhanced permeability and retention
Fab'	Fab' fragment of a mAb
FACS	Fluorescence-activated cell sorting
FBP	Folate-binding protein
FBS	Fetal bovine serum
FITC	Fluorescein isothiocyanate
FL	Follicular lymphoma
FMC63-C	anti-CD19 scFv from the FMC63 construct containing a terminal cysteine
FMC63-CHC	anti-CD19 scFv from the FMC63 construct containing a terminal cysteine and c-myc and His6 tags
GAH	Goat anti-human

GAM	Goat anti-mouse
Gly	Glycine
Gly4	GlyGlyGlyGly
GSH	Reduced glutathione
GSSG	Oxidized glutathione
Gu HCl	Guanidine hydrochloride
HAMA	Human anti-mouse antibody
HBS	HEPES-buffered saline
HD37-C	anti-CD19 scFv from the HD37 construct containing a terminal cysteine
HD37-CCH	anti-CD19 scFv from the HD37 construct containing a c-myc tag, a cysteine and a His5 tag
HD37-CHC	anti-CD19 scFv from the HD37 construct containing c-myc and His6 tags, and a terminal cysteine
HEPES	4-(2-hydroxyethyl)piperazine-1-ethanesulfonic acid
HER2	Human epidermal growth factor receptor 2
His	Histidine
His5	HisHisHisHisHis
His6	HisHisHisHisHisHis
HIV	Human immunodeficiency virus
HRP	Horseradish peroxidase
HSPC	Hydrogenated soy phosphatidylcholine
Hz	Hydrazide

i.v.	Intravenous
IC <sub>50</sub>	The concentration of drugs inhibiting 50% of cell growth
IPTG	Isopropyl β-D-1-thiogalactopyranoside
K <sub>D</sub>	Equilibrium dissociation constant
L-Arg	L-arginine
LUV	Large unilamellar vesicle
mAb	Whole monoclonal antibody
Mal	Maleimide
Mal-PEG-DSPE	Maleimide-derivatized PEG-DSPE
MCL	Mantle cell lymphoma
MFI	Mean fluorescence intensity
MLV	Multilamellar vesicle
MRT	Mean residence time
MST	Mean survival time
MTT	3-(4,5-Dimethylthiazol-2-yl)-2,5-diphenyltetrazolium bromide
MUC4	Mucin 4
NBD-PE	1-oleoyl-2-[6-[(7-nitro-2-1,3-benzoxadiazol-4- yl)amino]hexanoyl]-sn-glycero-3-phosphoethanolamine
ND	Not determined
nH-4G7-GC	anti-CD19 scFv from the 4G7 construct containing His5 and Gly4 tags, and a terminal cysteine
NHL	Non-Hodgkin's lymphoma

Ni-NTA	Nickel-nitrilotriacetic acid
NK cells	Natural killer cells
OD	Optical density
P/S/G	Penicillin-streptomycin-L-glutamine
PBS	Phosphate-buffered saline
PBST	0.1% Tween 20 in PBS
PDP	Pyridyldithiopropionate
PE	Pseudomonas exotoxin
PEG	Polyethylene glycol
PEG <sub>2000</sub> -DSPE	PEG, molecular weight 2000, covalently coupled to DSPE
PEG <sub>3400</sub> -DSPE	PEG, molecular weight 3400, covalently coupled to DSPE
PK	Pharmacokinetics
PL	Phospholipid
PPE	Palmar-plantar erythrodysesthesia
PTK	Protein tyroine kinase
REAL	Revised European American lymphoma
RES	Reticuloendothelial system
RGF 4G7	anti-CD19 scFv from the 4G7 construct engineered for expression in algae
S.D.	Standard deviation
scFv	Single chain Fv fragment
SCID	Severe combined immunodeficient
SDS-PAGE	Sodium docecyl sulphate polyacrylamide gel electrophoresis

SH	Free sulfhydryl group
SIL	Stealth <sup>®</sup> immunoliposome
SIL-DXR	DXR-loaded SIL
SIL[FMC63-C]	SIL targeted via FMC63-C
SIL[FMC63-CHC]	SIL targeted via FMC63-CHC
SIL[FMC63 mAb]	SIL targeted via FMC63 mAb
SIL[HD37-CCH]	SIL targeted via HD37-CCH
SIL[HD37-CHC]	SIL targeted via HD37-CHC
SIL[HD37 Fab']	SIL targeted via HD37 Fab'
SIL[HD37 mAb]	SIL targeted via HD37 mAb
SIL[RGF 4G7]	SIL targeted via RGF 4G7
SIL-DXR[HD37-CHC]	SIL-DXR targeted via HD37-CHC
SIL-DXR[HD37 Fab']	SIL-DXR targeted via HD37 Fab'
SIL-DXR[HD37 mAb]	SIL-DXR targeted via HD37 mAb
SL	Stealth <sup>®</sup> liposome
SL-DXR	DXR-loaded SL
SMPB	Succinimidyl-4-(p-maleimidophenyl)butyrate
SUV	Small unilamellar vesicle
$t_{1/2}$	Half-life
$T_c$	Phase transition temperature
VCR	Vincristine
$V_d$	Volume of distribution
VEGF	Vascular endothelial growth factor

V <sub>H</sub>	Variable heavy chain
V <sub>L</sub>	Variable light chain
WHO	World Health Organization

**Chapter 1**

**Introduction, Hypothesis and Objectives**

## **1. Introduction, Hypothesis and Objective**

### **1.1. Introduction**

Despite significant advances in the understanding of tumor biology and the development of more effective anticancer therapeutics, cancer remains a major public health problem. In 2001, cancer was the second leading cause of death, after cardiovascular diseases, in the United States. It accounted for an estimated 1,268,000 new cases and 553,400 deaths (1). The National Cancer Institute of Canada has estimated that more than 160,000 new cases and more than 73,000 deaths due to cancer will occur in Canada in 2007 (2).

Some traditional small molecule anticancer drugs often suffer from low therapeutic indices due to their lack of specific cytotoxicity against cancer cells, as well as a lack of specificity in their biodistribution. Anticancer drugs such as doxorubicin exhibit cytotoxicity not only against rapidly dividing malignant cells, but also against rapidly dividing normal cells, e.g., cells in the bone marrow and hair follicles. This lack of specificity results in most of the adverse side effects (e.g., alopecia, stomatitis, diarrhea, malaise, immunosuppression, and bone marrow toxicities) associated with anticancer drugs. The pharmacokinetic (PK) profiles of some 'classical' anticancer drugs, having large volumes of distribution (Vd), are characterized by indiscriminate distribution of the anticancer drugs into both malignant and normal cells; this causes, for example, the dose-limiting cardiac toxicity of doxorubicin. The non-specific activities of anticancer drugs lead to problems such as sub-therapeutic dosing, early termination of

therapy due to side effects, or fatalities. Early termination of therapy may result in reduced response, leading to disease relapse and drug resistance.

Various approaches to improve the specificity of anticancer drugs have been tried. The two major lines of approach are to increase the specific cytotoxicities of anticancer drugs to cancer cells, or to increase the specific distribution of anticancer drugs to cancer cells. In the first approach, research into unique signalling pathways and targets in malignant cells have resulted in the development and marketing of a new generation of “targeted” anticancer drugs, such as imatinib (Gleevec<sup>®</sup>) (3), gefitinib (Iressa<sup>®</sup>) (4), erlotinib (Tarceva<sup>®</sup>) (5) and various antitumor antibodies. These targeted anticancer drugs inhibit specific signaling pathways (e.g., the epidermal growth factor receptor, EGFR) that are essential for tumor pathogenesis.

This type of targeted therapy is thought to hold great promise for the treatment of cancers since these drugs have increased specific cytotoxicity against malignant cells, and some have been shown, when used in combination with traditional anticancer drugs, to result in significantly improved therapeutic effects over conventional treatments alone (6-8). Use of these drugs can also be associated with some level non-specific toxicity against normal cells, since normal cells also express some of the receptors (e.g., EGFR) that are targeted by these drugs. In addition, for some of these drugs (e.g., gefitinib), their therapeutic effects in the clinic remain less than ideal with minimal increases in survival time over placebo. However, certain subsets of patients seem to receive benefit, and more research is needed on how to stratify patients into responders and non-responders in order to maximize their therapeutic potential (9-11). Also, further research is needed to discover new targets and novel agents with greater therapeutic activities.

In the second approach, the specific delivery of conventional anticancer drugs to malignant cells has also been explored as a means to increase the specificity of anticancer drugs. This has resulted in the development of drug delivery systems (DDS) such as liposomes, microspheres, polymer micelles, ligand-drug conjugates and polymer-drug conjugates (12). By exploiting the unique physical properties of cancer cells or solid tumors, DDS can increase the accumulation of therapeutics such as conventional anticancer drugs, toxins or radionucleotides in solid tumors. Exploitable properties include the expression of antigens that are either unique to, or are overexpressed on the cancer cell surface, or the presence of fenestrated gaps in the endothelium of solid tumor vasculature. Examples of targeted delivery via tumor-associated antigens are radiolabeled antibodies (e.g.,  $^{131}\text{I}$ -tositumomab) (13), immunotoxins (e.g., HD37-dgRTA, an anti-CD19 antibody conjugated with the ricin A chain) (14), and antibody-drug conjugates (e.g., the BR96 mAb conjugated with doxorubicin) (15). Other DDS, such as liposomes (16) and polymer micelles (17), can specifically localize and deliver anticancer drugs to solid tumors by extravasation through fenestrated gaps in the endothelium of the tumor vasculature (18).

## **1.2. Liposomes as a Nano-particulate Drug Delivery System**

Since the first description of liposomes in the 1960s, liposomes have emerged as the prototype of DDS and have entered the mainstream of clinical use (16, 19). Several liposomal drugs, such as liposomal amphotericin B (Ambisome<sup>®</sup>), liposomal doxorubicin (Myocet<sup>®</sup>), liposomal daunorubicin (DaunoXome<sup>®</sup>) and PEGylated liposomal doxorubicin (Doxil/Caelyx<sup>®</sup>), are currently on the market (Table 1.1) and many others (e.g., liposomal vincristine) are in various stages of development. Liposomal DDS are

**Table 1.1. Currently marketed liposomal drugs.** Adapted from (16).

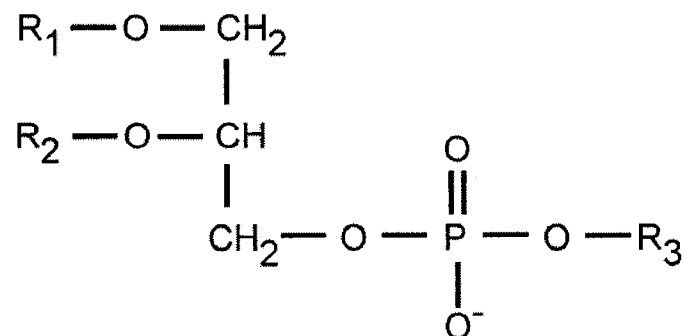
<b>Brand name</b>	<b>Drug</b>	<b>Formulation</b>	<b>Indications</b>	<b>Manufacturer</b>
AmBisome <sup>®</sup> (20)	Amphotericin B	Liposome	Fungal infections, visceral leishmaniasis	Gilead/Astellas
Myocet <sup>®</sup> (21)	Doxorubicin	Liposome	Metastatic breast cancer	Cephalon
Doxil/Caelyx <sup>®</sup> (22)	Doxorubicin	PEGylated liposome	Kaposi's sarcoma, refractory breast cancer, and refractory ovarian cancer	Alza/Johnson & Johnson
DaunoXome <sup>®</sup> (23)	Daunorubicin	Liposome	HIV-related Kaposi's sarcoma	Gilead
DepoCyt <sup>®</sup> (24)	Cytosine arabioside	Liposome	Lymphomatous meningitis and neoplastic meningitis	SkyePharma/ Enzon

generally composed of amphiphilic phospholipids (PL) and cholesterol (Chol) that can self-associate in an aqueous environment into spherical vesicles, with a phospholipid bilayer membrane and an aqueous interior.

One of the initial applications of liposomes was to model the composition and function of biological membranes (25). Liposomes were first described as encapsulation vehicles for enzymes and drugs in the 1970s (26, 27). Since, for clinical applications, their diameters are generally in the nanometer size range (~ 50-150 nm), liposomes are classified as nanomedicines. The lipids currently used in preparation of liposomes for clinical applications are generally considered to be biocompatible, biodegradable, non-immunogenic and to have a low toxicity profile (Fig. 1.1) (28).

Drugs can be either entrapped in the aqueous interior of liposomes or associated with the membrane bilayer. In general, entrapment of drugs in the interior of liposomes can result in a higher payload (i.e., > 1000 drug molecules per liposome) than ligand-targeted conjugates and polymer-conjugates of anticancer drugs (1–10 drug molecules per ligand or polymer) (29). Entrapment of drugs in liposomes can result in significant changes in the PK parameters of the entrapped drug, including decreased Vd, increased area under the curve (AUC) and half-life ( $t_{1/2}$ ), and decreased clearance (CL), compared to the free drug. This is illustrated by a polyethylene-glycolated (PEGylated) liposomal formulation of the anticancer drug doxorubicin (DXR), Doxil/Caelyx<sup>®</sup> and a classical liposomal formulation of DXR, Myocet<sup>®</sup>, in Table 1.2. The changes in PK for PEGylated liposomal DXR result in a clinically relevant reduction in cardiac toxicity (a sometimes fatal dose-limiting toxicity of DXR) (30), in comparison to free DXR. The presence of PEG on the surface of liposomes increases the circulation time of

### Common phospholipid structure



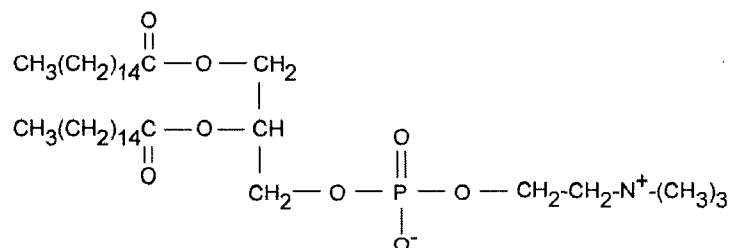
### Fatty acyl chains (R<sub>1</sub> and R<sub>2</sub>)

Palmitate	(C16:0)	CH <sub>3</sub> (CH <sub>2</sub> ) <sub>14</sub> CO <sup>-</sup>
Stearate	(C18:0)	CH <sub>3</sub> (CH <sub>2</sub> ) <sub>16</sub> CO <sup>-</sup>
Oleate	(C18:1)	CH <sub>3</sub> (CH <sub>2</sub> ) <sub>7</sub> CH=CH(CH <sub>2</sub> ) <sub>7</sub> CO <sup>-</sup>

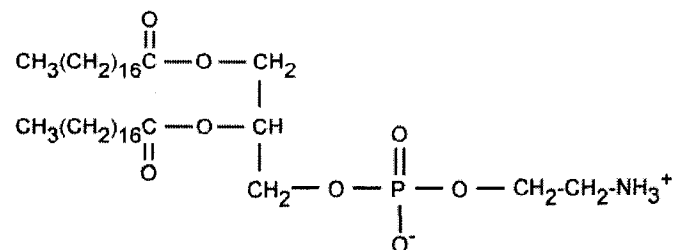
### Head group (R<sub>3</sub>)

Choline	CH <sub>2</sub> -CH <sub>2</sub> -N <sup>+</sup> -(CH <sub>3</sub> ) <sub>3</sub>
Ethanolamine	CH <sub>2</sub> -CH <sub>2</sub> -NH <sub>3</sub> <sup>+</sup>

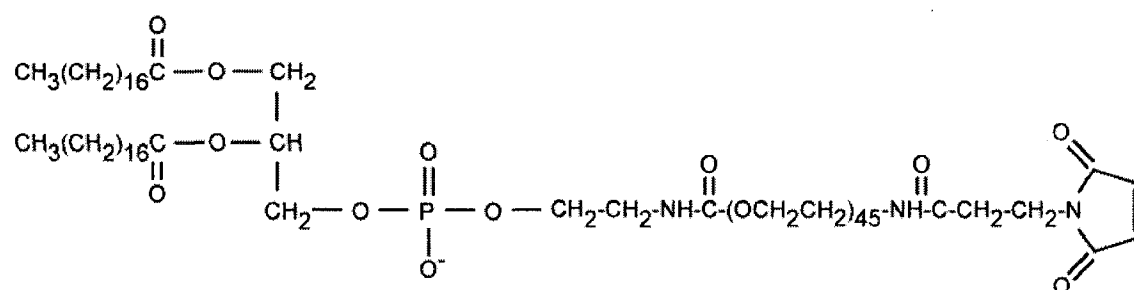
### Hydrogenated Soy Phosphatidylcholine (HSPC)



### Distearoylphosphatidylethanolamine (DSPE)



### Maleimide-derivatized PEG-DSPE



### Cholesterol

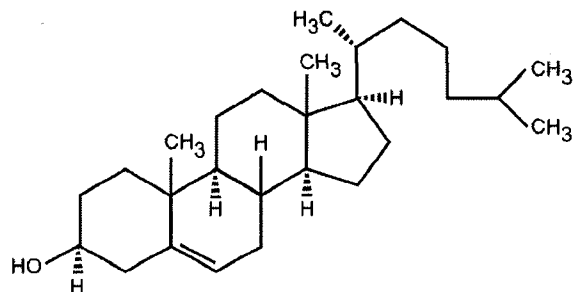


**Figure 1.1. Structures of some common liposome-forming lipids** (Adapted from G.J.R. Charrois).

**Table 1.2. Comparison of PK parameters for free DXR and liposomal DXR in human.**

	<b>DXR Dose (mg/ m<sup>2</sup>)</b>	<b>t<sub>1/2</sub>α<sup>a</sup> (h)</b>	<b>t<sub>1/2</sub>β<sup>b</sup> (h)</b>	<b>t<sub>1/2</sub>γ<sup>c</sup> (h)</b>	<b>Vd<sub>ss</sub><sup>d</sup> (L)</b>	<b>AUC<sup>e</sup> (mg*h/L)</b>	<b>CL<sup>f</sup> (L/h)</b>	<b>Ref.</b>
<b>Free DXR</b>	25	0.2	2	40	365	≈ 1	≥ 45	(31, 32)
<b>Doxil/ Caelyx<sup>®</sup></b>	25	3.2	45	-	4.1	609	0.08	(32)
	50	1.4	46	-	5.9	902	0.09	(32)
<b>Myocet<sup>®</sup></b>	25	0.3	7	-	18.8	18.5	23.3	(33)
	90	0.5	14	-	14.6	13.5	21.8	(33)

<sup>a</sup> Half-life of the alpha distribution phase (t<sub>1/2</sub>α); <sup>b</sup> Half-life of the beta elimination phase (t<sub>1/2</sub>β); <sup>c</sup> Half-life of the gamma elimination phase (t<sub>1/2</sub>γ); <sup>d</sup> Volume of distribution at steady state (Vd<sub>ss</sub>); <sup>e</sup> Area under the blood concentration versus time curve (AUC); <sup>f</sup> Clearance (CL)

Doxil/Caelyx<sup>®</sup> in comparison to Myocet<sup>®</sup>. Due to differences in lipid composition between the two formulations, Doxil/Caelyx<sup>®</sup> also exhibits increased drug retention in comparison with Myocet<sup>®</sup>.

Because DDS often function as sustained release systems, encapsulation or conjugation of drugs within the DDS can change the toxicity profile, as well as the pharmacokinetics and biodistribution (PK/BD), of the drug from that seen for a bolus injection of the free drug to a profile more like that seen for free drug infusions. For example, the PEGylated formulation of liposomal DXR has substantially reduced cardiac toxicity, but increased dose-limiting skin toxicity termed the hand-foot syndrome or palmar-plantar erythrodysesthesia (PPE), which is not commonly observed with bolus administration of the free drug, but has been described for free drug infusions of doxorubicin and 5-fluorouracil (34-37). PPE can be minimized by changes to the dosing schedule including dose reduction and lengthening of the dosing interval (38).

### **1.2.1. Classical Liposomes**

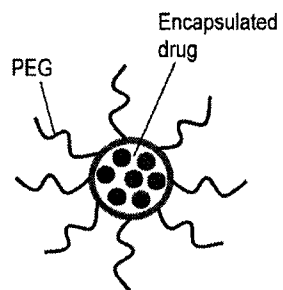
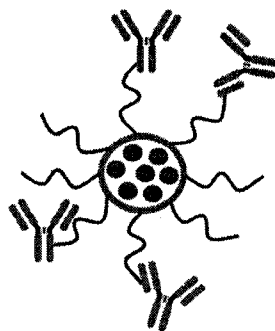
Classical liposomes are composed of natural lipids without surface modifiers. The exposed polar head groups of the phospholipids attract plasma proteins, and adsorption of plasma proteins (opsonins) to the surface of classical liposomes leads to recognition and uptake of the liposomes by cells of the reticuloendothelial system (RES), resulting in their clearance from circulation in a dose-dependent, saturable manner (39). Despite their lack of dose-dependent PK, several formulations of classical liposomes have been marketed, including Myocet<sup>®</sup> (liposomal doxorubicin) for the treatment of metastatic breast cancer. Human PK parameters for Myocet<sup>®</sup> are given in Table 1.2.

### 1.2.2. Sterically Stabilized and Stealth<sup>®</sup> Liposomes

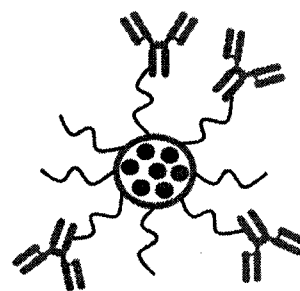
Stealth<sup>®</sup> liposomes (SL) are coated with polyethylene glycol (PEG)-lipid derivatives (Fig. 1.2A). Other sterically stabilized liposomes may be coated with hydrophilic polymers or peptides (40, 41). The grafting of hydrophilic PEG molecules on the surface of SL attract water molecules, which has been postulated to prevent opsonization (or attract dysopsonins) leading to reduced uptake by the RES. The end result is increased circulation half-lives relative to classical liposomes, and dose-independent, zero order PK (39, 42).

The long circulation times of SL allow the liposomes to take advantage of the enhanced permeability of tumor vasculature and decreased lymphatic drainage from tumors, resulting in their accumulation in solid tumors; this process is known as the enhanced permeability and retention (EPR) effect, or “passive targeting” (43-45). Normally, endothelial cells lining the vasculature have tight junctions between them, which prevent extravasation of plasma proteins and large macromolecules from the blood. Recruitment and growth of new blood vessels (i.e., angiogenesis) in tumors result in abnormal vasculature, where fenestrations in the endothelium (up to 800 nm in diameter) are sufficiently large to allow for extravasation and accumulation of liposomes (~ 50–200 nm in diameter) in the interstitial space of tumors (46, 47). Once localized in tumors, therapeutics released from liposomes are in close proximity to the tumor cells, which leads to increased uptake.

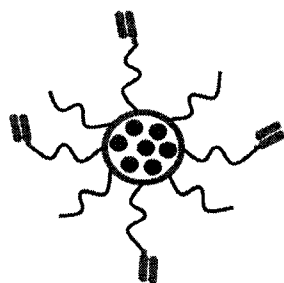
In comparison to free anticancer drugs, anticancer drugs such as DXR, when encapsulated in SL (SL-DXR, e.g., Doxil/Caelyx<sup>®</sup>), have increased accumulation in solid tumors and decreased accumulation in normal tissue such as the heart (48, 49). As a

A. Stealth<sup>®</sup> Liposome (SL)B. Stealth<sup>®</sup> immuoliposomes (SIL) conjugated with mAb via maleimide method

C. SIL conjugated with mAb via hydrazide method



D. SIL conjugated with Fab'



E. SIL conjugated with scFv

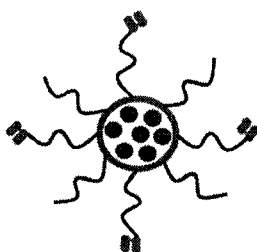


**Figure 1.2. Schematic representation of Stealth<sup>®</sup> and immunoliposomes coupled to various antibody constructs. Adapted from (12).**

result, Doxil/Caelyx<sup>®</sup>, has increased efficacy and decreased toxicities compared to free DXR, resulting in an increased therapeutic index (50, 51). Doxil/Caelyx<sup>®</sup> has received approval for treatment of Kaposi sarcoma, and refractory ovarian and breast cancers. In comparison to Myocet<sup>®</sup>, Doxil/Caelyx<sup>®</sup> has longer circulation time in humans with  $t_{1/2}$  of 45 h, Vd of 4.1 L and CL of 0.08 L/min (Table 1.2).

### 1.2.3. Ligand-targeted Liposomes

Sterically stabilized or Stealth<sup>®</sup> liposomes only “passively” target solid tumors and do not bind to malignant cells within the tumors. Furthermore, sterically stabilized liposomes are theoretically less effective against hematological malignancies due to the lack of the EPR effect against malignant cells in the blood or against micro-metastases that have yet to develop their own vasculatures. Ligand-targeted Stealth<sup>®</sup> liposomes (Stealth<sup>®</sup> immunoliposomes, SIL), have either small molecule ligands such as peptides, or antibodies (including fragments of antibodies) covalently attached to the outer surface of liposomes, which allow them to target cancer cells that either selectively express or overexpress tumor-associated receptors or antigens. Examples of ligands used for ligand-targeted liposomes included folate (52, 53), transferrin (54), and peptides containing the NGR or RGD motif, which bind to aminopeptidase N (CD13) or to  $\alpha_v\beta_3$ -integrin, respectively (55, 56).

Immunoliposomes can be targeted with whole monoclonal antibodies (mAb) or fragments of antibodies, for example, F(ab')<sub>2</sub>, Fab', or single chain Fv (scFv) fragments (Fig. 1.3). In various *in vitro* and animal models of cancers, many studies have demonstrated that targeted delivery of anticancer drugs with immunoliposomes results in an increased therapeutic effect over untargeted liposomes (57-59). In an early example in

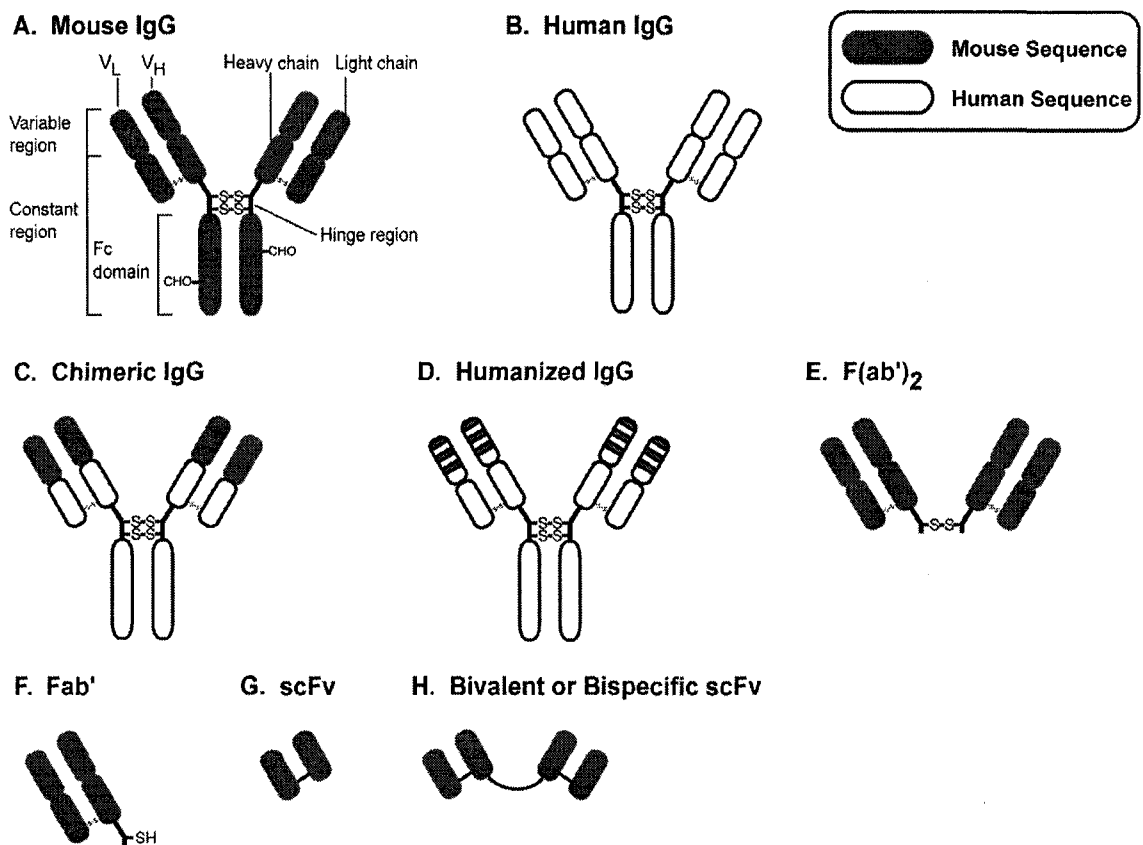


**Figure 1.3. Schematic representation of various antibody constructs.** **A)** Mouse IgG. The  $V_L$  and  $V_H$  regions contain the antigen binding domains (i.e., CDR). **B)** Human IgG. **C)** Chimeric IgG with murine  $V_L$  and  $V_H$  regions and human constant regions. **D)** Humanized IgG with murine CDR sequence grafted onto human IgG backbone. **E)** F(ab')<sub>2</sub> generated by pepsin digestion of the Fc domain of IgG. **F)** Fab' can be generated by reduction of the disulfide bond in the hinge region of F(ab')<sub>2</sub>. **G)** ScFv which contains recombinant  $V_L$  and  $V_H$  regions linked by a short peptide sequence (usually 4 Gly). Various tags (e.g., poly-His) and amino acid sequences (e.g., terminal Cys, with a sulfhydryl group for coupling to liposomes) can be engineered into the scFv construct. **H)** Bivalent scFv with two scFv, directed against the same epitope, joined by a poly-peptide linker. Bispecific scFv can be constructed by linkage of two scFv directed against two different antigens. Adapted from (12).

a murine model of squamous cell carcinoma of the lung, Ahmad et al. showed that targeted delivery of immunoliposomal DXR via the 174H.64 mAb, directed against a unique epitope expressed on proliferating squamous cell carcinoma, resulted in a significant decrease in the number of tumor foci and an increase in life span of the animals over free DXR and untargeted liposomal DXR (60). Using a metastatic model of human B-lymphoma, Lopes de Menezes et al. showed that targeting liposomal DXR via the anti-CD19 FMC63 mAb resulted in increased therapeutic activity over untargeted liposomal DXR and the free drug (61). In another series of experiments using the same model, Sapra et al. demonstrated increased therapeutic activity, manifested as prolonged or disease-free survival times, over the free drugs and untargeted liposomal drugs, in mice treated with liposomal DXR targeted via the FMC63 whole mAb or Fab' (62), or liposomal vincristine (VCR) targeted via either FMC63 or anti-CD20 mAb, Rituximab<sup>®</sup> (63). In murine models of human breast cancer, Park et al. showed that targeted delivery of liposomal DXR via the anti-HER2/*neu* mAb, Fab' or scFv resulted in tumor regression, and disease-free survival in mice bearing tumors with high expression of the HER2/*neu* oncogene (64).

In addition to the specific delivery of anticancer drugs to antigen expressing cells, synergistic effects may be achieved when anticancer drugs are delivered via immunoliposomes targeted with antibodies that are capable of initiating anti-proliferative signals (65). Therefore, some clear advantages exist for the targeted delivery of liposomal anticancer drugs over traditional untargeted liposomes. The identification of increasing numbers of tumor-specific antigens, and the development and marketing of numerous antibodies directed against these antigens present great opportunities for the

development of targeted DDS. Despite the availability of untargeted liposomal anticancer drugs for more than a decade and the intense research in immunoliposome technologies, no immunoliposomal anticancer drugs are presently being marketed, although some are near clinical trials (66, 67).

### 1.3. Preparation of Liposomes

In general, liposomes for clinical use are composed of amphiphilic long chain phospholipids (PL) and cholesterol (Chol) (Fig. 1.1). In an aqueous environment the amphiphilic PL self-assemble into vesicles with a bilayer membrane where the polar head-groups face the aqueous environment and the non-polar acyl groups form the interior of the bilayer. Sterically stabilized liposomes contain hydrophilic polymers such as PEG conjugated to a long-chain PL that serves to anchor the PEG in the PL bilayer. At temperatures below the solid to liquid-crystalline phase transition temperature ( $T_C$ ) of the phospholipids, the membrane is in an ordered, rigid state, and at temperatures above the  $T_C$  the membrane becomes disordered and fluid, resulting in increased permeability. The relative rigidity and permeability of the liposome membrane influences the rate of drug release.

Liposomes may be prepared by several methods, which include thin-film hydration (68), reverse phase evaporation (69), solvent injection (70), detergent dialysis (71) and freeze thaw (72). These methods generate large liposomes termed multilamellar vesicles (Fig. 1.4). Multilamellar vesicles (MLV) are less desirable for *in vivo* applications since they are above the cut-off size for tumor extravasation, have low entrapped volumes, and have considerable size heterogeneity, which makes pharmaceutical characterization difficult (68, 73, 74). Several methods, including

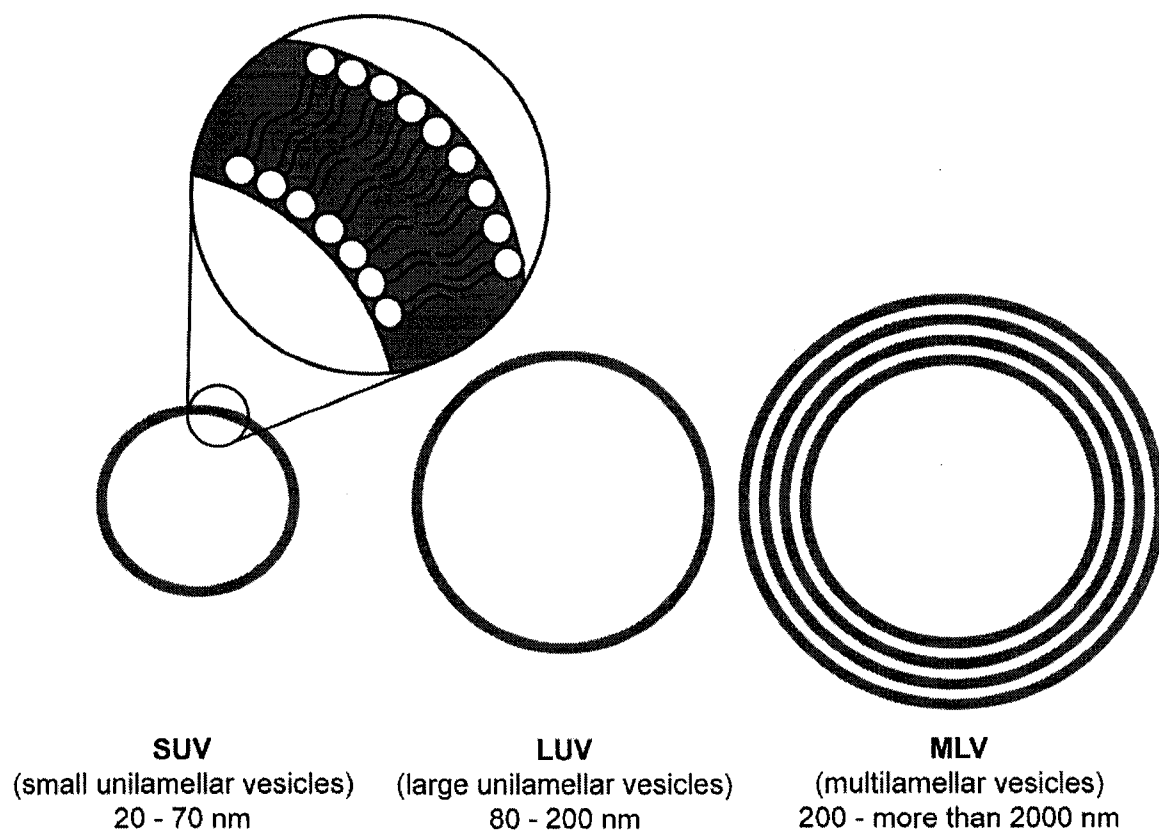


**Figure 1.4. Classification of liposomes based on size and lamellarity.** Adapted from (74).

sonication and extrusion through polycarbonate membranes, can be employed for reducing the size of the MLV to produce homogeneous preparations of unilamellar liposomes. Sonication of MLV results in small unilamellar vesicles, SUV, with diameters of ~ 30-50 nm (75), and extrusion produces large unilamellar vesicles, LUV, with diameters of ~ 50-150 nm, depending on the pore size of the polycarbonate membrane (76, 77). LUVs have higher entrapped volumes than SUVs and are therefore more suitable for *in vivo* drug delivery (69). For this thesis, liposomes were composed of lipids that have  $T_C$  well above 37 °C and liposomes were prepared by thin-film hydration followed by extrusion, through polycarbonate membranes, to diameters in the range of ~ 100-120 nm.

#### **1.4. Drug-loading Methods**

Drugs may be associated with liposomes in many ways, depending on the physical and chemical properties of the drug. Hydrophobic drugs may be embedded between the acyl chains in the inner core of the bilayer, amphipathic drugs may intercalate between phospholipid headgroups on either side of the membrane and hydrophilic drugs may be solubilized in the aqueous interior of liposomes or associate with the inner and outer bilayer surface via electrostatic forces (28). For entrapment of hydrophobic drugs such as paclitaxel, the drugs are generally dissolved in organic solvents with the appropriate lipids and then the mixture is dried or lyophilized. The dried drug-lipid mixture is then hydrated to produce MLV with the drug associated with the hydrophobic interior of the bilayer; smaller vesicles can be obtained subsequently by methods such as extrusion or sonication (28, 78). For simple entrapment of hydrophilic drugs, dried or lyophilized lipid mixtures may be hydrated in drug-containing buffers,

with subsequent removal of the un-encapsulated drugs via size exclusion chromatography, affinity chromatography, or dialysis. A drawback with this method is that the encapsulation rates are generally very low (28).

Alternatively, amphipathic weak bases such as DXR ( $pK_a = 8.3 - 8.5$ ) may be loaded into preformed liposomes via a technique termed “remote loading”, which relies on a differential gradient (pH or chemical) across the liposome membrane (79-81). When loading DXR into liposomes that have a pH gradient across the bilayer (outside, neutral; inside, acidic), diffusion of DXR in its uncharged form across the membranes into the acidic interior of liposomes results in protonation of the drug, trapping the drug within the liposomes. This method can encapsulate DXR with high efficiency ( $> 95\%$ ); dissipation of the pH gradient over time results in release of the drug from liposomes (79, 82). In a variation of the pH gradient method, DXR can be loaded into liposomes via an ammonium sulfate gradient (81, 83). Diffusion of ammonia from the liposomes results in an acidic interior and the formation of a stable, gel-like precipitate of DXR with the sulfate ions, which traps the drug inside the liposomes (Fig. 1.5). For this thesis, DXR-loaded liposomes were prepared by the ammonium sulfate gradient method since this method can result in encapsulation efficiency of  $> 95\%$  with little leakage of drug during prolonged storage.

#### **1.4.1. Rate of Drug Release**

For drugs such as DXR, which can be stably encapsulated, drug release is a result of dissipation of the pH gradient, resulting in the generation of uncharged DXR within the liposome interior. Both the dissipation of the  $H^+$  gradient and the subsequent release of uncharged DXR depend on the fluidity/rigidity of the membrane bilayer, which is a

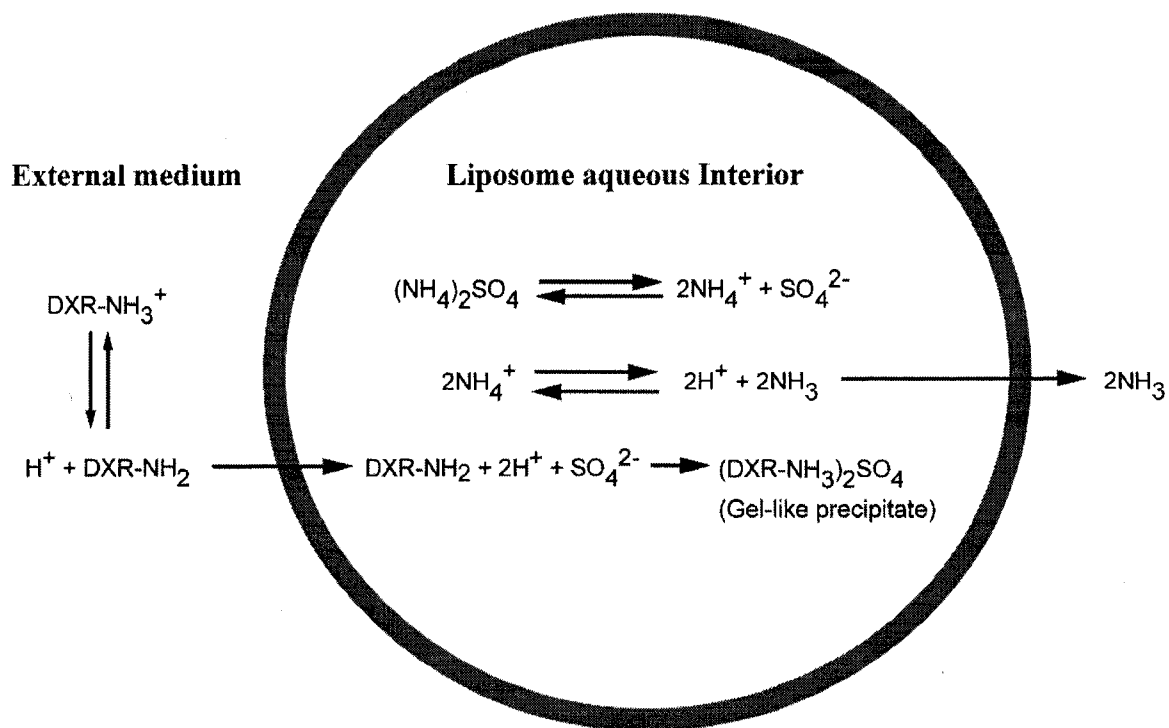


**Figure 1.5. Schematic presentation of remote loading of DXR using the ammonium sulfate gradient.** Doxorubicin has a pKa of 8.3-8.5. At an exterior pH of 7.4, uncharged DXR enters liposomes by crossing the lipid bilayer and becomes protonated in the acid interior of the liposomes. The protonated DXR is trapped inside the liposomes and reacts with  $\text{SO}_4^{2-}$  to form a gel-like precipitate. The acid interior pH is generated by the release of ammonia into the external medium. Using this method, the efficiency of encapsulation of DXR can approach 100%. Adapted from (83).

function of its lipid composition. Several studies have demonstrated that the leakage rate of DXR from remote-loaded liposomes is related to the  $T_C$  of lipid components. The plasma level DXR was shown to be significantly lower and clearance was significantly higher, when DXR was encapsulated in SL composed of lipids with a lower  $T_C$  (more fluid membrane) compared to SL composed of lipids with a higher  $T_C$  (more rigid membrane) (33, 84, 85).

The rate of drug release can, in turn, influence the therapeutic activity and the side effects of liposomal drugs. Charrois and others showed in mice that DXR encapsulated in liposomes with an intermediate rate of drug release resulted in significant weight loss, possibly due to toxicity to the gastrointestinal tract compared to DXR-loaded liposomes that had either a higher or lower rate of release (85). Allen et al. also demonstrated that, at equal doses of DXR, liposomal DXR with rates of drug release at either extreme did not exhibit any toxicity, but liposomal DXR with intermediate rates of drug release ( $t_{1/2} = 65\text{--}125$  h *in vivo*) resulted in severe gastro-intestinal toxicity (86). In another series of studies, Johnston et al. demonstrated that maximal therapeutic activity can be achieved by optimization of the rate of drug release from liposomes and rate of drug release at either extreme resulted in decreased activity (87). These experiments suggest that both the therapeutic activity and toxicity of liposomal drugs are related to the rate of drug release as shown in Figure 1.6. Therefore, it is now thought to be possible to optimize the rate of drug release to achieve the maximum therapeutic activity while minimizing toxicity for individual liposomal drugs.

Interestingly, Allen et al. demonstrated that the toxicity of liposomal DXR with intermediate rates of drug release can be ameliorated through antibody-mediated

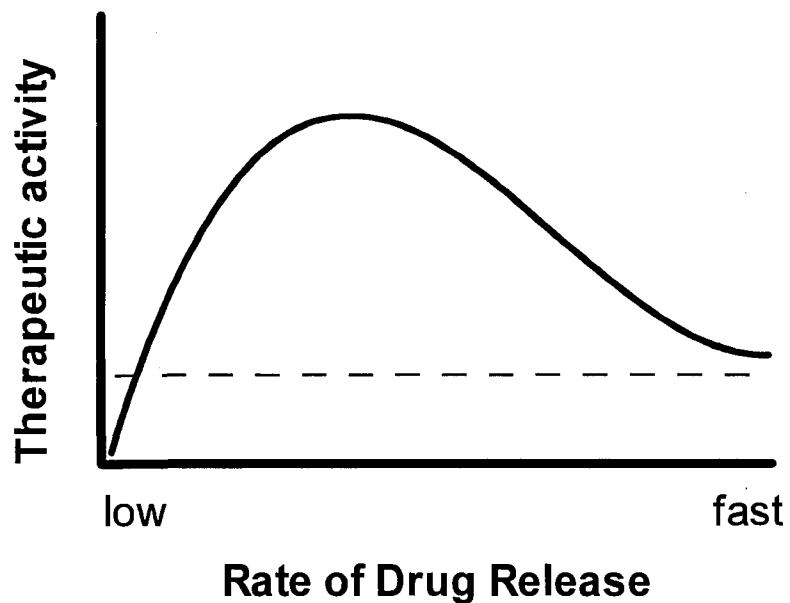


**Figure 1.6. Theoretical relationship between the rate of drug release and therapeutic activity.** Adapted from (87). As the rate of drug release approaches zero, the therapeutic activity should approach zero as well since little drug is released, i.e., bioavailable. The dashed line represents the therapeutic activity of the free drug, which by definition is fully bioavailable. At the maximal rate of drug release, the therapeutic activity of the liposomal drug should approximate that of the free drug.

targeting of the liposomal DXR in a murine model of B cell lymphoma (86). In these experiments, the authors showed that the toxicity of liposomal DXR having intermediate rates of drug release was reduced when those formulations were targeted to the B cells via an anti-CD19 mAb. The decrease in toxicity may be related to the increase in clearance or to increases in the specific biodistribution of the liposomes to the CD19<sup>+</sup> malignant B cells as a result of conjugation of anti-CD19 mAb to the surface of the liposomes.

### **1.5. Antibody-coupling Methods**

Antibodies or ligands can be coupled to liposomes by covalent or non-covalent bonds. For preparation of Stealth<sup>®</sup> immunoliposomes (SIL), whole antibodies or fragments of antibody are generally covalently coupled to the modified PEG termini distal to the surface of liposomes. Various modifications to the PEG termini permit the covalent coupling of ligands, including pyridyldithiopropionoylamino-PEG (PDP-PEG) (88), hydrazide-PEG (Hz-PEG) (89) or maleimide-PEG (Mal-PEG) (90).

In the PDP-PEG method, antibodies are functionalized with maleimide groups using succinimidyl-4-(p-maleimidophenyl)butyrate (SMPB) prior to coupling to liposomes containing thiolated PDP-PEG-distearoylphosphadidylethanolamine (PDP-PEG-DSPE), via formation of thio-ether bonds. In the Mal-PEG method, antibodies are thiolated and coupled to liposomes containing Mal-PEG-DSPE via thio-ether bonds. The advantage of the Mal-PEG method is that this method requires fewer steps and allows for more rapid coupling of antibodies to liposomes. A drawback with both PDP-PEG and Mal-PEG methods is that functionalization and thiolation of whole antibodies occur randomly and may occur in multiple locations resulting in random orientation of

antibodies relative to the surface of SIL (Fig. 1.2B). This can lead to increased clearance of the liposomes from circulation via two different mechanisms: cross-linking of the immunoliposomes and rapid clearance of the resulting aggregates or the exposure of Fc groups in the case of whole mAb, with clearance of the immunoliposomes via Fc receptor-mediated mechanisms.

The Hz-PEG method involves oxidation of the carbohydrates in the Fc region of the whole antibody into reactive aldehydes, and the formation of hydrazone bonds with the hydrazide groups on the PEG-terminus. Since coupling is through the Fc region of whole mAb (Fig. 1.2C), this method interferes with the binding of the Fc region to Fc receptors; mAb-coupled SIL formed by this method exhibit similar PK to untargeted liposomes (61).

In Chapter 4 of this thesis, the Mal-PEG coupling method was used since this method can be applied to Fab' fragments of mAb via thiol groups in the hinge region, and to scFv fragments containing reduced sulfhydryl groups. Since they lack the Fc region, Fab'-coupled SIL made by the Mal-PEG method have similar clearance to untargeted SL and circulate much longer than SIL coupled via this method to whole mAb (62, 91, 92). It is expected that SIL coupled with scFv will have clearance similar to SL and Fab'-SIL, since scFv fragments also lack the Fc region.

For non-covalent coupling of antibodies to liposomes, many studies have used antibodies and PEG-lipids functionalized with proteins or small molecules that have strong affinities for each other. For example, various antibody constructs have been linked to liposomes with some success via the strong biotin and avidin interaction (93, 94), via folate and the folate-binding protein (FBP) (95), and via poly-His tag and nickel

nitrilotriacetic acid (Ni-NTA) (96). Non-covalently coupled SIL may be less desirable than covalently coupled SIL for *in vivo* applications, due to the potential for immune reactions (e.g., to avidin) or since the interaction between the linkage molecules (e.g., poly-His and Ni-NTA) may be competed away by serum proteins or cell surface receptors, resulting in liposomes without any targeting moieties and therefore the loss of targeting (97).

### 1.6. Post-insertion Approach

In addition to conventional coupling, where antibody or ligands are coupled directly to liposomes containing derivatized PEG-lipids such as Mal-PEG-DSPE, immunoliposomes can also be prepared using the post-insertion method (98, 99). For the post-insertion method, ligands, antibody, or fragments of antibody, are first coupled to micelles of derivatized PEG-lipid, under conditions similar to conventional coupling. The antibody-conjugated PEG-lipids are then incubated with preformed liposomes, either drug-loaded or empty, under conditions that result in insertion of the conjugated PEG-lipids into the outer leaflet of the liposome membrane (Fig. 1.7). For efficient insertion, liposomes and antibody-conjugated PEG-lipid micelles are incubated together at a temperature that is near the  $T_C$  of the lipids in the liposomal membrane, but that does not result in denaturation of the antibody protein.

Production of immunoliposomes containing different drugs is relatively simple using the post-insertion method, relative to conventional coupling, since a large batch of antibody can be coupled to PEG-lipid micelles and subsequently post-inserted into liposomes containing the drug of choice. In addition, for antibody constructs with low storage stability (e.g., scFv), coupling to PEG-lipid micelles may increase stability of the

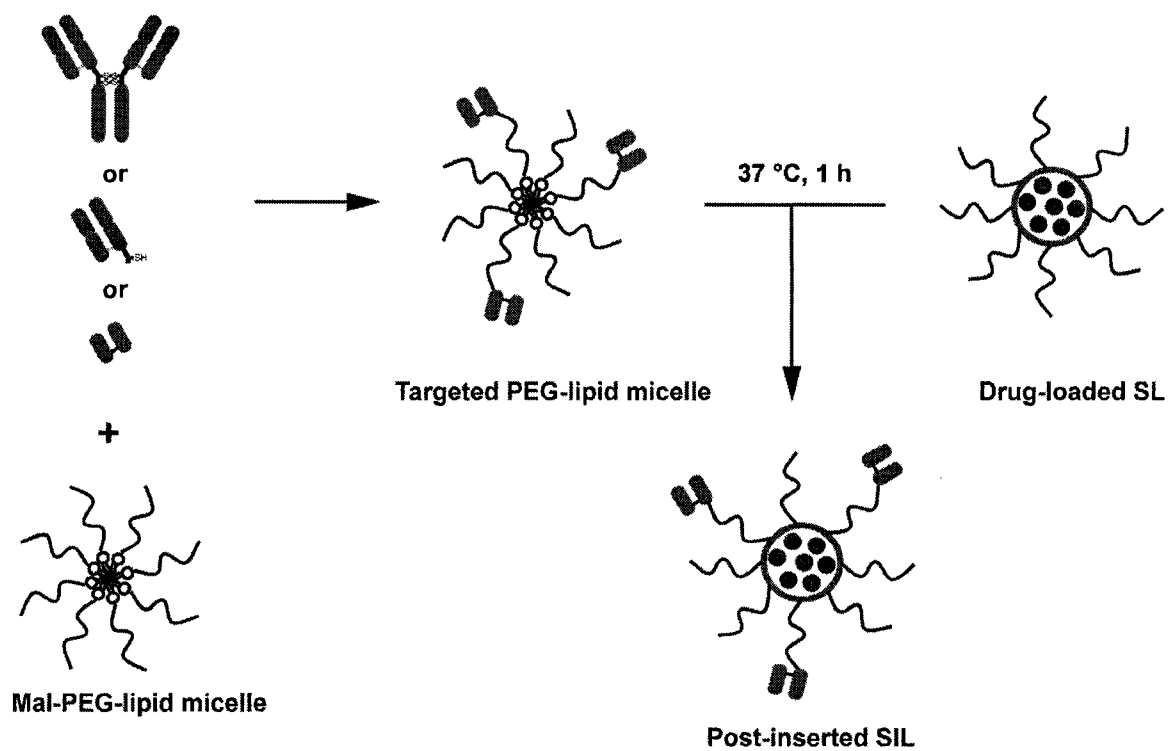


**Figure 1.7. Schematic representation of the post-insertion method.** Adapted from (T.M. Allen).

antibody constructs, and maintain their activity during storage, as will be shown in this thesis (Chapter 5). Immunoliposomes prepared by the post-insertion method have been shown to have cell binding, rate of drug release, and PK/BD similar to immunoliposomes prepared by conventional coupling (99, 100). Immunoliposomes in Chapter 3 were prepared by both conventional coupling and post-insertion.

### **1.7. Choice of Target**

For specific delivery of anticancer drugs to target cells, immunoliposomes and ligand-targeted therapeutics such as liposomes and antibody-drug conjugates, are targeted to surface antigens that are uniquely expressed or over-expressed on target cells. Ideally, expression of the antigen should be homogeneous allowing all malignant cells to be targeted. Unfortunately, cancer cells are heterogenic in nature and cells that do not express the target antigen may escape toxicity, resulting in disease relapse after initial treatment or the selection of drug-resistant cells. Some of the tumor cells that do not express the target antigen may be killed by the “by-stander effect”, where drugs released from antigen-expressing cells after death may enter neighboring cells by passive diffusion. To address this possibility, immunoliposomes and other immunoconjugates have been directed against multiple cancer cell antigens to increase the probability of binding to different populations of antigen-expressing cells (63). Also, for optimal targeting, the target antigen should not be shed from cells. Antigen shedding may result in decreased efficacy, since the number of antigens present on cells may be reduced and the shed antigens in blood may bind to and interfere with the binding of immunoliposomes to target cells.

A growing number of surface antigens are now being studied for targeted delivery of immunoliposomal anticancer drugs. These include the B-cell antigens CD19 (61) and CD20 (63); an epitope of the major histocompatibility complex class II antigen variant chain CD74 on B-lymphoid cells (101); the disialoganglioside GD<sub>2</sub> on neuroblastoma cells (92), EGFR (91) and HER2/*neu* (65).

### **1.7.1. Targeting to Tumor Antigens or Antigens Against Tumor-associated Cells**

Recent advances in the understanding of tumor biology and the relationship between tumor cells and tumor-associated cells such as tumor vasculature endothelial cells and tumor-associated macrophages, have led to various studies examining the delivery of targeted liposomal drugs to tumor-associated cells as well as to tumor cells themselves. In a neuroblastoma model, Pastorino et al. demonstrated that liposomal DXR targeted via a peptide containing the NGR sequence, to CD13 on endothelial cells of angiogenic tumor vasculature, resulted in reduced angiogenesis and increase survival in mice over untargeted liposomal DXR (55). A subsequent study showed that an even better therapeutic response can be achieved by a combination treatment of liposomal DXR targeted to a tumor-specific antigen, GD<sub>2</sub>, and an antigen specific for tumor vasculature-specific antigen, CD13, compared to liposomal DXR targeted to either antigen alone (102). Recent studies have also highlighted the potential benefits of targeting tumor-associated macrophages, where selective depletion of macrophages is associated with smaller tumors in mice compared to mice with an intact pool of macrophages (103).

### 1.7.2. Internalizing vs. Non-internalizing Antigens

Immunoliposomes may be targeted against non-internalizing antigens or against internalizing antigens where binding to the antigen mediates endocytosis of the antigen-antibody complex. Although targeting of liposomal drugs will, in general, result in increased therapeutic activity over untargeted liposomal drugs, there is now evidence to suggest that targeted delivery of immunoliposomal anticancer drugs via internalizing antigens can increase therapeutic activity, since substantially more anticancer drugs may be delivered to sites of action within the target cell following their release from endosomes and lysosomes. Sapra et al. showed, in a model of B-cell lymphoma, that for cell cycle non-specific drugs such as DXR, targeted delivery of liposomal drugs via an internalizing antigen, CD19, resulted in increased cytotoxicity and therapeutic effects over targeted delivery via the non-internalizing (or slowly internalizing) antigen, CD20 (104). In addition, it has been shown in various breast cancer models, that increased therapeutic effects were observed with liposomal DXR targeted to HER2/*neu* over untargeted liposomal DXR; this was attributed to be a result of increased internalization of the targeted liposomal drugs into tumor cells (65, 90, 105).

Upon binding to their respective antigen, the immunoliposomes are internalized into the lysosomal apparatus, consisting of endosomes and lysosomes. These are acidic compartments, rich in enzymes, where breakdown of the liposomes and release of the encapsulated drug occurs. Drugs such as DXR and VCR are stable in this environment, but acid- or enzyme-labile drugs such as cytarabine (Ara-C) may be inactivated and any potential therapeutic effects nullified.

Antigen-mediated endocytosis is influenced by several factors, including the antigen density on target cells, the nature of the epitope against which an antibody is targeted, and the rate of internalization and recycling or re-expression of antigen on the cell surface (106). The internalization of antigens may be induced by crosslinking of certain cell surface antigens. In these situations, an increase in antigen density results in a decrease in the distances between neighboring antigens and an increase in the probability of antigens crosslinking, which may lead to an increase in internalization. The relationship between endocytosis of immunoliposomes and antigen densities was demonstrated by several groups, using immunoliposome targeted to various antigens. Internalization of immunoliposomal DXR was associated with an increased therapeutic effect, which required a minimum antigen density of in the range of  $10^5$  sites per cell for *in vivo* activity (64, 107). Some studies have suggested that antigen-mediated internalization may be epitope dependent. Neve et al. demonstrated that binding of a monovalent anti-HER2/*neu* scFv (F5) was able to result in higher cellular uptake than several other anti-HER2/*neu* antibody constructs, including the anti-HER2/*neu* whole mAb, trastuzumab (108).

In another series of experiments, immunoliposomal DXR targeted to HER2/*neu* via the N-12A5 mAb did not result in increased efficacy over untargeted liposomal DXR, suggesting the immunoliposomes were not internalized, while immunoliposomes targeted to a different epitope on HER2/*neu* via another mAb resulted in internalization of the immunoliposomes and enhanced efficacy (106, 109, 110). Some antigens may require binding of bivalent antibodies for internalization, which may be a result of cross-linking of the antigens (111, 112).

Coupling of monovalent antibody constructs such as Fab' and scFv to liposomes will restore multivalent presentation of the constructs on the surface of liposomes and allow for multiple binding to antigens on the cell surface. The rate of recycling of internalized antigens to the cell surface can affect subsequent binding of immunoconjugates to their antigens after the initial round of binding. Paulos et al. investigated the rate of recycling of the folate receptor, and its effect on the uptake of folate-drug conjugates in various tumor and normal cells (113). These studies demonstrated a large variability in the time course of receptor recycling in different cells, ranging from 5.7–20 h, and observed a decrease in uptake of folate-drug conjugates when cells were not allowed sufficient time for receptor recycling.

#### **1.8. Choice of Targeting Ligand**

As discussed above, liposomal anticancer drugs may be targeted via small ligands such as folate, peptides containing the NGR or RGD sequence, antibodies or fragments of antibodies. Antibodies and antibody fragments are the most studied for targeting liposomal drugs since they have the advantage of being highly specific for their target antigens. In addition, synergistic activity may be observed when signaling antibodies are combined with combinations of anticancer drugs (114-116). However, the production of antibodies and fragments, which require expression and purification from biological systems, is much more cost intensive than production of small ligands and peptides, which can be chemically synthesized.

### 1.8.1. Monoclonal Antibodies and Fragments of Antibodies

Whole mAb is a bivalent molecule with two antigen-binding domains per mAb (Fig. 1.3). The variable regions in the heavy ( $V_H$ ) and light chains ( $V_L$ ) contain the complementarity-determining regions (CDR), which recognize and bind to a specific epitope on antigens. The Fc region can bind to Fc-receptors on macrophages and other cells, resulting in uptake of the mAb, which is the primary mode of clearance of mAb from circulation. Fc binding can also activate secondary signals in other cells, e.g., activation of mast cells, resulting in degranulation. The main mechanism of action for some mAb (e.g., rituximab) in the treatment for cancer, is thought to be binding of the mAb to the antigen and initiation of the killing of the target cells through activation of effector cells such as killer T-cells and natural killer (NK) cells, via Fc-related antibody-dependent cellular cytotoxicity (ADCC) or complement-dependent cytotoxicity (CDC).

Recent studies have shown that some mAb (e.g., the anti-HER2 mAb, trastuzumab) can inhibit cell signaling pathways that are essential for tumor growth, in addition to initiation of ADCC (117, 118). Early studies using murine mAb in humans found that murine mAb were immunogenic and resulted in the formation of human anti-mouse antibodies (HAMA) and rapid removal of the mAb from circulation (119-121). In addition, it was found that the murine Fc domains were not as effective at activation of ADCC or CDC in humans as are human Fc domains (122).

Despite their immunogenic nature and lower therapeutic potential, some murine mAbs such as muromonab (Orthoclone OKT3<sup>®</sup>) and ibritomomab (Zevalin<sup>®</sup>), have been approved for clinical use (Table 1.3). Chimeric mAb (123), humanized mAb (124) and fully human mAb (125) were developed to decrease immunogenicity (Fig 1.3), increase

**Table 1.3. Partial list of currently marketed monoclonal antibodies.**

<b>Brand (generic) name</b>	<b>Target</b>	<b>Isotype</b>	<b>Indication</b>	<b>Manufacturers</b>
Rituxan <sup>®</sup> (rituximab)	CD20	Chimeric IgG <sub>1</sub>	Relapsed or refractory low grade or follicular NHL	Genentech/Biogen Idec
Herceptin <sup>®</sup> (trastuzumab)	HER2	Humanized IgG <sub>1</sub>	HER2- overexpressing metastatic breast cancer	Genentech
Avastin <sup>®</sup> (bevacizumab)	Vascular endothelial growth factor (VEGF)	Humanized IgG <sub>1</sub>	Metastatic carcinoma of the colon or rectum and late stage NSCLC	Genetech
Zevalin <sup>®</sup> (ibritomomab tiuxetan)	CD20	Murine IgG <sub>1</sub>	Relapsed or refractory low grade or follicular NHL (including Rituxan <sup>®</sup> - refractory NHL)	Biogen Idec
Orthoclone OKT3 <sup>®</sup> (muromonab)	CD3	Murine IgG	Acute allograft rejection	Ortho Biotech
Remicade <sup>®</sup> (infliximab)	TNF- $\alpha$	Chimeric IgG <sub>1</sub>	Psoriasis, rheumatoid arthritis, ankylosing spondylitis, Crohn's disease and ulcerative colitis	Centocor
Xolair <sup>®</sup> (omalizumab)	IgE	Humanized IgG <sub>1</sub>	Moderate to severe persistent asthma	Genentech

circulation time and increase therapeutic potential of mAb for therapeutic use in human. Small antibody fragments such as Fab' and scFv are postulated to be less immunogenic than mAb due to the lack of the Fc domain, against which most HAMA response is directed (120). Fab's are monovalent fragments of a mAb containing the light chain and a portion of the heavy chain (Fig. 1.3). Single chain Fv fragments are small fragments of antibodies containing only the V<sub>H</sub> and V<sub>L</sub> domains linked by a flexible polypeptide linker (Fig. 1.3).

In the older targeting literature, immunoliposomes were targeted principally with murine whole mAb, but increasingly Fab' and now scFv are being used as targeting agents. With the commercial availability of humanized and fully human mAb, which is more clinically acceptable than murine mAb, there is renewed interest in using mAb to target DDS. The use of humanized and fully human Fab' or scFv to target DDS may also be possible in the future. It is therefore important to examine the differences in PK, biodistribution and outcomes for DDS targeted by the various antibody constructs. This thesis examines the PK and therapeutics of murine mAb, Fab' and scFv directed against the same CD19 epitope.

### **1.8.2. Affinity, Avidity and Antibody Density**

Antibody affinity describes the strength of a single interaction of an antibody with its antigen. Avidity is the combined strength of multiple interactions of an intact whole antibody (having two binding sites) or a multivalent antibody construct with its antigen. Affinity describes the binding of Fab' or scFv antibody fragments, both of which have only one antigen-binding site per molecule. However, for whole mAb and for immunoliposomes, including immunoliposomes targeted by Fab' and scFv, there is

multivalent presentation of the antibody and antibody fragments and hence multiple interactions with their respective antigens. In this case, the term avidity is used to describe the combined strength of the interactions with antigens.

For immunoliposomal drugs, the relationship between the avidity of antibodies, the antibody densities on liposomes and the antigen densities on the target cells, and their respective effects on cell binding has not been fully addressed. Examination of immuno-drug conjugates, targeted via different Fab' fragments that bind to the same antigen with different avidities, has shown that increased cytotoxicity is observed in immunoconjugates with higher avidity. This suggests that higher avidity is more favorable for targeted delivery of anticancer drugs (126). However, it has been postulated that antibody-targeted delivery *in vivo* may be impeded by the “binding-site barrier”, where antibodies bind to the first antigens encountered. This can result in accumulation of the most of the antibodies (or immunoliposomes) in the perimeter of the solid tumor rather than penetration into the interior of the tumor (127, 128). Theoretically, the effect of the binding-site barrier would be more pronounced for antibodies with high avidities than for those with low avidities. However, Kirpotin et al. found that the distribution of anti-HER2/*neu* immunoliposomes within breast tumors, targeted by antibodies with high avidity for HER2/*neu*, was similar to untargeted liposomes, and they did not observe any binding-site barrier for their immunoliposomes (105). For blood-borne malignancies or cancer cells that are easily accessible from the vasculature, including micro-metastases or tumor-associated endothelial cells, treatment with immunoliposomes targeted via antibodies with high avidity may result in more

favorable therapeutic response, since immunoliposomes targeted via high avidity antibodies can tightly bind to the antigen at the first encounter.

Various techniques are available for affinity or avidity selection of mAb and antibody fragments. Antibody-producing B cells from immunized mice can be isolated and selected, based on avidity, for producing mAb against an antigen (129). For recombinant Fab' and scFv fragments, affinity selection may be performed by phage-display or ribosome-display (130, 131). In addition to manipulation of the avidity of antibody constructs, increased binding of immunoliposomes may be achieved through increasing the density of antibodies on the surface of liposomes. For antibody fragments, higher surface density may be more desirable since it leads to greater avidity, resulting in increase probability of contact and binding of the immunoliposomes to the targeted antigen. It has also been shown that endocytosis and total cell binding, *in vitro*, can increase as a function of the density of Fab' and scFv fragments on the surface of liposomes (90, 132). However, for whole mAb-targeted immunoliposomes, increases in surface mAb density may result in decreased therapeutic effect due to increased Fc receptor-mediated clearance of the immunoliposomes *in vivo*.

The avidity of a molecule increases with increases in the number of binding domains available on that molecule. Therefore, higher avidity is expected when a bivalent mAb is compared with its monovalent antibody fragments, i.e., Fab' or scFv. Several studies have shown that increases in avidity can be achieved through multimerization of monovalent antibody fragments such as scFv (133, 134). The multivalent presentation of antibody fragments (Fig. 1.2D and E) on the surface of liposomes can also restore the multivalency of these monovalent antibody fragments.

Sapra et al. demonstrated that, at similar densities of antigen-binding domains on the surface of immunoliposomes, the binding of immunoliposomes targeted via an anti-CD19 Fab' to CD19<sup>+</sup> cells, is similar to immunoliposomes targeted via the parental mAb (62). The multimeric presentation of antibodies on the surface of liposomes is also expected to enhance the therapeutic benefits of anti-tumor antibodies. Chiu et al. demonstrated that the multimeric presentation of antibodies, such as rituximab and trastuzumab, on the surface of liposomes resulted in increased activity *in vitro* over the free antibodies and downregulation of key modulators of pro-survival signals (135).

It has been shown that increased antigen densities on target cells are associated with greater binding of immunoliposomes and greater response to targeted therapy (64, 107). However, in a clinical setting, it may be difficult to manipulate the levels of expression of a particular tumor antigen in patients in order to increase the response to targeted therapy. However, the apparent antigen density and antigen-binding capacity can be increased by targeting liposomal drugs against multiple antigens. Laginha and Allen showed that immunoliposomal DXR conjugated with both anti-CD19 and anti-CD20 mAb exhibited increased total cell binding and cytotoxicity compared to immunoliposomes conjugated with either anti-CD19 mAb or anti-CD20 mAb alone, at similar antibody densities (136).

### **1.8.3. Pharmacokinetics of Immunoliposomes**

In general, murine mAb-targeted immunoliposomes exhibit rapid, biphasic clearance from circulation in mice, due to recognition of the Fc region by macrophages in the liver and spleen. It has been found that the rate of clearance is also dependent on the

density of mAb on the surface of liposomes, as injection of immunoliposomes with mAb densities above  $\sim 60\text{--}75 \mu\text{g}/\mu\text{mol PL}$  resulted in their rapid clearance (88, 109).

As discussed above, rapid clearance of mAb can be reduced by using coupling methods such as the hydrazide method, which reduce the exposure of the Fc domain of mAb on the surface of liposomes. However, the hydrazide method is relatively inefficient and results in a covalent bond that has increased lability relative to the maleimide method. Hence, it is not the preferred method, unless acid lability is desired.

It has been shown in various animal models, in which immunoliposomes targeted via Fab' vs. mAb were compared, that SIL targeted via Fab' fragments have considerably improved PK over mAb-targeted SIL; blood levels of Fab'-targeted immunoliposomes were similar to untargeted SL (62, 92, 137). Similarly, liposomes targeted via scFv fragments are expected to have PK similar to Fab'-targeted immunoliposomes and untargeted SL due to the lack Fc domain and less foreign peptide sequences. Few studies have examined the PK properties of scFv-targeted immunoliposomes (138), and to date comparisons of PK/BD and therapeutic effects of scFv-targeted immunoliposomes in relation to the parental mAb and Fab' have not been reported. Such comparisons are made in this thesis.

#### **1.8.4. Methods of Producing Whole Antibodies and Fragments of Antibodies**

As mentioned above, the most common antibody constructs used for targeting immunoliposomes are mAb, Fab' and increasingly scFv. Although not currently used to any degree, liposomes could also be targeted via other types of antibody construct, such as bispecific mAb (Fig. 1.3), in which each of the two binding regions on a mAb is

directed against a different antigen. Whole mAb are traditionally produced using mouse hybridoma cells (139), either in animal ascites, or, more recently, from cell culture supernatant. Production of mAb by hybridoma cells in ascitic fluid is one of the most efficient methods of producing whole mAb, but, due to ethical issues, it is seldom used now. In general, production of mAb by hybridoma in culture supernatant is less economical and less efficient than animal ascites since large volumes of growth media are required and production yields are usually lower (140, 141). Other expression systems, such as mammalian cells, transgenic animals and plants have been used, as full length mAb are usually expressed in mammalian systems to ensure proper folding and glycosylation of the mAb (142). The chimeric anti-CD20 mAb, rituximab, and the humanized anti-HER2/*neu* mAb, trastuzumab, are produced in suspension cultures of Chinese hamster ovary cells. It has been demonstrated that mAb can also be produced in the milk of transgenic animals (143-146). However, several disadvantages are associated with production of mAb in transgenic animals, including that the animals usually suffer from low live-birth rates, the milk may carry animal pathogens, and it may take several years to establish a stable herd of animals (142). Recently, it has been shown that recombinant mAb can be produced in tobacco plants (147, 148). Plants are free from human pathogens, but there are significant differences in glycosylation of mAb between plant and mammalian cells, with variations in the types of carbohydrate conjugated to mAb (149).

MAb are commonly purified from hybridoma cells using affinity chromatography, usually Protein A or Protein G columns, which bind to the Fc domain. Fab' may then be generated directly from the purified mAb by enzymatic digestion of the

Fc domain or cleavage of the mAb at the hinge region (150) (Fig. 1.3). Alternatively, recombinant Fab' may be expressed in *E. coli* cultures. Purification of Fab' is commonly done using Protein A or Protein G affinity columns to remove the Fc domains after cleavage of intact mAb, or alternatively using Protein L affinity columns that have affinity for the light chain.

ScFv fragments are commonly expressed in inducible *E. coli* cultures, although expression in yeast cultures and plants has also been described (151, 152). Expressed scFv may be extracted from either the periplasmic space or from inclusion bodies in the cytoplasm of the bacteria. Molecular tags, such as poly-Histidine (poly-His, usually with 5x His or 6x His) (153) and FLAG, an octa-peptide consisting of AspTyrLysAspAspAspLys (154), are usually engineered into the scFv sequence for affinity-based purification and identification of the protein. For proper folding and formation of internal disulfide bonds, scFv are commonly fused to a leader sequence which directs the scFv to the oxidizing environment of the periplasmic space of the bacteria where formation of disulfide bonds can occur (142). Native and folded scFv can then be extracted from the periplasmic space.

ScFv are commonly extracted from the periplasmic space using osmotic shock, which transiently increases the permeability of the outer membrane of the bacteria allowing release of the scFv into the extraction buffer. Induced expression of scFv in *E. coli* often results in excessively high protein concentration in the cytoplasm, a reducing environment that promotes unfolding of scFv, leading to aggregation and formation of inclusion bodies. Since most of the expressed scFv are deposited in inclusion bodies, numerous strategies have been developed to recover scFv from these insoluble aggregates

in order to increase extract yields. These methods generally involve denaturation and dissolution of inclusion bodies, and refolding of the denatured scFv in various buffers (155-157). Other strategies, such as expression of scFv in genetically modified *E. coli* with a more oxidizing cytoplasm in order to improve recovery of native proteins, have also been described (158). In this thesis, extraction of scFv from periplasmic space and inclusion bodies was examined, and the yields were compared for several scFv constructs.

There are several potential advantages of using scFv fragments over whole antibodies or larger fragments for liposome targeting. These include: 1) lower production cost for scFv fragments generated from bacterial culture relative to whole antibodies generated from animal ascites or cell culture; 2) the ability to select scFv with the desired affinity and specificity using phage display; 3) the option of engineering tags into scFv constructs, which can aid in their identification and purification; 4) ability to engineer fully human fragments or fragments with low levels of non-human content, which will reduce the risk of immunogenic reactions. Based on these potential advantages, one of the objectives of this thesis is to explore the production and use of scFv fragments as targeting agents for immunoliposomal delivery of anticancer drugs.

### **1.9. Model System**

Lymphomas are traditionally classified into Hodgkin's and Non-Hodgkin's lymphomas (NHL). Various systems of classification have been proposed, including, the Kiel Classification System (159), the International Working Formulation (160), the Revised European-American Lymphoma (REAL) classification system (161) and the

REAL-based WHO classification system (162), the latter being the most recent and encompassing.

Non-Hodgkin's lymphoma (NHL), the most common form of B lymphoid disease, is the 5<sup>th</sup> most common cause of new cases of cancer in North America, accounting for approximately 4 to 5 percent of new cases of cancer each year (1, 163). Non-Hodgkin's lymphoma is a heterogeneous group of cancers with 85-90% of lymphomas bearing a B-cell phenotype and 10-15% bearing a T-cell phenotype (164, 165). Diffuse large B-cell lymphoma (DLBCL) is the most prevalent form of NHL (166). The exact cause of NHL is unclear; however, several well-established risk factors have been found and these include: infections such as HIV (167) and Epstein-Barr virus (168), immunosuppression secondary to organ transplantation (169), genetic predisposition (170), and environmental factors related, for example, to occupation (171).

B-lymphoid malignancies are primarily monoclonal, with a high percentage of cells (> 90%) expressing antigens such as CD19, CD20 and CD22 on their cell surface. These antigens are found primarily on mature B-cells and can be utilized as targets to direct therapeutics specifically against malignant B cells, which arise later in the differentiation process. Targeting cells expressing these antigens spares the stem cells that give rise to mature B cells. Since stem cells do not express CD19, 20 and 22, stem cells, therefore, should escape the cytotoxicity mediated by therapies against these antigens, allowing repopulation of normal B cells in the blood after eradication of the malignant cells.

For NHL, the responses to chemotherapy are generally heterogeneous, depending on the subtype of the lymphoma. For indolent lymphomas such as follicular lymphoma

(FL), standard chemotherapy is currently CHOP plus rituximab, a combination of cyclophosphamide, doxorubicin, vincristine, prednisone, and the anti-CD20 mAb, rituximab. Rates of complete response (CR) to CHOP are generally in the order 10–20%, while for some aggressive lymphomas such as DLBCL, rates of CR are generally greater than 60% (165). The rates of CR are further increased to 55-87% with the addition rituximab to CHOP (6-8, 172). Unfortunately, for some lymphomas such as mantle cell lymphoma (MCL), the response to chemotherapy, including CHOP plus rituximab, is limited and they are considered incurable with current therapies (173). In addition, a substantial percentage of patients with NHL who responded to initial therapy will develop recurrent disease, which results from the incomplete eradication of residual cells. Therefore, there is a clinical need for better therapeutics for some aggressive and incurable forms of NHL, as well as relapsed or recurrent diseases. This thesis examined the therapeutic potential of immunoliposomal DXR targeted to CD19 as a treatment for the eradication of residual cells or early metastatic disease.

### **1.9.1. B-cell Antigen: CD19**

In this thesis, CD19 was chosen as the target antigen for studying the delivery of liposomal DXR via various antibody constructs. CD19 is a 95 kDa surface glycoprotein with two extracellular immunoglobulin-like domains and a 240 amino acid long cytoplasmic tail which contains domains similar to proteins found in the Epstein-Barr virus (174, 175). The CD19 molecule is exclusively expressed on B cells from early pre-B-cells to mature B-cells, including malignant cells arising within the B-cell lineage (176). In some aggressive forms of lymphoma, such as MCL and multiple myeloma, the

expression of CD19 is lost. Bone marrow stem cells and B-cell progenitors do not express CD19 (176, 177).

Current evidence suggests that CD19 is important in the selection, activation, proliferation and differentiation of B cells. The functions of CD19 are mediated by multiple signalling pathways, which include phospholipase C as one of the mediators of the CD19 signal (178). Cross-linking of CD19 on B cells induces a sustained increase in intracellular  $Ca^{2+}$  (179, 180) and internalization of CD19 (177, 181). CD19 has also been shown to amplify signalling pathways mediated by the Src family of protein tyrosine kinases (PTK), which are involved in the growth and differentiation of cells (182). It is postulated that CD19 is crucial to activation of B cells, since *in vitro* binding of mAb to CD19 inhibits mitogen-induced activation and proliferation (179).

CD19 is suggested to be associated with at least 4 other cell surface molecules, including CD21 (183), CD81 and Leu 13 (184, 185), and induction of proliferation by CD19 is dependent on co-ligation with other surface molecules. Co-ligation of CD19 with other molecules such as CD21 lowers the threshold for B-cell activation and increases the magnitude of the response to stimulation (186). Abnormal activation, proliferation and differentiation of B cells have been observed in knockout mice lacking CD19 (187). In CD19-deficient mice, affinity maturation of antibody-secreting B-cells was impaired by the lack of CD19, and these CD19<sup>-</sup> B cells exhibit poor primary responses to antigens and reduced efficiency of selection (188).

Due to its unique expression and signalling properties, CD19 has been studied as a potential target for cancer therapy. Anti-cancer therapy directed against CD19 would theoretically result in specific killing of CD19-expressing B cells, and since CD19<sup>-</sup> bone

marrow stem cells would be unaffected, the normal B-cell pool can be repopulated. Single agent treatment using an anti-CD19 mAb in animal models demonstrated the potential benefits of anti-CD19 therapy (189). Due to the signalling properties of CD19, synergistic effects of anti-CD19 mAb therapy with conventional anti-cancer therapy can be achieved (190, 191). Other studies, which used CD19 as a target, e.g., immunoconjugates or immunoliposomal anticancer drugs, have demonstrated specific killing of CD19-expressing cells and anti-tumor effects in animal models, highlighting the potential benefits of anticancer therapy delivery via CD19 (14, 61, 104).

### 1.9.2. Doxorubicin

Doxorubicin (MW = 543.53 g/mol), marketed as Adriamycin<sup>®</sup>, is an anthracycline antibiotic isolated from *Streptomyces peucetius* (Fig. 1.8). It is a widely-used anticancer drug and has shown activity against various types of cancers including breast, ovarian and hematological malignancies (31). Doxorubicin is a cell cycle independent drug and is commonly used with other anticancer drugs in combinations such as CHOP (cyclophosphamide, doxorubicin, vincristine and prednisone), or ABVD (doxorubicin, bleomycin, vinblastine and dacarbazine). Doxorubicin has multiple mechanisms of action including intercalation into the DNA helix thereby inhibiting transcription and protein synthesis, inhibition of topoisomerase II resulting in inhibition of DNA repair after double-strand breakage, and generation of free radicals resulting in oxidative stress and apoptosis (31, 192).

Doxorubicin is a hydrophobic weak base (pKa = 8.3–8.5). The free drug has a high volume of distribution (Vd = 365 L) when injected into human. Plasma levels of DXR exhibit a triexponential elimination profile, with  $t_{1/2\alpha}$  of 10 min,  $t_{1/2\beta}$  of 1-3 h and

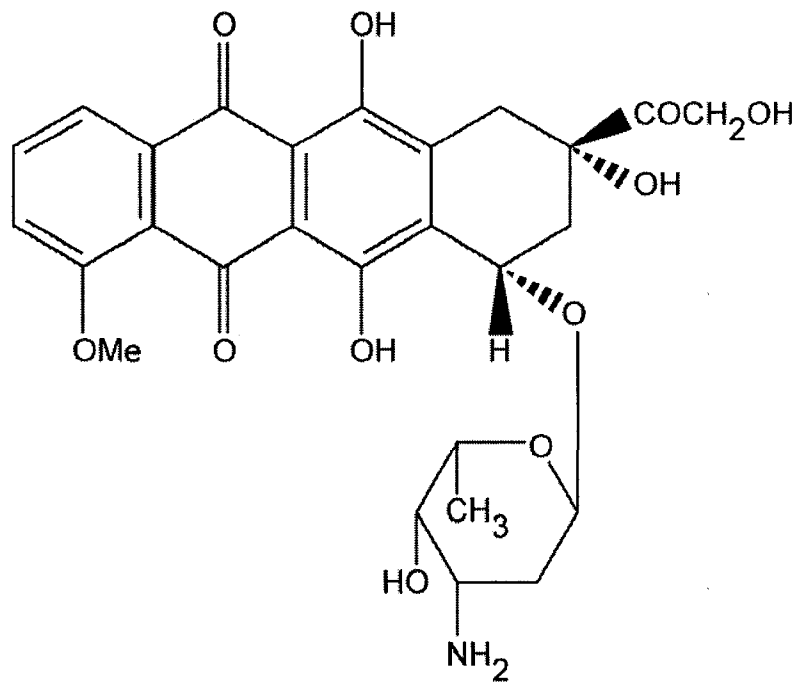


**Figure 1.8. Structure of doxorubicin.**

$t_{1/2\gamma}$  of 30–50 h (31). The clearance of DXR from blood is greater than 45 L/h. The primary metabolite of doxorubicin, doxorubicinol, which is an active metabolite, is produced via carbonyl reduction by aldo-keto reductases. Due to its high  $V_d$  and slow redistribution, DXR distributes into deep tissues and remains in the tissue for long periods of time, resulting in numerous adverse effects, including myelosuppression, alopecia, mucositis, nausea and vomiting. Cardiotoxicity, usually in the form of congestive heart failure, is a major dose-limiting toxicity that is uniquely associated with peak concentrations of doxorubicin and anthracyclines in the heart following bolus administration (31). The life-time cumulative dose for DXR is recommended not to exceed 500 mg/m<sup>2</sup>.

Encapsulation of DXR into long circulating Stealth<sup>®</sup> liposomes (Doxil<sup>®</sup>/Caelyx<sup>®</sup>) alters the PK/BD of the free drug (Table 1.2) with decreased  $V_d$ , decreased distribution to normal tissue and increased localization in tumors. This combination results in an increase in the therapeutic index of the drug and significantly reduces cardiac toxicities, despite doses in excess of the recommended cumulative dose of free DXR of 500 mg/m<sup>2</sup> (51, 193). Liposome encapsulation of DXR shifts the adverse effects of the drug towards those seen for free drug infusions (34). Administration of Doxil<sup>®</sup> at a dose intensity of greater than 10-12 mg/m<sup>2</sup>/week is associated with a skin toxicity (194), termed palmar-plantar erythrodysesthesia (PPE), which is thought to be a result of the accumulation of the long-circulating formulation in capillaries of the skin of hands, feet and pressure points.

### 1.10. Hypothesis

It is hypothesized that a suitable scFv construct can be readily produced in sufficient quantities, and of suitable purity and stability, for its use as a targeting moiety for targeted liposomal delivery of anticancer drugs to B-cell malignancies. It is further hypothesized that scFv fragments will have overall better suitability for clinical development than whole monoclonal antibodies or Fab' fragments.

### 1.11. Objectives

The research project will encompass the following objectives:

- 1) Optimization of the production, purification and characterization of different anti-CD19 scFv constructs, and determination of the most suitable scFv fragment for experiments, taking into account factors such as ease of production, yield, stability, target epitope, and affinity.
- 2) Screening of B cell lines for expression of B antigens (e.g., CD19, CD20, and CD22) and choosing an appropriate cell line for future experiments.
- 3) Optimization of coupling procedures for attachment of scFv fragments to liposomes.
- 4) Determination of the *in vitro* cytotoxicity of scFv-targeted liposomal drugs in relation to the liposomal drugs targeted via mAb and Fab'.
- 5) Determination of the PK/BD and therapeutic outcome of scFv-targeted liposomal drugs, in comparison with liposomal drugs targeted via mAb and Fab', in animal xenograft models of B-cell malignancies.

**Chapter 2**  
**Materials and Methods**

## 2. Materials and Methods

### 2.1. Materials

Hydrogenated soy phosphatidylcholine (HSPC) and methoxypoly(ethylene glycol) (MW 2000), covalently linked to distearoylphosphatidylethanolamine (mPEG<sub>2000</sub>-DSPE), were generous gifts from ALZA Corporation, Inc. (Mountain View, CA). Cholesterol (Chol), maleimide-derivatized PEG<sub>2000</sub>-DSPE (Mal-PEG<sub>2000</sub>-DSPE) and 1-oleoyl-2-[6-[(7-nitro-2-1,3-benzoxadiazol-4-yl)amino]hexanoyl]-sn-glycero-3-phosphoethanolamine (NBD-PE) were purchased from Avanti Polar Lipids (Alabaster, AL). Maleimide-derivatized PEG<sub>3400</sub>-DSPE (Mal-PEG<sub>3400</sub>-DSPE) was custom synthesized by Nektar Therapeutics (Huntsville, AL). Bio-Rad Protein Assay Reagent was purchased from Bio-Rad Laboratories (Mississauga, ON).  $\beta$ -mercaptoethanol ( $\beta$ -ME), 2-iminothiolane (Traut's Reagent), L-arginine (L-Arg), 5,5'-Dithiobis(2-nitrobenzoic acid) (DTNB, Ellman's reagent), Protein L Agarose columns, goat anti-mouse fluorescein isothiocyanate (GAM-FITC) conjugate, goat anti-human FITC conjugate (GAH-FITC), ANTI-FLAG<sup>®</sup> M2 mAb-FITC, 3-(4,5-Dimethylthiazol-2-yl)-2,5-diphenyltetrazolium bromide (MTT) and RPMI 1640 media were obtained from Sigma Chemical Co. (St. Louis, MO). 1,4-dithiothreitol (DTT) was purchased from Fisher Scientific (Nepean, ON). Nuclepore<sup>®</sup> polycarbonate membranes (pore sizes, 0.4, 0.2, 0.1, and 0.08  $\mu$ m) were purchased from Northern Lipids (Vancouver, BC) or Fisher Scientific (0.4  $\mu$ m). Chol-[1,2-<sup>3</sup>H-(N)]hexadecyl ether (<sup>3</sup>H-CHE, 1.48-2.22 TBq/mmol), <sup>14</sup>C-doxorubicin (<sup>14</sup>C-DXR), Sephadex G-50, Sephadex G-25, Sepharose CL-4B and Aqueous Counting Scintillant (ACS) were purchased from GE Healthcare (Baie d'Urfe,

PQ).  $^{125}\text{I}$ -Sodium iodide ( $^{125}\text{I}$ -NaI, 185 MBq), Solvable™ and Ultima Gold™ and ACS were purchased from Perkin Elmer Life Sciences (Woodbridge, ON). Nickel-nitrilotriacetic acid (Ni-NTA) column and murine anti-polyhistidine (anti-His) mAb were purchased from Qiagen (Hilden, Germany). Immobilized Pepsin and IODO-Beads® were purchased from Pierce (Rockford, IL). Penicillin-streptomycin-L-glutamine (P/S/G, 10000 U/mL, 10000  $\mu\text{g/mL}$ , 29.2 mg/mL, respectively), and fetal bovine serum were obtained from Invitrogen (Burlington, ON). Bacto Tryptone, Bacto Yeast Extract and Bacto Agar were from BD (Sparks, MD). Isopropyl  $\beta$ -D-1-thiogalactopyranoside (IPTG) was purchased from Rose Scientific (Edmonton, AB). All other chemicals were of the highest grade available.

## 2.2. Cell lines

The CD19<sup>+</sup> human Burkitt's lymphoma cell lines (Daudi, Ramos, Namalwa and Raji) and the CD19<sup>-</sup> human T-lymphoma cell line (Molt4) were purchased from the American Type Culture Collection. The cells were cultured in suspension in RPMI 1640 media supplemented with 10% (V/V) fetal bovine serum, and 1% (V/V) P/S/G in a humidified 37 °C incubator with a 5% CO<sub>2</sub> atmosphere.

## 2.3. Antibodies

The murine anti-CD19 mAb, FMC63 mAb (IgG<sub>2a</sub>) and HD37 mAb (IgG<sub>1</sub>), were produced from the FMC63 (195) and HD37 hybridomas (179), obtained from Dr. H. Zola (Children's Health Research Institute, Adelaide, Australia) and Dr. B. Doerken (Charité, University Medicine, Berlin, Germany) via Dr. E. Vitetta (University of Texas Southwestern Medical Center, Dallas, TX), respectively. The murine anti-CD22 mAb,

RF-B4-B3 (IgG<sub>1</sub>), was a generous gift from Dr. E. Vitetta. The chimeric anti-CD20, rituximab (Rituxan<sup>®</sup>), was purchased from the University of Alberta Hospital pharmacy.

Various anti-CD19 scFv were used in this study. The plasmid for expressing HD37-c-myc-Cys-His5 scFv (HD37-CCH) was provided courtesy of Dr. S. Kipriyanov, Affimed Therapeutics AG, Heidelberg, Germany (196). The plasmid for HD37-c-myc-His6-Cys (HD37-CHC) was provided courtesy of Dr. S. Kipriyanov and Inex Pharmaceuticals (Burnaby, BC). The plasmid for HD37-Cys (HD37-C) was prepared by removing the tags from a HD37-c-myc-His6-Cys (HD37-CHC) construct as described (197). The n-strep-His5-4G7-Gly4-Cys scFv (nH-4G7-GC) was provided courtesy of Dr. G. H. Fey (University of Erlangen-Nuremberg, Erlangen, Germany) in a denatured form which needed to be refolded. The RGF 4G7 scFv (RGF 4G7), which contains a N-terminus FLAG tag and a Cys at the C-terminus, was expressed in and purified from algae under the direction of Dr. S.E. Franklin (San Diego, CA). The plasmid for the FMC63-c-myc-His6-Cys (FMC63-CHC) was provided courtesy of Dr. H. Zola (Children's Health Research Institute, Adelaide, Australia). The tagless FMC63-Cys (FMC63-C) construct was prepared as described (197). For scFv constructs, c-myc, poly-His and FLAG tags were used for purification and/or identification. The Cys residue was used for coupling to liposomes via thio-ether bonds with maleimide of Mal-PEG-DSPE.

#### **2.4. Animals**

Six to eight weeks old female BALB/c CR Alt BM (BALB/c) mice were purchased from Health Sciences Laboratory Animal Services (HSLAS, University of Alberta, Edmonton, AB) and were kept in standard housing. Female 6 to 8 weeks old

ICR severe compromised immunodeficient (SCID) mice were purchased from Taconic Farms (Germantown, NY) and were kept in the virus antigen-free rooms of HSLAS. All animal studies were conducted in accordance with the Canadian Council on Animal Care Guidelines and Policies with approval from the Health Sciences Animal Policy and Welfare Committee for the University of Alberta.

## **2.5. Expression and Extraction of ScFv from the Periplasmic Space of *E. coli* and Inclusion Bodies**

For HD37-CHC, HD37-CCH, HD37-C, FMC63-CHC, and FMC63-C, recombinant plasmids carrying the scFv genes were used to transform *E. coli* RV308 by the heat shock method (198) and expressed in shaker cultures. Cultures were grown at 26 °C and expression of the scFvs was induced with 0.2 mM of IPTG at 22 °C when the optical density at 600 nm (OD<sub>600</sub>) reached 0.8. Cells were harvested by centrifugation after 16 h of induction.

For extraction of scFv from the periplasmic space of *E. coli*, cells were incubated with the periplasmic extraction buffer (100 mM Tris HCl, 20% W/V sucrose, 1 mM EDTA, pH 8.0) for 1 h on ice. Cells were then centrifuged and the extracted scFv fragments were collected in the supernatant as periplasmic extract. Purification scFv containing poly-His was performed via affinity chromatography using Ni-NTA columns. After extraction, the periplasmic extract, containing scFv, was extensively dialyzed in Ni-NTA Dialysis Buffer (1 M NaCl, 50 mM Tris HCl and 40 mM imidazole, pH 7.0). The dialyzed extract was then incubated overnight at 4 °C with Ni-NTA at a 50:1 (V:V) ratio, with gentle rocking. After the incubation, the Ni-NTA was packed into a column and washed with washing buffers (1 M NaCl, 50 mM Tris HCl, and 50 or 80 mM imidazole,

pH 7.0). The scFv was then eluted with elution buffer (1 M NaCl, 50 mM Tris HCl and 300 mM imidazole, pH 7.0). Elution fractions were analyzed on SDS-PAGE gels and scFv-containing fractions were extensively dialyzed in phosphate-buffered saline (PBS, (8 g/L NaCl, 0.2 g/L KCl, 1.15 g/L Na<sub>2</sub>HPO<sub>4</sub>, 0.2 g/L KH<sub>2</sub>PO<sub>4</sub>, pH 7.4) with or without 50–250 mM imidazole. The tagless HD37-C and FMC63-C scFv constructs were purified from the periplasmic extract using a Protein L agarose column as previously described (199). Briefly, the periplasmic extract was extensively dialyzed in PBS at pH 7.4 before loading onto the column at 20 mL/h, using a peristaltic pump. The column was washed with PBS (pH 7.4) to remove non-specifically bound proteins. The scFv was eluted with elution buffer (100 mM glycine, pH 2.0) and immediately neutralized with addition of 1 M Tris at pH 9.0 to achieve a final pH of 7.4.

The FMC63-CHC, HD37-C and FMC63-C scFv constructs were also isolated from cytoplasmic inclusion bodies (insoluble protein aggregates) and were purified as previously described with slight modification (199). Cell pellets harvested after induction of expression were resuspended in Lysis Buffer 1 (50 mM Tris, 200 mM NaCl, 1 mM EDTA, pH 8.0) and lysed by either French Press or sonication. The cells were then centrifuged at 10,000 g at 4 °C and the inclusion bodies were collected as pellets. The inclusion bodies were resuspended and incubated in 0.1% Triton X-100 for 0.5 h at room temperature and were then centrifuged at 10,000 g at 4 °C. The inclusion bodies were washed with Lysis Buffer 1 and resuspended in Lysis Buffer 2 (100 mM Tris, 200 mM NaCl, 1 mM EDTA, pH 8.3). A previously described step-wise dialysis method, with modification, was used for refolding the denatured HD37-C (200). Inclusion bodies were solublized in Lysis Buffer 2 containing 6 M guanidine hydrochloride (Gu HCl) and

were centrifuged at 10,000 g at 4 °C. Soluble protein was collected in the supernatant and before dialysis the protein concentration was adjusted to 100 µg/mL. Dialysis was conducted with sequential daily decreases of Gu HCl (6, 3, 2, 1, 0.5, 0 M). At the 1 M and 0.5 M Gu HCl stages, 400 mM of L-arginine and 375 µM of oxidized glutathione (GSSG) were added to assist the proper formation of disulfide bonds. The nH-4G7-GC scFv, which was also extracted from inclusion bodies, was received in the denatured form and was refolded using the above procedure.

## **2.6. Western Blot Analysis**

Purified proteins were separated on SDS-PAGE using a 10% Tris SDS-PAGE gel and transferred to a Hybond ECL nitrocellulose membrane (201) using a Trans-Blot apparatus (Bio-Rad, Mississauga, ON) following the manufacturer's instructions. The ECL membrane was blocked with 5% skim milk in 0.1% Tween 20 in phosphate buffer saline, pH 7.3 (PBST) for 1 h. The membrane was washed with PBST and incubated with murine anti-His mAb or murine anti-c-myc mAb for 1 h. After incubation, the membrane was washed with PBST and incubated with goat anti-mouse HRP (GAM-HRP, Upstate, Lake Placid, NY). Finally, the membrane was washed 4 times with PBST and enhanced chemiluminescent-based detection was done according to the manufacturer's protocol (ECL Western blot analysis system, Amersham Biosciences, PQ).

## **2.7. Preparation of Liposomes and Doxorubicin Loading**

Untargeted SL and DXR-loaded SL were composed of HSPC:CHOL:mPEG<sub>2000</sub>-DSPE at a 2:1:0.1 molar ratio to phospholipid. <sup>3</sup>H-CHE was added as a non-exchangeable, non-metabolized lipid tracer (202, 203). Liposomes, extruded to a

diameter of  $110 \pm 20$  nm, were prepared as previously described (83, 204) in HEPES-buffered saline (HBS, 5.96 g/L HEPES, 8.18 g/L NaCl, pH 7.4) at a concentration of 20 - 30 mM phospholipid (PL). When required, DXR was loaded into SL using the ammonium sulfate gradient method as described previously (83).

## 2.8. Preparation of Immunoliposomes

For iodination of mAb, F(ab')<sub>2</sub>, and scFv, a previously described method was used (61). Briefly, 1 mg of antibody construct in 300  $\mu$ L of HBS pH 8.0 was incubated with 185 MBq of <sup>125</sup>I-Na in a vial containing IODO-Beads<sup>®</sup> at 22 °C for 1 h. Unreacted free <sup>125</sup>I-Na was removed by chromatography via a Sephadex G25 column, equilibrated in HBS, pH 8.0. The specific activity of the <sup>125</sup>I-labeled antibody construct was determined from its gamma radioactivity.

In some cases, liposomes for coupling to mAb and antibody fragments contained 0.01 mol % of Mal-PEG-DSPE. In Chapter 3, scFv fragments were coupled to liposomes containing Mal-PEG<sub>2000</sub>-DSPE at a 1:500 molar ratio of scFv to HSPC as previously described (90), with slight modifications. For HD37-CHC, scFv was reduced with either 2.5 or 5 mM  $\beta$ -ME at 22 °C for 1 h. HD37-C was reduced with 14 mM  $\beta$ -ME 22 °C for 1 h. HD37-CCH was reduced with 5 mM DTT at 22 °C for 30 min. For nH-4G7-GC, scFv was reduced with 1 mM DTT at 22 °C for 1 h. RGF 4G7 was reduced with 0.11 mM 2-MEA in HBS pH 6.0 at 37 °C for 15 min. <sup>125</sup>I-labeled scFvs were used as tracers. Unreacted reducing agents were removed from samples by chromatography using Sephadex G-25 columns. Within 15 min after elution from Sephadex G-25 columns, scFv fragments were combined with liposomes containing Mal-PEG<sub>2000</sub>-DSPE and were allowed to incubate overnight at 22 °C with stirring.

Immunoliposomes targeted with the RGF 4G7 scFv (SIL[RGF 4G7]) were also constructed using the previously published post-insertion method, with slight modifications (91, 98, 99). The RGF 4G7 scFv was incubated with 0.1, 5 or 15 mM of 2-MEA HCl for 15 min in HBS (pH 6.0) at either 37 °C or 22 °C. <sup>125</sup>I-labeled RGF 4G7 scFv was added as a tracer prior to reduction. The reduced scFv was separated from the reducing agent by chromatography using Sephadex G25 columns, equilibrated with de-oxygenated HBS (pH 7.4). Shortly before coupling, a dried film of Mal-PEG<sub>2000</sub>-DSPE was hydrated in de-oxygenated HBS (pH 7.4) to form 10 mM Mal-PEG<sub>2000</sub>-DSPE micelles. For the coupling of scFv to micelles, the RGF scFv was mixed with Mal-PEG<sub>2000</sub>-DSPE micelles at a 1:4 molar ratio of scFv to Mal-PEG<sub>2000</sub>-DSPE, and incubated for 16 h at 22 °C. For insertion of scFv-Mal-PEG<sub>2000</sub>-DSPE into liposomes, scFv-micelle conjugates, trace-labelled with <sup>125</sup>I-scFv, were incubated with preformed liposomes at a ratio of 1.3–1.6 nmol scFv/μmol of PL at 55 °C for 0.5 h or 22 °C for 16 h. The resulting liposomes, SIL[RGF 4G7], contained PEG-scFvs inserted into their outer monolayer. The post-inserted liposomes were separated from free scFv and un-inserted scFv-Mal-PEG<sub>2000</sub>-DSPE by chromatography using a Sepharose CL-4B column.

In Chapter 4, HD37-C and HD37-CCH scFv fragments were coupled to liposomes containing Mal-PEG<sub>3400</sub>-DSPE at a 1:500 scFv:HSPC molar ratio, as described above. The scFv fragments were reduced for 1 h at room temperature with 14 mM β-ME and with 5 mM DTT for HD37-C and HD37-CCH, respectively. <sup>125</sup>I-labeled scFvs were used as tracers. HD37 and FMC63 mAbs were thiolated with Traut's reagent at a ratio of Traut's:IgG of 20:1 (mol/mol) in degassed HBS (pH 8.0) for 1 h. After thiolation, unreacted Traut's reagent was removed from the sample via Sephadex G-50 columns

equilibrated with degassed HBS (pH 7.4).  $^{125}\text{I}$ -labeled HD37 and FMC63 mAbs were used as tracers. Immediately after the column chromatography, the thiolated antibody was added to liposomes at 1:1000 mAb:HSPC molar ratio and incubated overnight at room temperature with stirring. Unconjugated antibody and antibody-free liposomes were removed by chromatography on Sepharose CL-4B columns in PBS, pH 8.0.

In Chapter 5, Stealth<sup>®</sup> immunoliposomes were prepared using a modification of the post-insertion method (98, 99). For generation of free thiol groups, both the HD37-CCH and the HD37 F(ab')<sub>2</sub> fragments were reduced with 5 mM of DTT in HBS (pH 8.0) for 15–20 min at room temperature.  $^{125}\text{I}$ -labeled scFv or Fab' were used as tracers for quantitation of scFv and Fab' fragments on the final liposomes. Unreacted reducing agents were removed by chromatography on Sephadex G-25 columns equilibrated in degassed HBS (pH 7.4). HD37-CCH or HD37 Fab' fragments were quickly coupled to Mal-PEG<sub>2000</sub>-DSPE micelles for 16 h at room temperature (22 °C) with continuous stirring, at a 1:4 molar ratio of either scFv or Fab' to Mal-PEG<sub>2000</sub>-DSPE.

HD37 mAb was thiolated with Traut's reagent at a molar ratio of 10:1 (Traut's reagent:HD37 mAb) in degassed HBS (pH 8.0) for 1 h.  $^{125}\text{I}$ -labeled HD37 mAb was used as a tracer. After thiolation, unreacted Traut's reagent was removed by chromatography on Sephadex G-50 columns equilibrated with degassed HBS (pH 7.4). Immediately after the column, the thiolated mAb was coupled to Mal-PEG<sub>2000</sub>-DSPE/mPEG<sub>2000</sub>-DSPE (1:4 molar ratio) micelles at a molar ratio of 1:10 (mAb:Mal-PEG<sub>2000</sub>-DSPE) for 16 h at room temperature with continuous stirring.

For insertion of mAb or fragments, conjugated to Mal-PEG<sub>2000</sub>-DSPE micelles, into the outer membrane of liposomes, HD37-CCH-, HD37 Fab'-, or HD37 mAb-

conjugated lipid micelles were incubated with preformed SL for 16 h at room temperature with continuous stirring. Unconjugated antibody and antibody-free lipid micelles were separated from mAb or fragment-conjugated SIL by chromatography on Sepharose CL-4B columns in HBS (pH 7.4). For all experiments, SIL targeted via HD37-CCH, HD37 Fab' or HD37 mAb, were compared at similar surface CD19 binding sites densities, taking into account that each mAb contains two CD19 binding domains.

## **2.9. Separation of Coupled RGF 4G7-micelles from Free RGF 4G7 and**

### **Determination of Free Thiol Groups**

In Chapter 3, a Sephadex G-100 column (150 kDa exclusion limit) was used to separate coupled RGF 4G7 scFv-Mal-PEG<sub>2000</sub>-DSPE micelles from uncoupled scFv. 2, 4-Dinitrophenol threonine (DNP-threonine, 285 Da) was used to characterize the column volume of the 1 mL G-100 column. A small amount of RGF 4G7 was coupled to Mal-PEG<sub>2000</sub>-DSPE micelles using the method described above. For detection of the scFv, trace amount of <sup>125</sup>I-labeled RGF 4G7 scFv was mixed with unlabeled scFv prior to coupling. The coupled mixture was applied to a G-100 column to separate coupled scFv-micelles from free scFv. Elution fractions were collected and the scFv was detected by measuring gamma radioactivity in each fraction. In a separate control experiment, free <sup>125</sup>I-labeled RGF 4G7 scFv was applied to the same G-100 column. Fractions were collected and gamma radioactivity of each fraction was measured.

The Ellman's Assay was used for quantification of free thiol (SH) groups on reduced RGF 4G7 scFv after desalting on G25 columns. A standard curve was constructed using reduced glutathione (GSH), which contains 1 SH per molecule. The GSH was combined with 100  $\mu$ L of 1 M Tris pH 8, 50  $\mu$ L of DTNB solution (2 mM

DTNB and 50 mM  $\text{NaC}_2\text{H}_3\text{O}_2$ ), and  $\text{H}_2\text{O}$  to a total volume of 1 mL. Absorbance was measured at 412 nm and the amount of SH on the RGF 4G7 was determined according to the standard curve.

## 2.10. Flow Cytometry Studies

Fluorescence-activated cell sorting (FACS) experiments were conducted to determine expression of several B-cell antigens (i.e., CD19, CD20 and CD22) in various B-cell lines. Briefly,  $1 \times 10^6$  Raji, Namalwa, Daudi, Ramos or Molt4 cells were incubated with 50  $\mu\text{g}/\text{mL}$  of FMC63 mAb, RF-B4-B3 mAb, or rituximab for 1 h at 4 °C, and then washed with cold PBS. Binding of mAb was detected in a Becton Dickinson FACScan (BD Biosciences, Mississauga, ON) after labeling with 20  $\mu\text{L}$  of a 1/50 dilution of GAM-FITC or a 50  $\mu\text{L}$  of a 1/32 dilution of GAH-FITC in HBS, pH 7.4. The binding of mAb to cells was indicated by increased fluorescence intensity associated with cells. Controls included untreated cells, cells treated with GAM-FITC and cells treated with GAH-FITC.

FACS experiments were also conducted to determine the binding of various scFvs to Namalwa or Raji cells. Briefly,  $1 \times 10^6$  cells in the exponential growth phase were seeded in sterile tubes. Cells were incubated with scFvs for 1 h at 4 °C, and then washed with cold PBS. Binding of scFvs was detected in a Becton Dickinson FACScan after labeling with 20  $\mu\text{L}$  (200 ng/mL) murine anti-His mAb in HBS, pH 7.4, followed by 20  $\mu\text{L}$  of a 1/50 dilution of GAM-FITC in HBS, pH 7.4. Controls included untreated cells, cells treated with anti-His mAb, cells treated with ANTI-FLAG<sup>®</sup> M2 mAb-FITC (Sigma), cells treated with GAM-FITC, and cells treated with anti-His mAb plus GAM-FITC.

Experiments to determine equilibrium dissociation constants ( $K_D$ ) were performed as described (205), with slight modifications. Briefly,  $2 \times 10^5$  Raji cells were incubated with various concentrations of scFv in PBS supplemented with 10% FBS (PBS/FBS) at a final volume of 1 mL for 3 h at 4 °C. Cells were then washed twice with PBS/FBS. For HD37-CCH, cells were then incubated with 20  $\mu$ L of murine anti-His mAb (200 ng/mL) in PBS/FBS for 1 h at 4 °C, washed twice with PBS/FBS, then incubated with 20  $\mu$ L of a 1/50 dilution of GAM-FITC in PBS/FBS for 30 min at 4 °C. For HD37 mAb and FMC63 mAb, cells were incubated with 20  $\mu$ L of a 1/50 dilution of GAM-FITC in PBS/FBS for 30 min at 4 °C. For RGF 4G7, cells in PBS/FBS were incubated with ANTI-FLAG<sup>®</sup> M2 mAb-FITC for 1 h at 4 °C, at a final concentration of 4.6  $\mu$ g/mL, according to the manufacturer's instructions. As a final step, all cells were washed twice with PBS/FBS and resuspended in 0.5 mL of 4% formaldehyde in PBS. Fluorescence was measured in a Becton Dickinson FACScan and were normalized using the SPHERO<sup>™</sup> FITC Calibration Particle Kit (Spherotech, Libertyville, IL). The mean fluorescence intensity (MFI) was plotted as a function of increasing concentrations of mAb or scFv. The binding data was fitted with a one site binding model using GraphPad Prism (San Diego, CA). The binding data were analyzed by the Lineweaver-Burk method using the equation:  $1/\text{MFI} \approx 1/\text{MFI}_{\text{max}} + (K_D/\text{MFI}_{\text{max}})(1/[\text{mAb or scFv}])$ , where  $\text{MFI}_{\text{max}}$  was the maximal MFI obtained from the Y-intercept and the  $K_D$  was calculated from the slope of the linear regression line.

### **2.11. *In vitro* Cell Binding Studies Using Tritium-labeled Liposomes**

Cellular binding studies were performed as previously described (206). The association with B-lymphoid cells was determined for targeted and non-targeted

liposomes, labeled with  $^3\text{H}$ -CHE. Briefly,  $1 \times 10^6$  Raji or Namalwa cells were seeded in sterile tubes. Cells were incubated with various formulations of liposomes for 1 h at 37 or 4 °C, at PL concentrations ranging from 0.1 to 3.2 mM. For competition experiments, cells were pre-incubated for 15 min with 100  $\mu\text{g}$  of HD37 mAb (7.5- to 120-fold in excess of the number of CD19 binding sites on the surface of liposomes) and then immunoliposomes were added. Cells were then washed 3 times with cold PBS, and the amount of  $^3\text{H}$ -CHE counts associated with cells was determined by scintillation counting (Beckman LS-6800 Scintillation Counter, Beckman Coulter Canada, Inc., Mississauga, ON). Data were presented as nmol PL associated with  $1 \times 10^6$  cells and fitted with a one site binding model using GraphPad Prism. Specific binding was calculated by subtracting cell-associated radioactivity counts of SL from SIL.

### **2.12. *In vitro* Cytotoxicity Studies**

Cytotoxicity studies employed the MTT tetrazolium assay as previously described (61). Briefly,  $8 \times 10^5$  Raji cells or  $5 \times 10^5$  Molt4 cells were incubated with various formulations of DXR-loaded liposomes (SL-DXR or SIL-DXR). In Chapter 4, cells were incubated with either free DXR, untargeted liposomal DXR (SL-DXR), SIL-DXR[HD37-CCH], free HD37-CCH, or a mixture of unconjugated HD37-CCH and SL-DXR in media for 1 h at 37 °C. In Chapter 5, cells were incubated with either free DXR, SL-DXR, SIL-DXR[HD37-CCH], SIL-DXR[HD37 Fab'] or SIL-DXR[HD37 mAb] in media for 1 h at 37 °C. Cells were then thoroughly washed, resuspended in fresh media and were allowed to grow for another 48 h in full media. At the end of 48 h, viable cells were detected by the addition of MTT as described (61). Treated cells were compared to untreated cells to calculate percent of viable cells. Very little leakage of drug from the liposomes is

expected during a 1 h incubation since the liposomes have leakage half-lives in excess of 90 h (85). Therefore, an increase in the cytotoxicity of immunoliposomal DXR, in comparison with untargeted liposomal DXR, suggests CD19-mediated uptake of the immunoliposomal DXR during the incubation period.

### 2.13. Pharmacokinetics and Biodistribution Studies

*In vivo* pharmacokinetics (PK) and biodistribution (BD) studies were conducted in naïve BALB/c or Raji-bearing SCID mice (injected i.v. into the tail vein with  $2.5 \times 10^6$  Raji cells). Mice (3/time point) were injected i.v. with saline (control) or various formulations of DXR-loaded liposomes (i.e., SL-DXR, SIL-DXR[HD37-CCH], SIL-DXR[HD37 Fab'] and SIL-DXR[HD37 mAb]) at a dose of 3 mg DXR/kg. For experiments with Raji-bearing SCID mice, DXR-loaded liposomes were injected 24 h post-implantation. The *in vivo* fate of both the liposomes and the drug were traced with radiolabeled markers ( $^3\text{H}$ -CHE and  $^{14}\text{C}$ -DXR, respectively). Samples of blood and major organs (i.e., liver, spleen, lung, heart, kidneys) were excised from individual euthanized animals at selected time points. Samples were solublized with Solvable™, decolorized with 30% hydrogen peroxide, and counted for  $^3\text{H}$  and  $^{14}\text{C}$  radioactivity in 10 to 20 mL of Ultima Gold™ scintillation fluor after light adaptation for 1 h (Beckman LS 6500 liquid scintillation counter). For analysis of the blood concentration data, the total blood volume was assumed to be 7% of the weight of each mouse. For the analysis of biodistribution to organs, a blood correction factor was applied to the organ data to account for the presence of radioactivity in the blood within the organs (207). Results were expressed as % injected PL- and drug-associated radioactivity. In order to examine the effect of the presence of the scFv tags, Raji-bearing SCID mice were injected with

SL-DXR, SIL-DXR[HD37-CCH], or SIL-DXR targeted via the tagless HD37-C construct (SIL-DXR[HD37-C]) and treated as above. Blood concentration data were analyzed using WinNonLin Software (Pharsight<sup>®</sup> Corporation, Mountain View, CA) and fitted with either an i.v. bolus one-compartment or i.v. bolus multi-compartment model.

#### **2.14. Therapeutic Studies**

SCID mice (7/group) were injected i.v. into the tail vein with  $2.5 \times 10^6$  Raji cells. At 24 h post-implantation, when most of the cells have exited the circulation (208), mice were injected i.v. with saline (control), or with a dose of 3 mg DXR/kg of free DXR, SL-DXR, SIL-DXR[HD37-CCH], SIL-DXR[HD37 Fab'] or SIL-DXR[HD37 mAb]. The maximum tolerated dose of DXR for SCID mice is 3 mg/kg (209). Mice were monitored and were euthanized when they developed hind leg paralysis, which was indicative of infiltration of the bone marrow and compression of the spinal cord by cancer cells (210). In another experiment, Raji-bearing SCID mice were treated with the above formulations at a dose of 1 mg DXR/kg at 24 h post-implantation.

#### **2.15. Statistical Analysis**

Comparisons of means were done using the GraphPad InStat software (GraphPad Software, Inc., Version 3.0, San Diego, CA) with one-way analysis of variance (ANOVA) and the Tukey post-test. Analysis of PK/BD data was done using GraphPad Prism software (GraphPad Software, Inc., Version 4.0, San Diego, CA) with two-way ANOVA and the Bonferroni post-test. Analysis of survival studies was done using GB-STAT software (Dynamic Microsystems, Inc., Version 8.0, Silver Spring, MD) with

Kaplan-Meier analysis and the log rank test for equality of survival. Differences were considered significant when the  $P$  values were less than 0.05.

### **Chapter 3**

## **Expression, Purification and Screening of Various Constructs of Anti-CD19 Single Chain Fv Fragments**

### **3. Expression, Purification and Screening of Various Constructs of Single Chain Fv Fragments**

#### **3.1. Abstract**

The pan-B-cell antigen CD19 is an attractive target for directing immunoliposomal anticancer drugs to B-lymphoid cancers. Single chain Fv (scFv) may be a more suitable targeting agent for the manufacture of liposomal drugs than Fab' and mAb in terms of production, ease of manipulation and pharmacokinetics. Various anti-CD19 scFv constructs were available from collaborators, and they were used for feasibility studies of scFv-targeted liposomes. Various properties including affinity, stability, and coupling to liposomes were examined in order to choose a suitable candidate for comparison with Fab' and mAb.

#### **3.2. Introduction**

The CD19 antigen is a pan-B-cell antigen that is primarily expressed on mature B cells and is not expressed outside of the B-cell lineage. CD19 is an attractive target for the study of antibody-directed therapeutics since it is expressed on most type of B-lymphoid malignancies and binding of the antigen by antibodies leads to internalization of the antigen-antibody complex (211, 212). Various studies have examined anti-CD19 antibody-drug conjugates for the treatment of B-lymphoid cancers, using whole mAb from mouse as the targeting agent (14, 213). However, there are issues related to the clinical use of murine mAb such as rapid clearance and low circulation times, and possible human-anti-mouse antibody (HAMA) responses against the mAb, which can be attributed to recognition of the Fc domain of the mAb (120, 214). To avoid the issues

associated with mAb, in animal models of human B-lymphoid cancers many groups have explored the use of drug conjugates with Fab' and scFv fragments, both lacking the Fc domain (62, 181, 215, 216). For clinical applications of immunoliposomes, scFv may be more favourable than Fab' and mAb since: 1) scFv is smaller and contains fewer foreign peptide sequences than Fab' or mAb; 2) scFv lacks the Fc region, which most HAMA responses are directed against; 3) scFv can be produced in various recombinant systems such as bacterial and algal cultures, with the potential for fewer manufacturing concerns; and 4) greater ease of manipulation of properties such as antigen binding for scFv compared to mAb.

Since their discovery, liposomes have entered the mainstream as the prototypical drug delivery system for toxic agents such as anticancer drugs (16). Various liposomal anticancer drugs, such as Doxil/Caleyx<sup>®</sup> (untargeted Stealth<sup>®</sup> liposomal doxorubicin), are currently in clinical use for various types of cancers. Antibody-targeted liposomes (immunoliposomes) have the capability of delivering large quantities of drug to antigen-expressing cells in a cell-specific manner. It has been shown in animal models that immunoliposomes (SIL) containing doxorubicin (DXR), targeted via an anti-CD19 mAb or Fab', have increased therapeutic effect over DXR-containing untargeted liposomes (SL-DXR) (61, 62). Due to the smaller size of scFv, it is hypothesized that immunoliposomal DXR (SIL-DXR) targeted via an anti-CD19 scFv may be less immunogenic than SIL targeted via Fab' or mAb.

One of the objectives of this thesis is to compare SIL-DXR targeted via anti-CD19 mAb, Fab' or scFv of the same origin in an animal model of human B-lymphoma. To complete this objective, an anti-CD19 scFv with suitable properties in terms of

antigen binding, expression yields, and stability needs to be chosen from the constructs provided by various collaborators. In this study, initial experiments were conducted for targeting liposome to CD19-expressing B-lymphoid cells, using different production and purification methods applied to various constructs of anti-CD19 scFv. ScFv directed against three different epitopes on CD19 were used. Two expression systems, bacterial and algal culture fermentation, were used to produce scFv. In addition, two extraction methods, extraction from bacterial periplasmic space or extraction from inclusion bodies with subsequent refolding, were used and some comparisons between the two methods were made. Various strategies for the coupling of scFv to liposomes and the binding of scFv-targeted liposomes to CD19-expressing cells were examined.

### **3.3. Antibodies and ScFv Constructs Used**

Details of experiments and of the mAb and scFv constructs used in this chapter are provided in Chapter 2. For this study, FMC63 mAb (anti-CD19), rituximab (anti-CD20) and RF-B4-B3 mAb (anti-CD22) were used for the screening of various B-cell lines for their respective antigens. HD37-CHC, FMC63-CHC, HD37-C, FMC63-C, nH-4G7-GC, HD37-CCH and RGF 4G7 scFv were used for expression and purification, binding, and for some initial coupling studies.

## **3.4. Results**

### **3.4.1. Screening of B-cell Lines**

Various B-cell lines (Namalwa, Raji, Daudi and Ramos) were screened for the expression of CD19, CD20 and CD22 (Fig. 3.1). All 4 B-cell lines tested positive for the

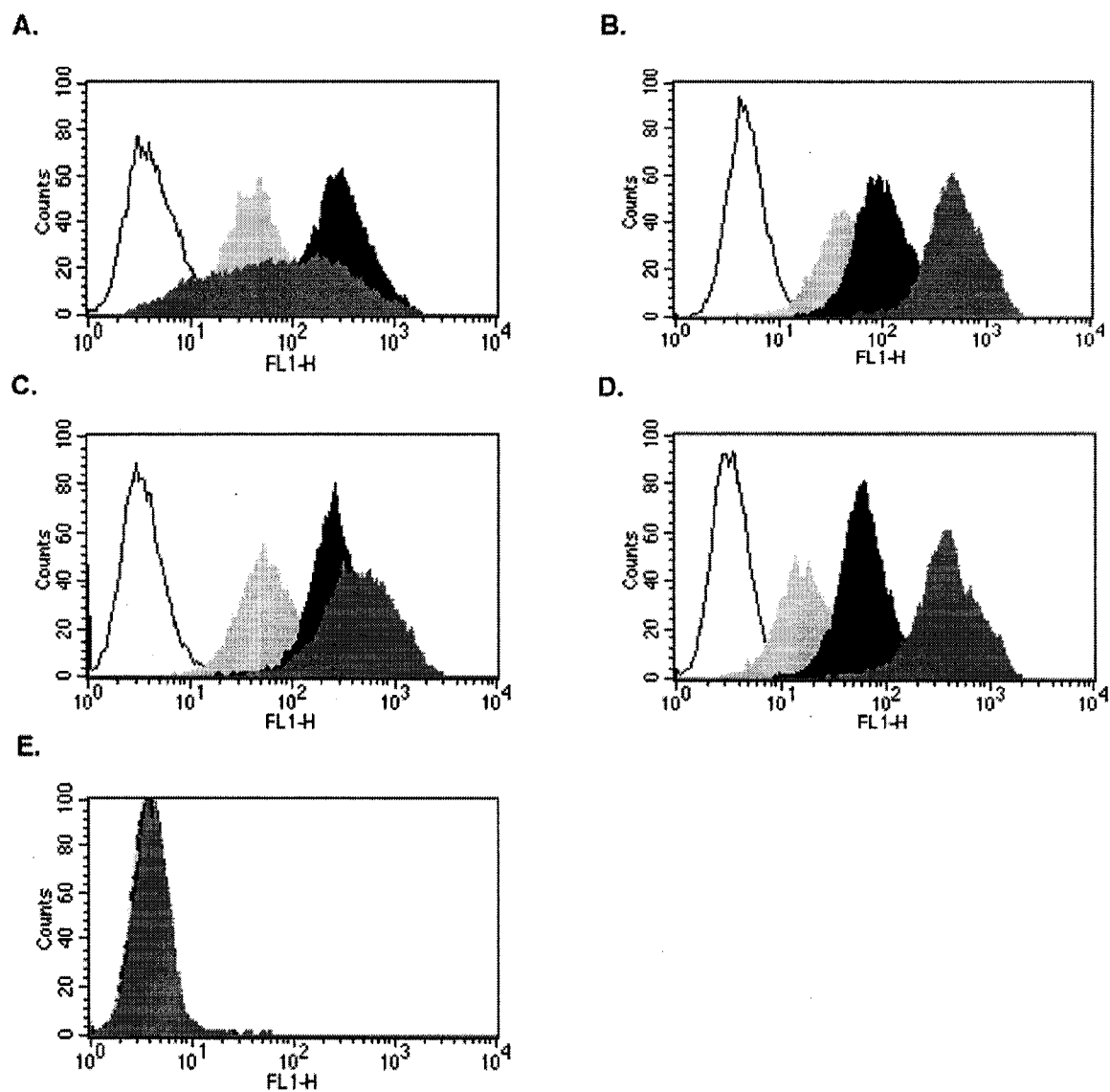


**Figure 3.1. Screening of various B-cell lines for expression of CD19, CD20, and CD22.** Cells were treated with 50  $\mu\text{g}/\text{mL}$  mAb for CD19, CD20 and CD22 as described in Chapter 2. **A)** Namalwa cells. **B)** Daudi cells. **C)** Raji cells. **D)** Ramos cells. **E)** Molt4 cells. CD19 (■); CD20 (▒); CD22 (□); no treatment control (□). Additional controls included cells treated with GAM-FITC and cells treated with GAH-FITC. The fluorescence of the GAM-FITC and GAH-FITC controls were the same as the auto-fluorescence of untreated cells

various B-cell antigens. Namalwa and Raji cells were used in this thesis since they expressed the CD19 antigen at slightly higher levels than Daudi and Ramos cells. The T-cell line (Molt4) was chosen as the negative control for this thesis since it did not express any of the antigens.

#### **3.4.2. Binding of the HD37-CHC and FMC63-CHC constructs to B cell lines**

Initial work using FMC63-CHC and HD37-CHC (1.4  $\mu\text{M}$ ) showed that free scFv bound to CD19<sup>+</sup> Namalwa cells (Fig. 3.2A and B). No binding was observed against CD19<sup>-</sup> Molt4 cells. At the same scFv concentration, the binding of HD37-CHC to Raji cells (Fig. 3.2C) was found to be slightly higher than FMC63-CHC (Fig. 3.2B).

#### **3.4.3. Extraction, Production Yield, Concentration and Stability**

Production yields of FMC63-CHC and HD37-CHC from the periplasmic space ranged from 0.1–0.3 mg/L of culture for both constructs (Table 3.1). Both scFv constructs were prone to aggregation at concentrations > 14  $\mu\text{M}$  (0.5 mg/mL). At lower concentrations, the HD37-CHC construct was stable and could be coupled to liposomes, but the resultant PL concentrations of the SIL were too low for experiments. Typically, scFv constructs were needed to be stable at concentrations roughly above 1 mg/mL (33  $\mu\text{M}$ ) in order to produce immunoliposomes in sufficient concentrations for experiments.

The HD37-CHC construct was also used to optimize the procedures for extraction of scFv from inclusion bodies and validate the presence of scFv in these insoluble aggregates. It was found that the HD37-CHC scFv was present in inclusion bodies and can be extracted from inclusion bodies at > 5 mg scFv/L culture (Fig. 3.3 and Table 3.1).

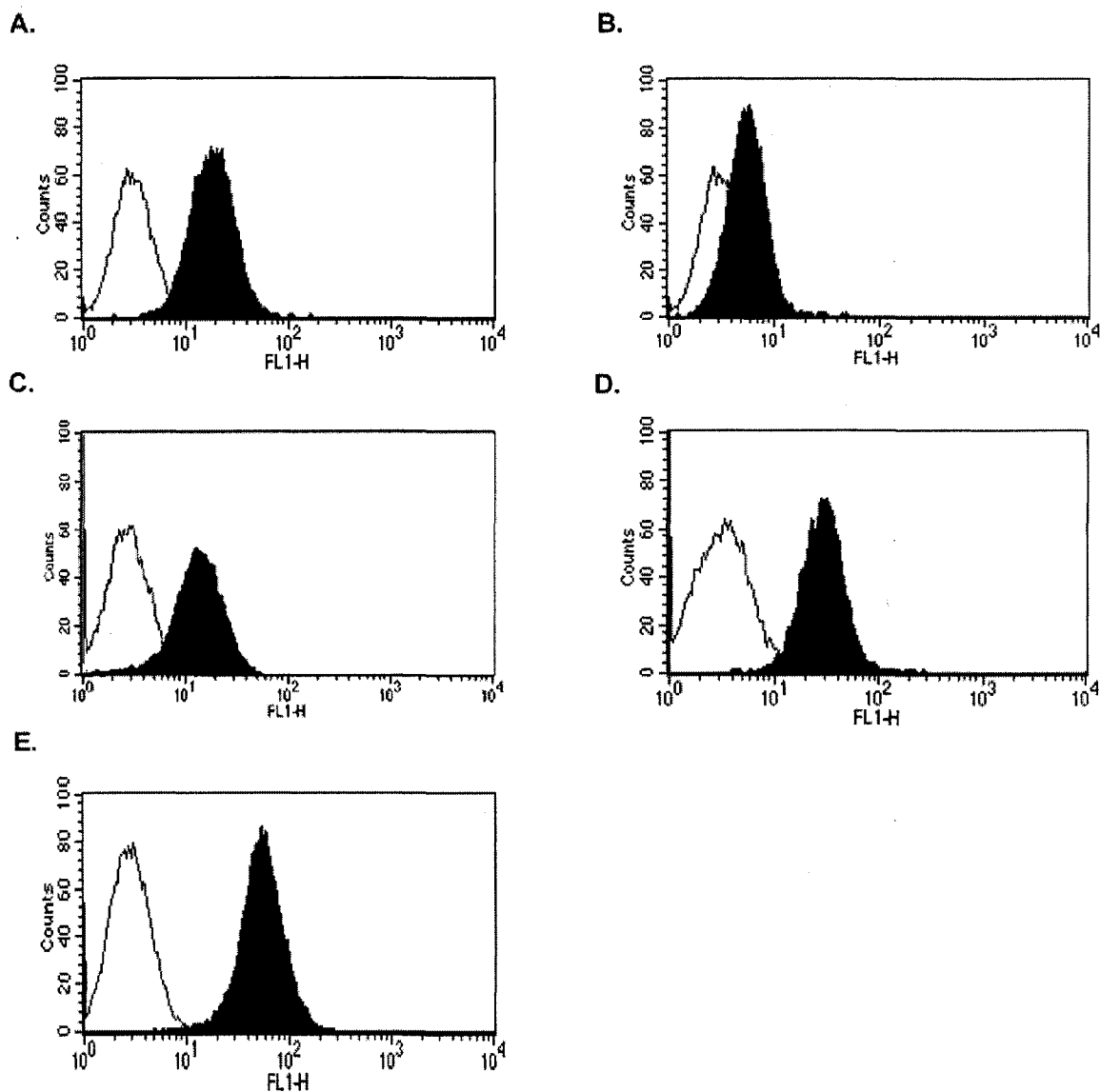


**Figure 3.2. FACS of all scFv constructs.** A)  $1 \times 10^6$  Namalwa cells incubated with  $1.4 \mu\text{M}$  of HD37-CHC. B)  $1 \times 10^6$  Namalwa cells incubated with  $1.4 \mu\text{M}$  of FMC63-CHC. C)  $1 \times 10^6$  Raji cells incubated with  $1.43 \mu\text{M}$  of HD37-CCH. D)  $1 \times 10^6$  Raji cells incubated with  $3.4 \mu\text{M}$  of nH-4G7-GC. E)  $1 \times 10^6$  Raji cells incubated with  $0.02 \mu\text{M}$  of RGF 4G7. Treated cells (■); no treatment control (□). Additional controls included cells treated with anti-His mAb, cells treated with ANTI-FLAG<sup>®</sup> M2 mAb-FITC, cells treated with GAM-FITC, and cells treated with anti-His mAb plus GAM-FITC. The fluorescence of the anti-His mAb, ANTI-FLAG<sup>®</sup> M2 mAb-FITC, GAM-FITC and anti-His mAb plus GAM-FITC controls were the same as the auto-fluorescence of untreated cells.

**Table 3.1. Production yields, concentration and stability of scFv constructs.**

<b>ScFv construct</b>	<b>Method of extraction</b>	<b>Typical yield (mg/L)</b>	<b>Prone to aggregation at conc. above 14 <math>\mu</math>M</b>
<b>HD37-CHC</b>	Periplasmic extraction	0.1-0.3	Yes
	Inclusion bodies	> 5	Yes
<b>FMC63-CHC</b>	Periplasmic extraction	0.1-0.3	Yes
<b>HD37-C</b>	Periplasmic extraction	0.1 0.3	No
	Inclusion bodies	1-2	No
<b>FMC63-C</b>	Periplasmic extraction	0.1-0.3	No
	Inclusion bodies	1-2	No
<b>nH-4G7-GC</b>	Inclusion bodies	ND	Yes
<b>HD37-CCH</b>	Periplasmic extraction	0.4-0.6	No
<b>RGF 4G7</b>	From algal cultures	ND	No

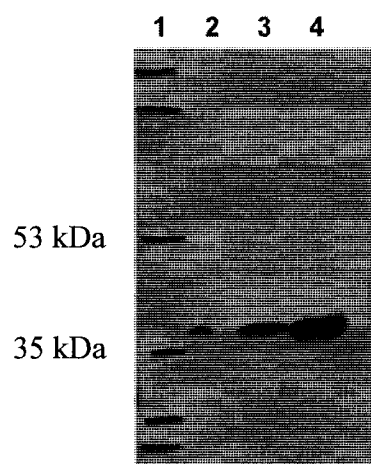


**Figure 3.3. Western blot of HD37-CHC scFv extracted from inclusion bodies.** HD37-CHC was detected by murine anti-c-myc mAb as described in Chapter 2. Lane 1: molecular weight markers. Lane 2 4: 4, 10, and 20  $\mu$ g of HD37-CHC respectively.

#### 3.4.4. Generation of Tagless Constructs, Production Yield, Refolding and Stability

Since molecular tags might not be preferred for clinical applications, two tagless constructs (i.e., HD37-C and FMC63-C) were engineered by Dr. D. Das and Dr. M. Suresh for targeting liposomes (197). When purified from the periplasmic space of *E. coli*, production yields were 0.1-0.3 mg/L of culture. To increase the amount of purified scFv, the tagless constructs were purified from inclusion bodies with yields of 1-2 mg of denatured protein/L of culture. The native scFv, after extraction from the periplasmic space, was refolded, as described in Section 2.3, Chapter 2. HD37-C and FMC63-C were stable at concentrations  $> 33 \mu\text{M}$  (1 mg/mL), which was favourable for coupling to liposomes.

The nH-4G7-GC scFv was refolded and the refolded scFv bound to Raji cells (Fig. 3.2D). The scFv, however, was not stable in isotonic buffers such as PBS. Arginine was used to stabilize the scFv during the last stages of the refolding procedure, and any attempts to remove the arginine from the refolding buffers resulted in substantial aggregation ( $> 50\%$ ). The aggregation was postulated to be the result of a hydrophobic leader sequence in the scFv.

#### 3.4.5. Binding Activity of Tagless Constructs

Due to the lack of tags for identification, the binding of HD37-C and FMC63-C to CD19<sup>+</sup> cells was assessed using a Protein L-FITC conjugate, as Protein L had been shown to bind to the HD37-CHC scFv (199). However, no binding to CD19<sup>+</sup> cells was observed for either native scFv extracted from the periplasmic space or for refolded HD37-C or FMC63-C. This was postulated to be due to a loss of affinity of the Protein

L-FITC for the construct, since binding of the parental HD37 mAb to CD19 also could not be detected by Protein L-FITC.

In order to further investigate the binding activity, refolded HD37-C was coupled to the surface of liposomes resulting in coupling densities of 0.7-0.9 nmol scFv/ $\mu$ mol PL (19.2-25.6  $\mu$ g scFv/ $\mu$ mol PL), which compares favourably with previous literature values (217). The binding to B-lymphoid cells *in vitro* was compared for SIL[HD37-C], untargeted liposomes (SL), and either SIL[HD37 mAb] or SIL[FMC63 mAb] (Fig. 3.4). SIL[HD37-C] had substantially lower binding to CD19-positive Raji or Namalwa cells than the binding of liposomes targeted via the FMC63 or HD37 mAbs; indeed, binding of SIL[HD37-C] was not different from control SL.

#### **3.4.6. Yield, Purification, Stability and Binding of HD37-CCH Purified from the Periplasmic Space**

After considerable time and effort, it was concluded that refolding denatured scFv from inclusion bodies is associated with too many potential problems and would not be suitable for this project. Subsequently, the HD37-CCH was purified from the periplasmic space of *E. coli* with production yield ranging from 0.4-0.6 mg/L of culture (Table 3.1). The scFv was stable in PBS at concentrations  $> 29 \mu$ M (1.0 mg/mL).

The HD37-CCH construct was coupled to liposomes (SIL[HD37-CCH]) resulting in 0.3 nmol HD37-CCH/ $\mu$ mol PL. Initial binding experiments with SIL[HD37-CCH] showed increased binding to Raji cells compared to SL. In competition experiments, binding of SIL[HD37-CCH] to Raji cells could be blocked by pre-incubating cells with HD37 mAb (Fig. 3.5).

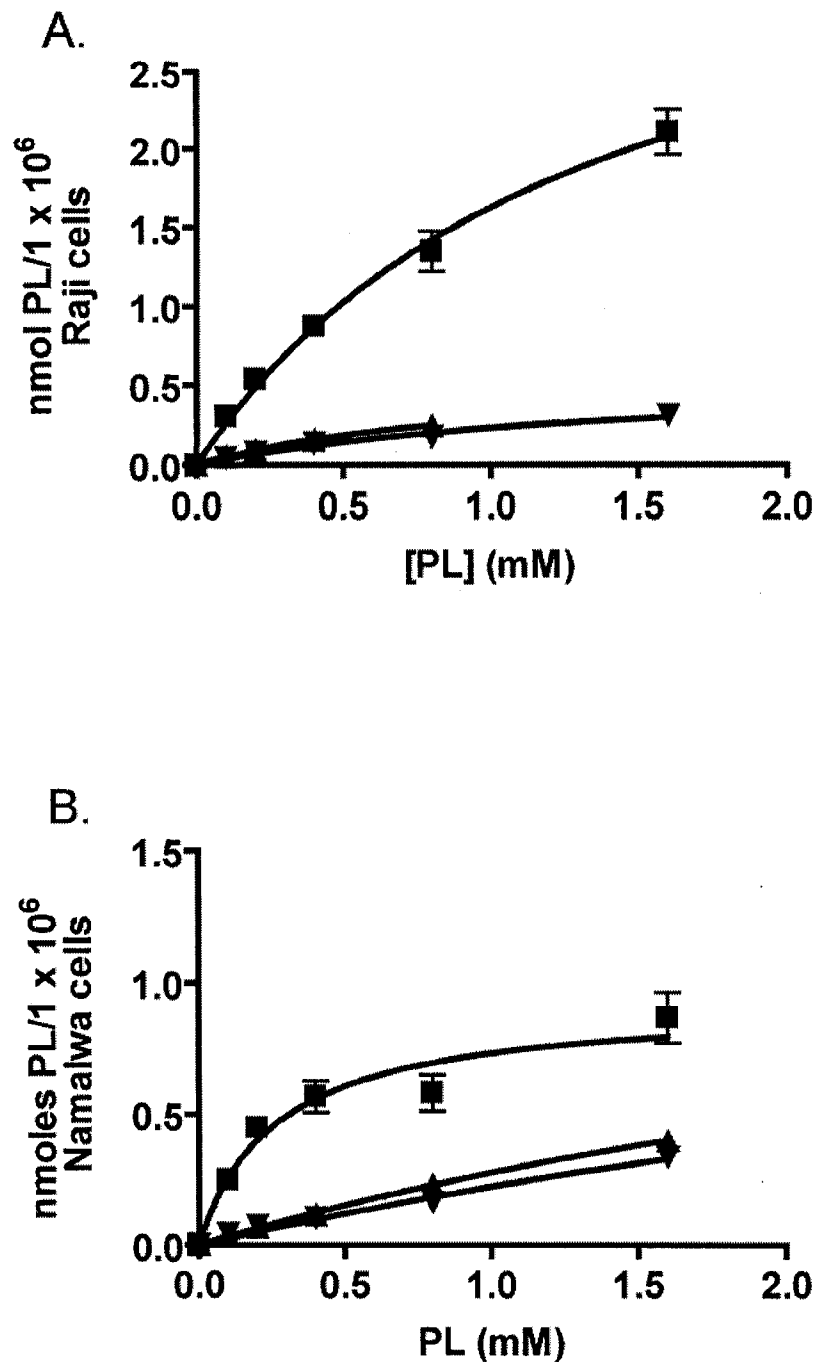


**Figure 3.4. Binding of immunoliposomes to B-lymphoid cells.**  $1 \times 10^6$  cells were incubated with the various liposome formulations at increasing PL concentrations. **A)** Raji cells. ■ SIL[HD37 mAb], ▲ SIL[HD37-C] and ▼ SL. **B)** Namalwa cells. ■ SIL[FMC63 mAb], ▲ SIL[HD37-C] and ▼ SL.

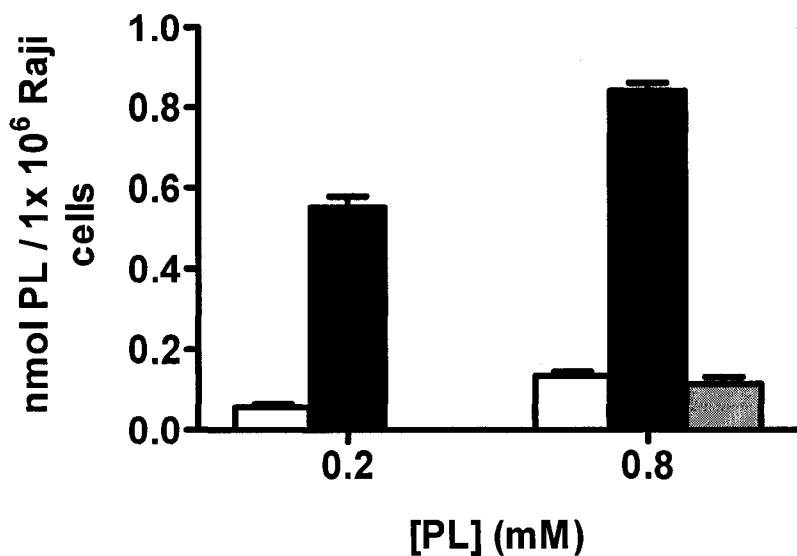


**Figure 3.5. Binding study of SIL[HD37-CCH] and SL to CD19<sup>+</sup> Raji cells.**  $1 \times 10^6$  cells were incubated with SIL[HD37-CCH] or SL at the indicated PL concentrations for 1 h at 37 °C. Binding was quantitated by scintillation counting of cell-associated liposomes labeled with <sup>3</sup>H-CHE. WHITE bar: SL, BLACK bar: SIL[HD37-CCH], GREY bar: cells incubated with 0.6 nmol (13X excess) of HD37 mAb 15 min prior to addition of SIL[HD37-CCH].

### 3.4.7. Coupling and Binding of RGF 4G7 scFv

The RGF 4G7 scFv was expressed by fermentation of algal cultures. Using FACS, the free RGF 4G7 scFv was shown to bind to Raji cells (Fig. 3.2E) with a  $K_D$  of in the range of  $1-2 \times 10^{-9}$  M (Fig 3.6). The  $K_D$  of RGF 4G7 was several-fold lower than that of the HD37-CCH construct ( $K_D \approx 6-9 \times 10^{-9}$  M) suggesting the RGF 4G7 construct has higher affinity for CD19 compared to HD37-CCH (Chapter 4). The RGF 4G7 was found to be stable at concentrations  $> 33 \mu\text{M}$  (1.0 mg/mL) (Table 3.1).

In order to optimize coupling and binding to Raji cells, various conditions were evaluated for coupling RGF 4G7 to liposomes (Table 3.2). The post-insertion method was used because previous experiments showed that coupling the HD37-CCH scFv to Mal-PEG<sub>2000</sub>-DSPE micelles increased the storage stability of the scFv (Chapter 5), which may help to increase the amount of scFv coupled to liposomes. Initially, the RGF 4G7 was reduced with 15 mM of 2-MEA (molar ratio of 1:411, scFv:2-MEA). Post-insertion of scFv-Mal-PEG-DSPE conjugates into the outer membrane of preformed liposomes resulted in 0.13 nmol RGF 4G7/ $\mu\text{mol}$  PL, which was lower than previous results obtained using the HD37-CCH construct. One possibility for this is that the association of the scFv with the surface of liposomes may have been via non-covalent interactions, e.g., Van der Waal's forces. The binding of these SIL[RGF 4G7] to Raji cells was similar to untargeted SL (not shown).

### 3.4.8. Trouble-shooting the Low Binding of SIL[RGF 4G7] to Raji Cells

The low binding of the SIL[RGF 4G7] to Raji cells was hypothesized to be due either to sub-optimal coupling conditions that resulted in low numbers of scFv on the

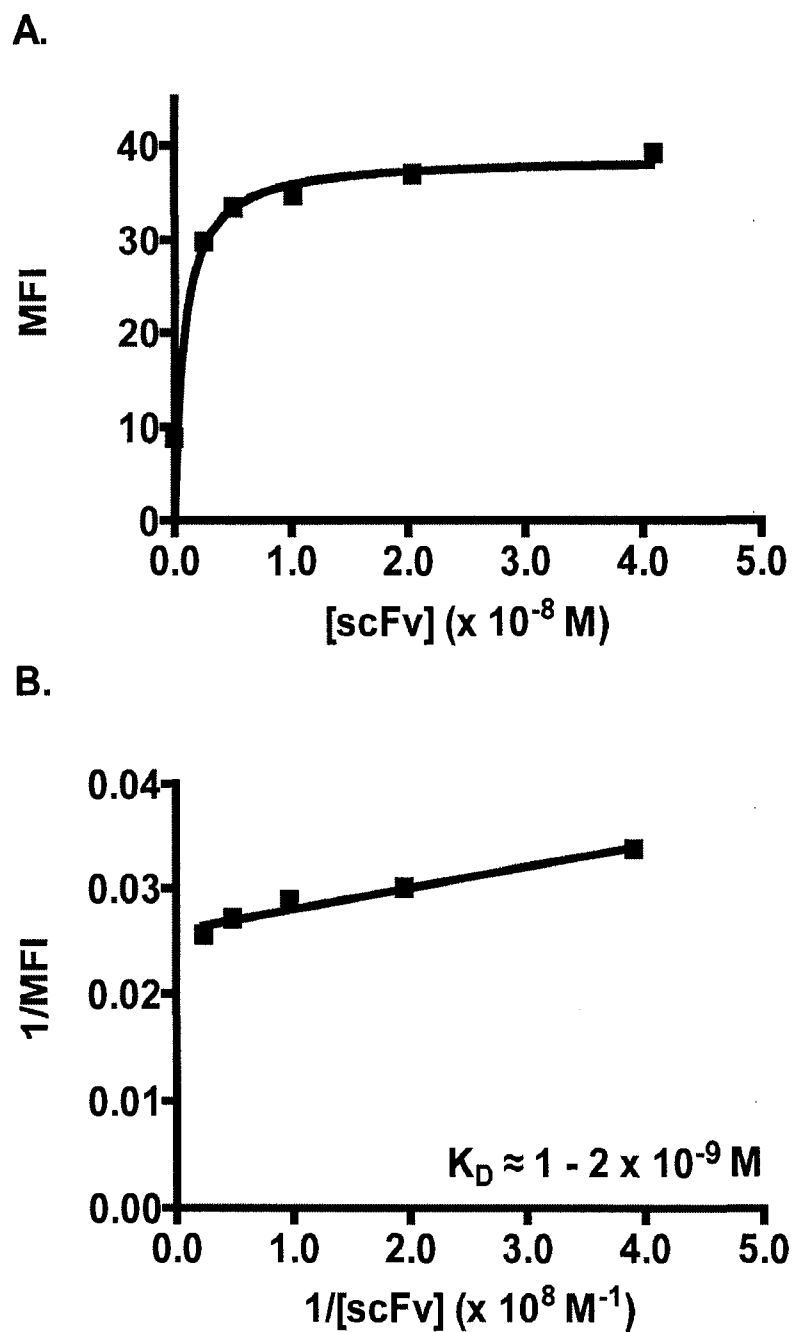


**Figure 3.6. Mean fluorescence intensity (MFI) as a function of concentration of RGF 4G7.** MFI was measured by FACS as described in Chapter 2. **A)** MFI as a function of increasing concentration of RGF 4G7. **B)** Double reciprocal plot of MFI vs. [RGF 4G7] for Lineweaver-Burk analysis of the equilibrium dissociation constant ( $K_D$ ).

**Table 3.2. Post-insertion and coupling conditions used for RGF 4G7 scFv.**

	<b>Molar ratio of scFv: 2-MEA</b>	<b>Temp.<sup>a</sup> (°C)</b>	<b>Free sulfhydryl / scFv</b>	<b>PI or coupling temp. (°C)</b>	<b>PI or coupling time (h)</b>	<b>scFv/μmol PL (nmol/μmol)</b>
<b>Post-insertion</b>	1:2	37	1.2	22	16	0.11
	1:137	37	ND	55	0.5	0.18
	1:318	22	ND	55	0.5	0.13
	1:411	37	ND	55	0.5	0.25
<b>Conventional coupling</b>	1:2	37	0.6	22	16	0.22

<sup>a</sup> Temperature of the reducing procedure

surface of the SIL, or to destruction of disulfide bonds within the scFv that are critical for proper tertiary structure and binding to CD19. To trouble-shoot the latter possibility, the concentration of 2-MEA was reduced to 5 mM in order to prevent excessive reduction of intermolecular disulfide bonds in the molecule.

For this experiment, scFv-conjugated Mal-PEG-DSPE micelles were prepared, as above, at 5 and 15 mM 2-MEA and the resulting RGF 4G7 micelles were mixed with preformed SL using the post-insertion method. For samples reduced with 5 mM or 15 mM 2-MEA, the amount of scFv associated with liposomes was found to be 0.18 nmol and 0.25 nmol RGF 4G7/ $\mu$ mol of PL, respectively. Binding to Raji cells of SIL[RGF 4G7] prepared at either 5 or 15 mM 2-MEA were again not different than untargeted SL (not shown).

In order to determine whether any covalent coupling between the free RGF 4G7 and the Mal-PEG-DSPE had occurred, free scFv was coupled to Mal-PEG-DSPE micelles (15 mM of 2-MEA for 15 min at 37 °C) and was applied to a G-100 column. It is expected that the RGF 4G7 would elute with the lipid micelles if covalent coupling occurred. Using DNP-threonine, the column volume of the 1 mL G-100 column was shown to be roughly 1 mL. Since the molecular weight of scFv-conjugated Mal-PEG-DSPE micelles is expected to be above the exclusion limit of the G-100 column, the scFv-conjugated micelles should elute in the void volume. When the mixture of coupled RGF 4G7-Mal-PEG-DSPE micelles was applied to the column, gamma counts appeared in fractions near the void volume suggesting that the scFv was eluted with the micelles (Fig. 3.7). As a control, free  $^{125}$ I-labeled RGF 4G7 scFv was applied to the column. The free  $^{125}$ I-labeled RGF 4G7 scFv eluted after the scFv-conjugated micelles, but before the

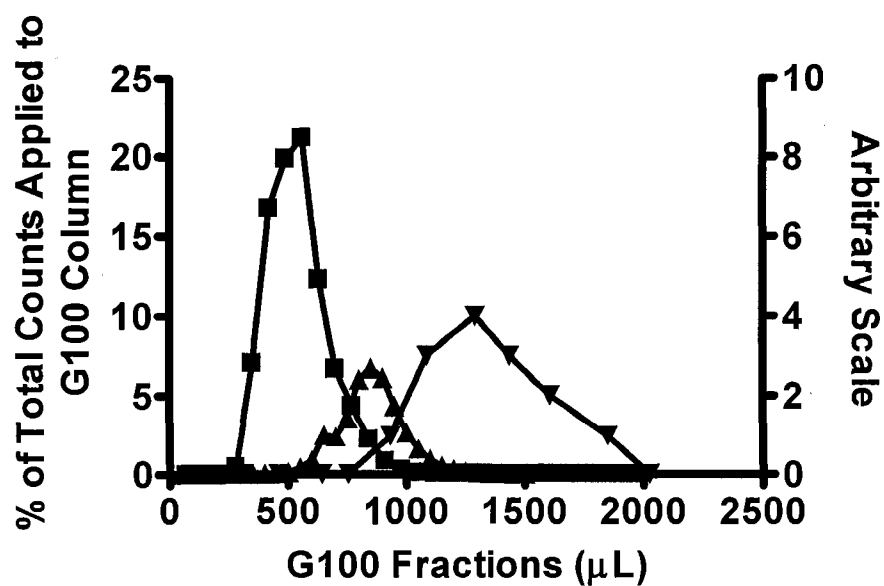


**Figure 3.7. Elution profile of a 1 mL G-100 column.** RGF 4G7 scFv-conjugated micelles and free <sup>125</sup>I-RGF 4G7 scFv were detected by gamma radioactivity (left Y-axis). DNP-threonine was detected by visual inspection of color (yellow) intensity of elution fractions (right Y-axis). RGF 4G7-micelles (■); Free <sup>125</sup>I-RGF 4G7 (▲); DNP-threonine (▼).

column volume. The results were not conclusive, but suggested that some covalent coupling of RGF 4G7 to Mal-PEG-DSPE may have occurred under the conditions tested.

In order to further characterize the reduction and coupling processes, Ellman's Assay was used to determine the number of free thiol groups present on the RGF 4G7 after reduction. This was done in order to test the hypothesis that excess 2-MEA may lead to destruction of internal disulfide bonds resulting in inactivation of the scFv and destruction of binding activity. RGF 4G7 was reduced with 2-MEA at a molar ratio of 1:2 (scFv:2-MEA); this resulted in 1.2 SH per scFv, suggesting that only the terminal Cys was reduced and the internal disulfide bonds remained intact.

When post-insertion of scFv-Mal-PEG-DSPE conjugates was again attempted, only 0.11 nmol RGF 4G7/ $\mu$ mol PL was detected, which was substantially lower than previous results obtained using the HD37-CCH construct. Again this suggested that only non-covalent association of the scFv with the surface of liposomes may have occurred. The binding of these SIL[RGF 4G7] to Raji cells was again no higher than the control untargeted liposomes (Fig. 3.8A).

Another control experiment was done in order to determine if the problem was only with RGF 4G7 constructs and not with the cells themselves. Raji cells were incubated with SL, SIL[RGF 4G7] or SIL[HD37 Fab'] (SIL targeted by HD37 anti-CD19 Fab') (Fig. 3.8B). The SIL[HD37 Fab'] had substantially higher binding than SL and SIL[RGF 4G7] indicating that CD19 antigens were present on the Raji cells.

In another set of experiments, direct coupling of RGF 4G7 to liposomes was also attempted. ScFv was reduced with 2-MEA at a molar ratio of 1:2 (scFv:2-MEA), which resulted in 0.6 free SH per molecule of scFv as measured by Ellman's assay. The amount

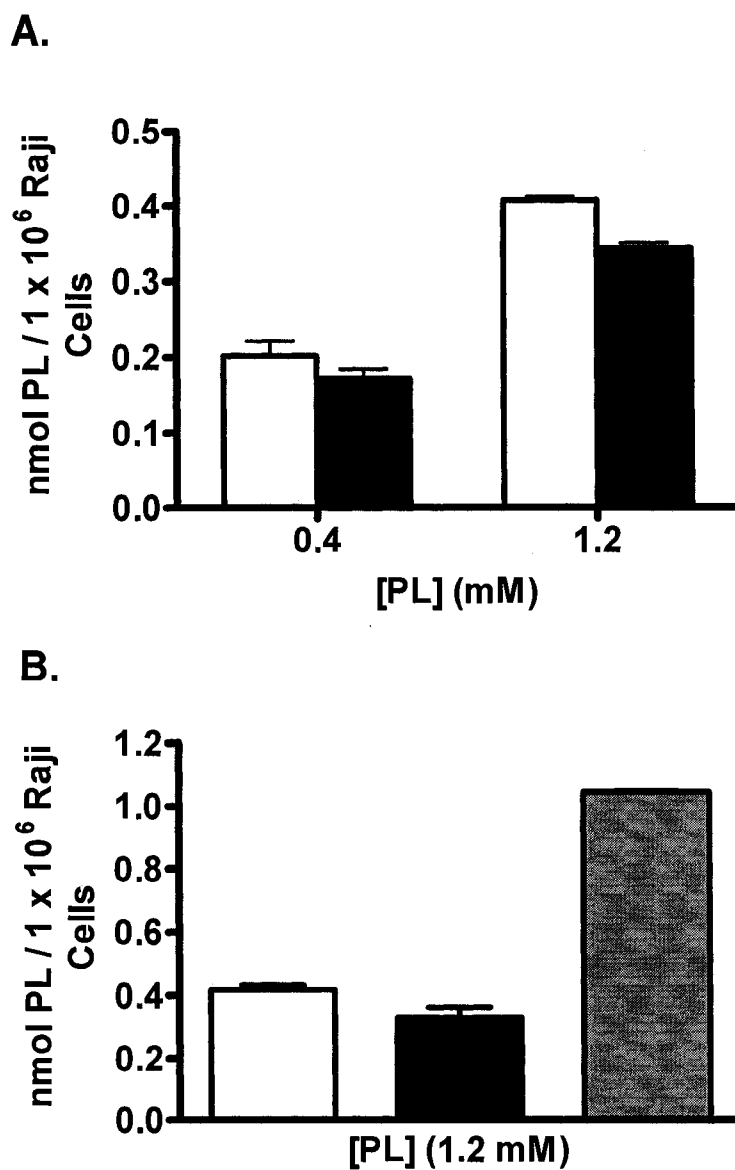


**Figure 3.8. Binding study of SIL[RGF 4G7] and SL to CD19<sup>+</sup> Raji cells.** A)  $1 \times 10^6$  cells were incubated with SIL[RGF 4G7] or SL at the indicated PL concentrations for 1 h at 37 °C. Binding was quantitated by scintillation counting of cell-associated liposomes labeled with <sup>3</sup>H-CHE. B)  $1 \times 10^6$  cells were incubated with SL, SIL[RGF 4G7] or SIL[HD37 Fab'] at a PL concentration of 1.2 mM for 1 h at 37 °C. WHITE bar: SL, BLACK bar: SIL[RGF 4G7], GREY bar: SIL[HD37 Fab'].

of scFv coupled to liposomes by the direct coupling method was also low (0.22 nmol/ $\mu$ mol PL) in comparison to previous results using other scFv constructs. Binding of the SIL[RGF 4G7] to Raji was again similar to untargeted SL (Fig. 3.9).

Subsequently, additional data has provided some clues to the cause of low coupling and binding of SIL[RGF 4G7]. Thermal stability studies have shown that RGF 4G7 formed insoluble aggregates when the scFv was subjected to temperatures similar to those used in the direct coupling method and the post-insertion procedure. Aggregation was shown to occur at each step of the procedure and an accumulated total of 60-75% of scFv was lost due to aggregation (Dr. S.E. Franklin, personal communication).

### 3.5. Discussion and Conclusions

This Chapter presented data on the use of various anti-CD19 scFv constructs to target liposomes to CD19<sup>+</sup> cells *in vitro*. The objective of the study was to find a scFv construct suitable for targeting liposome in comparison to mAb and Fab' fragments, and to explore different techniques for production and purification of scFv. From these results, it was found that each scFv construct requires individual optimization. Although it is not uncommon for expression and periplasmic space extraction yields to be in the range 0.1-1 mg/L of *E. coli* cultures, some studies have found that yields from 3-17 mg scFv/L of culture can be achieved (218).

The results from this study suggest that stability of scFv may be one of the most important factors that influence the success of a scFv as a targeting agent. Various studies have shown that *in vitro* stability of an scFv correlates positively with *in vivo* activity (219, 220). In addition, it has been shown that the stability of scFv fragments are temperature, pH and concentration sensitive, and substantial engineering of scFv

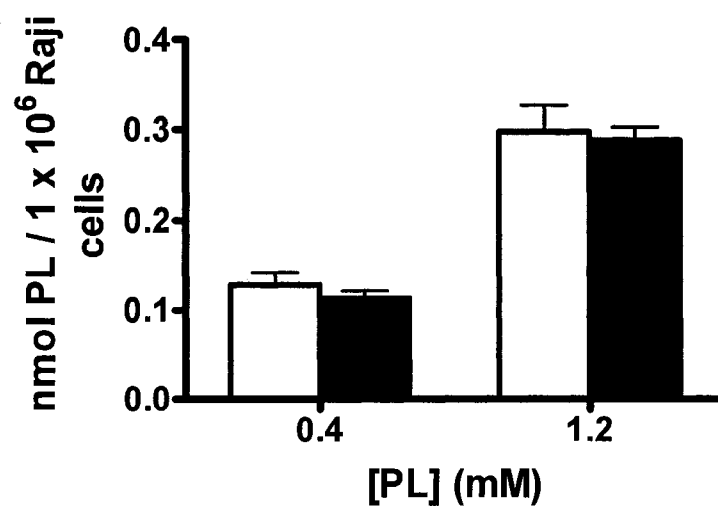


**Figure 3.9. Binding study of conventionally coupled SIL[RGF 4G7] and SL to CD19<sup>+</sup> Raji cells.**  $1 \times 10^6$  cells were incubated with SIL[RGF 4G7] or SL at the indicated PL concentrations for 1 h at 37 °C. Binding was quantitated by scintillation counting of cell-associated liposomes labeled with <sup>3</sup>H-CHE. WHITE bar: SL, BLACK bar: SIL[RGF 4G7].

constructs may be needed to alleviate such problems (221-223). Some studies have reported that low stability is an inherent issue associated with production and use of scFv, which may provide an explanation for the low stability of most of the scFv constructs used in this study; the lack of constant regions in scFv may play a partial role in this low stability (224). Most of the scFv constructs used in this study were not stable; they experienced aggregation and loss of activity at concentrations optimal for coupling to liposomes. In addition, the tested scFv constructs were also prone to aggregation during prolonged storage at 4 °C or -20 °C. Of the different constructs tested, only the HD37-CCH demonstrated sufficient stability for coupling to liposomes and affinity for Raji cells at 37 °C. This particular construct was therefore chosen for subsequent studies for comparison to its parental mAb and Fab'.

It can also be concluded that refolding scFv from inclusion bodies was more complex and difficult than originally anticipated. Refolding denatured scFv from inclusion bodies was mostly unsuccessful, despite the use of GSH, GSSG and arginine, all of which facilitate formation of internal disulfide bonds and proper folding of scFv constructs (156, 200, 225). During the refolding process, the scFv is in equilibrium with different, partially unfolded intermediates, which have exposed hydrophobic parts that are normally hidden in the native structure. Incomplete refolding will result in inactive proteins and aggregation (221, 222). In addition to the presence of a hydrophobic leader sequence in the nH-4G7-GC scFv construct, the existence of partially unfolded intermediates may provide a possible explanation for the high concentration of arginine needed to maintain this construct in solution during refolding. Although the refolded HD37-C construct was stable at concentrations optimal for coupling to liposomes, HD37-

C-coupled liposomes (SIL[HD37-C]) did not show any specific binding to CD19<sup>+</sup> cells. During the refolding process, the scFv can be trapped in a “thermodynamic sink”, where the protein remains in an intermediate state (226). This thermodynamic sink can lead to incomplete refolding, resulting in loss of activity, providing a possible explanation for the observations in this study.

The RGF 4G7 scFv was hypothesized to be more stable than the nH-4G7-GC since the RGF 4G7 scFv was expressed in algal cultures. Algal cultures do not require fusion of the construct to a hydrophobic leader sequence, which was necessary in the production of nH-4G7-GC expressed in bacteria. Indeed, the RGF 4G7 was stable in isotonic PBS as well as in concentrations optimal for coupling to liposomes. However, various coupling strategies were used to no avail in the coupling of this scFv on the surface of liposomes or its binding to Raji cells.

The hypothesis that low cell binding of the RGF 4G7 construct was a result of reduction of internal disulfide bonds can be excluded since a decrease in the molar ratio of scFv to reducing agent did not result in an increase in binding. The poor coupling and binding results are likely explained by the thermal stability data, which showed successive reductions in the amount of soluble scFv present in the samples during each subsequent step of either the direct coupling or the post-insertion procedure. Both 4G7 constructs (nH-4G7-GC and RGF 4G7) may have less intrinsic stability than the HD37-CCH construct, since both of the 4G7 constructs were prone to aggregation and did not show sufficient stability for targeting liposomes, when expressed and purified using either bacterial or algal expression systems.

Because the RGF 4G7 scFv has higher affinity for CD19 than the HD37-CCH (197), in the future it might be worthwhile to explore other strategies to increase the stability of the 4G7 scFv fragment. One strategy would be to select randomly mutated clones from a phage-display library that has both high affinity for CD19 and increased thermal stability (223). Alternatively the complementarity determining region (CDR) of 4G7 can be grafted onto the backbone of a more stable scFv construct (219).

In conclusion, for the purpose of finding a scFv suitable for targeting liposomes, it may be more time-efficient to employ a rational approach where a specific construct is initially chosen and then subsequently modified to optimize specific properties such as enhanced stability and affinity.

## Chapter 4

### **Expression and Purification of an Anti-CD19 Single Chain Fv Fragment for Targeting of Liposomes to CD19-expressing Cells**

(This chapter is published. Cheng W. W., Das D., Suresh M. R. and Allen T. M.; *Biochim. Biophys. Acta*, 1768(1): 21–29, 2007)

## 4. Expression and Purification of an Anti-CD19 Single Chain Fv Fragment for Targeting Liposomes to CD19-expressing Cells

### 4.1. Abstract

Antibody-targeted liposomal anticancer drugs combine the specificity of antibodies with large payloads of entrapped drugs. It was previously shown that liposomal doxorubicin (DXR) targeted via anti-CD19 monoclonal antibodies (mAb) or their Fab' fragments against the B-cell antigen CD19 led to improved therapeutic effects in murine B-cell lymphoma models relative to untargeted liposomal DXR. The use of anti-CD19 single chain fragments of the antibody variable region (scFv) as a targeting moiety is now being examined in order to test the hypothesis that scFv fragments have advantages over full-sized mAb or Fab' fragments. An anti-CD19 scFv construct, HD37-CCH, was expressed in *E. coli*. The HD37-CCH construct was selected for coupling studies due to its relative stability and activity. When coupled to liposomes, the HD37-CCH scFv showed increased binding *in vitro* to CD19-positive Raji cells, compared to untargeted liposomes. Cytotoxicity data showed that HD37-CCH scFv-targeted liposomes loaded with DXR were more cytotoxic than untargeted liposomal DXR. These results suggest that anti-CD19 scFv constructs should be explored further for their potential in treating B-lymphoid leukemias and lymphomas.

### 4.2. Introduction

The use of antibodies and antibody fragments as cancer therapeutics have flourished in recent years and led to the clinical approval of several monoclonal antibodies, including Rituxan<sup>®</sup> (rituximab) and Herceptin<sup>®</sup> (trastuzumab) (227, 228).

Currently, more than 150 mAbs are in clinical trials worldwide (229). Immunoconjugates, where mAbs are covalently linked to a few molecules of drugs, toxins or radioisotopes, have also been successfully commercialized, e.g., Zevalin<sup>®</sup> (ibritumomab tiuxetan), Bexxar (<sup>131</sup>I-tositumomab), and Mylotarg<sup>®</sup> (gemtuzumab ozogamicin) (13, 230, 231). Additive or synergistic effects have been demonstrated in patients when combinations of signaling antibodies such as rituximab and conventional chemotherapeutic drugs are administered (7, 232).

Although mAbs can be highly selective for their targets, their properties are not ideal for continued administration in patients since immune reactions can occur, particularly to antibodies containing foreign (e.g., mouse) regions (233). Antibody fragments, such as Fab' fragments (~55 kDa) and single chain fragments of the variable region (~35 kDa) lack the Fc domain, and thus the dominant immunogenic determinants. Fab' and scFv fragments can be selected by phage display and are more easily engineered than mAbs to control properties such as affinity or internalization capabilities (234). They can be produced by a variety of methods including bacterial and algal fermentation, which should decrease their production costs (142). Many laboratories are currently investigating the use of these small fragments for the treatment of cancers (62, 92, 138, 217, 235, 236).

Liposomes are phospholipid bilayer spheres that can encapsulate drugs in their aqueous interior. The grafting of PEG to the surface of liposomes (termed Stealth<sup>®</sup> liposomes) serves two purposes: the polymer terminus is a convenient location for the coupling of targeting ligands such as mAbs and derived fragments, and these liposomes have circulation half-lives of several hours, which allows sufficient time for the

liposomes to access and bind to the target cells (61, 63, 92, 236). Several liposomal drugs are currently on the market, including Caelyx/Doxil<sup>®</sup> (a Stealth<sup>®</sup> liposomal formulation of the anticancer drug doxorubicin, which is approved for AIDS-related Kaposi's sarcoma, refractory ovarian and metastatic breast cancers) (237). Currently no ligand-targeted liposomes are in the clinic, but extensive preclinical research activity is taking place in this area. The concept is similar to that of antibody-drug conjugates, with the advantage that targeted liposomes can deliver a far greater payload of drug per antibody, i.e., several hundred drug molecules per antibody, relative to less than 10 drug molecules per antibody for the antibody-drug conjugates. This can result in increased therapeutic effect for fewer antibodies, leading to reduced antibody-associated side effects and reduced expense (12, 237-239).

The Allen laboratory has had a long-standing interest in disease targets that are readily accessible from the vasculature, including B and T cell haematological malignancies and the vasculature of solid tumors. Non-Hodgkin's lymphoma, the most common B-cell malignancy, is the 5<sup>th</sup> most common cause of new cases of cancer in North America and accounts for approximately 4 to 5 percent of new cases of cancer every year (1, 2). B-cell malignancies generally respond well to initial chemotherapy, especially the combination of Rituxan<sup>®</sup> plus CHOP (cyclophosphamide, doxorubicin, vincristine and prednisone) (7, 8, 114). Unfortunately, a substantial percentage of patients who respond to initial therapy will relapse. This is thought to result from the incomplete eradication of residual malignant B-lymphoid cells and/or their progenitors, and justifies the search for therapies that can eradicate these cells. The CD19, CD20 and CD22 antigens are expressed on a high percentage of malignant B-lymphoid cells in

lymphoma patients (240, 241). Since these antigens are found primarily on mature B cells and not on their precursor cells, they are good targets for directing therapeutics against malignant B-lymphoid cells.

It was previously shown that anti-CD19-targeted liposomal DXR led to improved therapeutic effects in murine models of human B lymphoma (Namalwa) relative to free DXR or untargeted liposomal DXR (61, 62, 204, 206). The potential advantages of using scFv fragments, in relation to mAb and Fab', for targeting liposomes to B-cell malignancies, are now being explored in this study. In the current study, a construct of anti-CD19 scFv was tested for ease of production from *E. coli* fermentation and for ease of purification, storage and stability. Cell binding and cytotoxicity of the anti-CD19 scFv immunoliposomes were compared to untargeted liposomes.

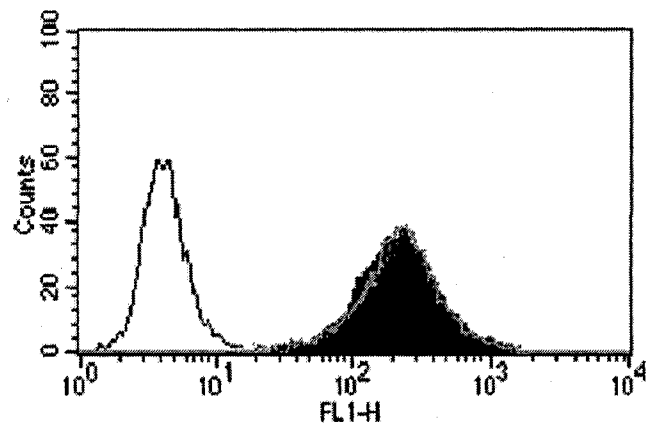
#### **4.3. Antibodies and ScFv Constructs Used**

For this study, the anti-CD19 FMC63 mAb, HD37 mAb, and the HD37-CCH scFv were used (see Chapter 2 for details).

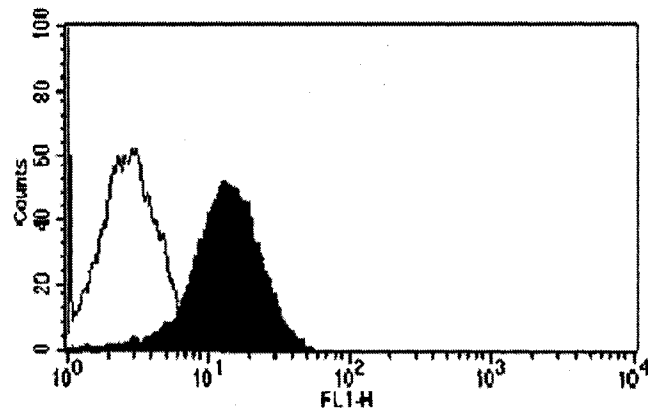
#### **4.4. Results**

Using FACS, both parental full-length CD19 mAbs, FMC63 and HD37, were demonstrated to bind similarly to the B-lymphoid cell line Namalwa (Fig. 4.1A). As well, the scFv fragment, HD37-CCH, extracted from the periplasmic space also bound to another CD19<sup>+</sup> B-cell line, Raji (Fig 4.1B). Using a Lineweaver-Burk analysis, the  $K_D$  of FMC63 mAb was found to be in the range of  $1-3 \times 10^{-9}$  M (Fig 4.2). The  $K_D$  of the HD37 whole mAb was in the range of  $2-3 \times 10^{-9}$  M (Fig. 4.3), which was approximately

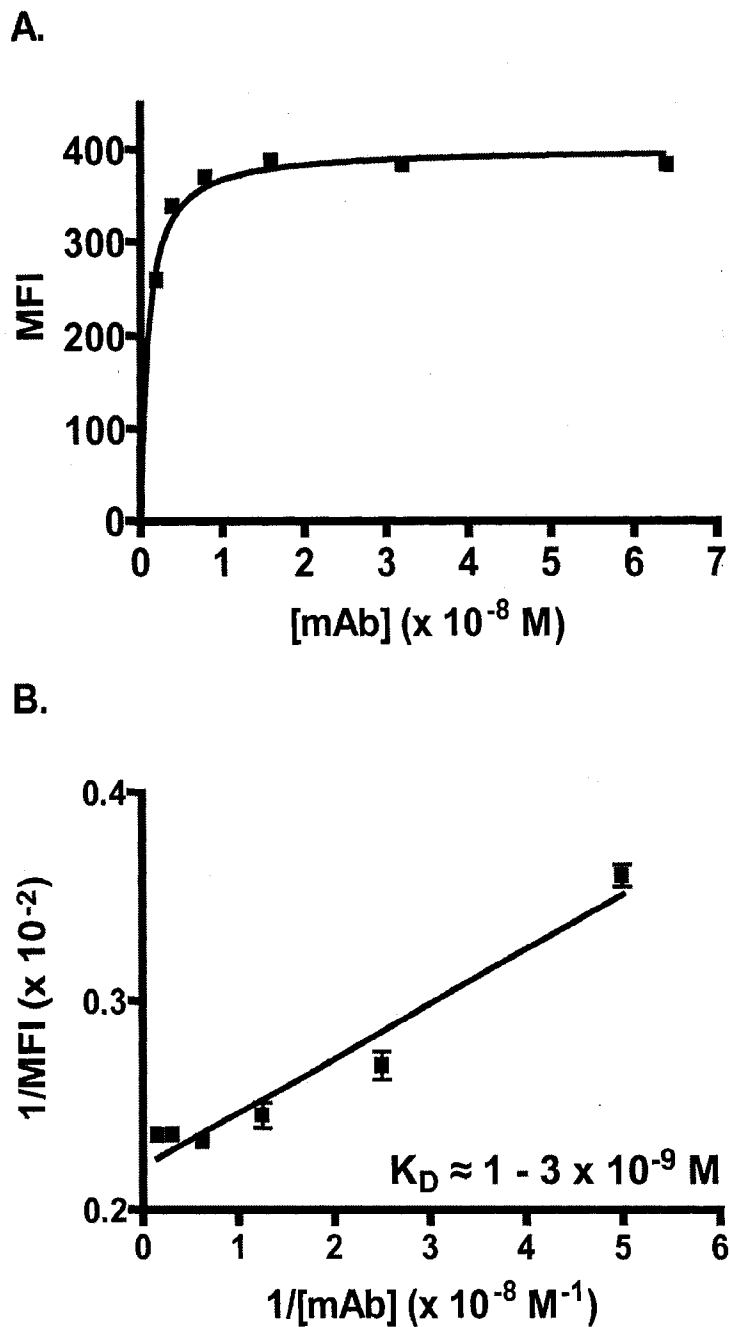
A.



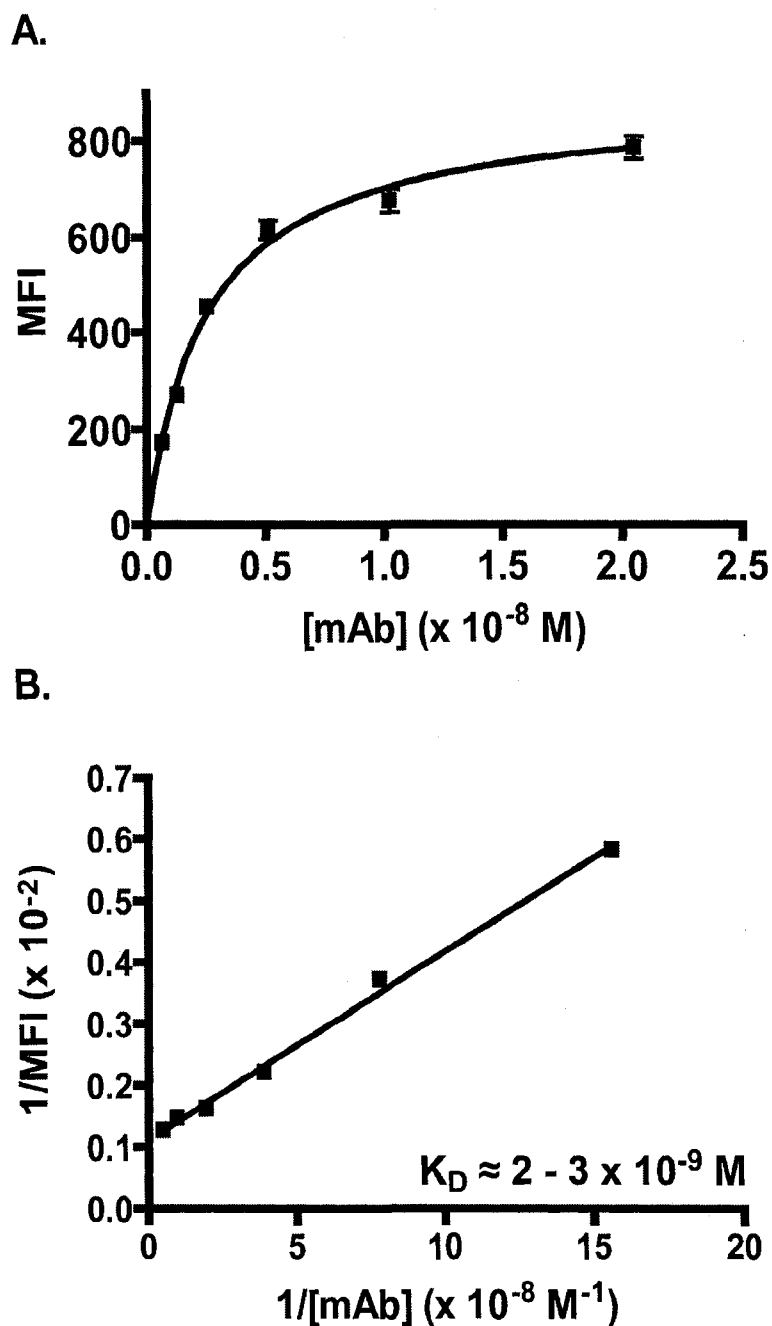
B.



**Figure 4.1. Flow cytometry analysis.** A)  $1 \times 10^6$  Namalwa cells treated with  $10 \mu\text{g}$  of either FMC63 mAb or HD37 mAb. HD37 mAb (■); FMC63 mAb (□); no treatment control (□). B) Binding of periplasmic extracted HD37-CCH with Raji cells. HD37-CCH (■); no treatment control (□). Additional controls, in which the fluorescence were the same as the auto-fluorescence of untreated cells, included cells treated with GAM-FITC, cells treated with anti-His mAb, and cells treated with anti-His mAb plus GAM-FITC.



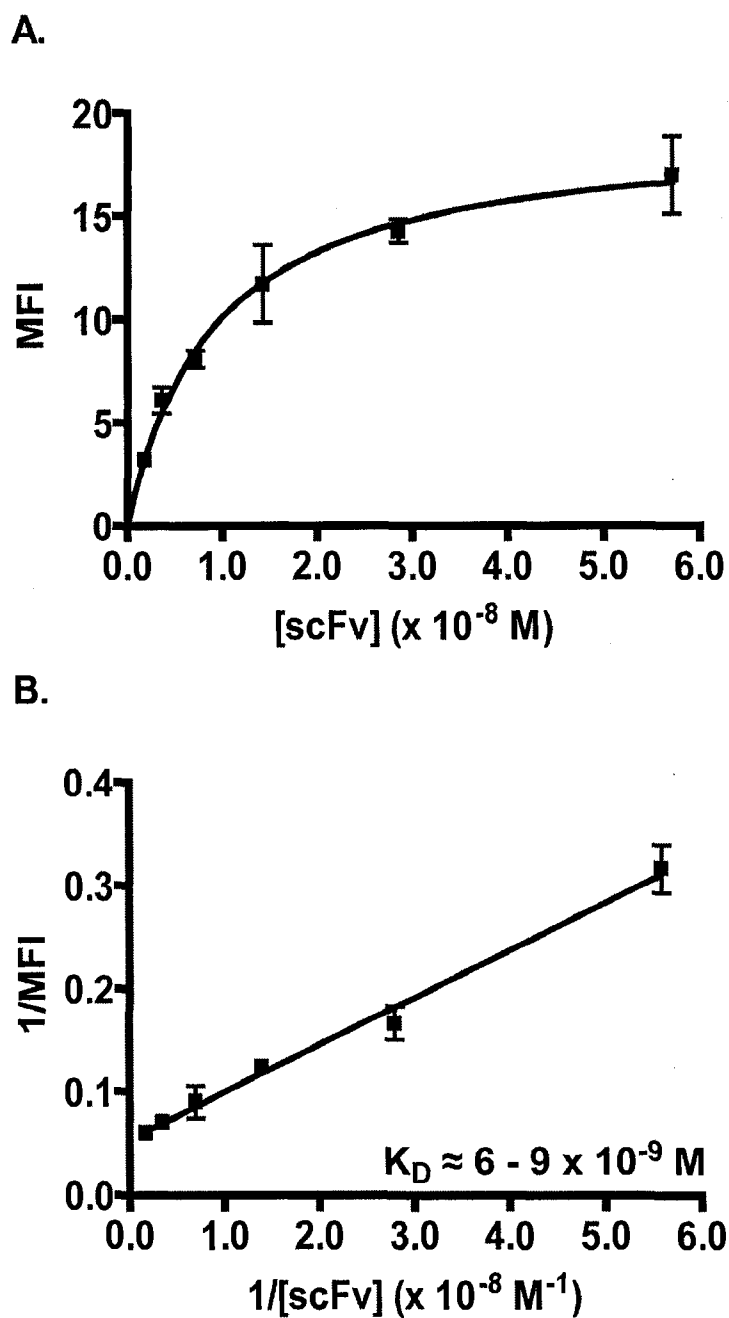
**Figure 4.2. Mean fluorescence intensity (MFI) as a function of concentration of FMC63 mAb.** MFI was measured by FACS as described in Chapter 2. **A)** MFI as a function of increasing concentration of FMC63 mAb. **B)** Double reciprocal plot of MFI vs. [FMC63 mAb] for Lineweaver-Burk analysis of the equilibrium dissociation constant ( $K_D$ ).



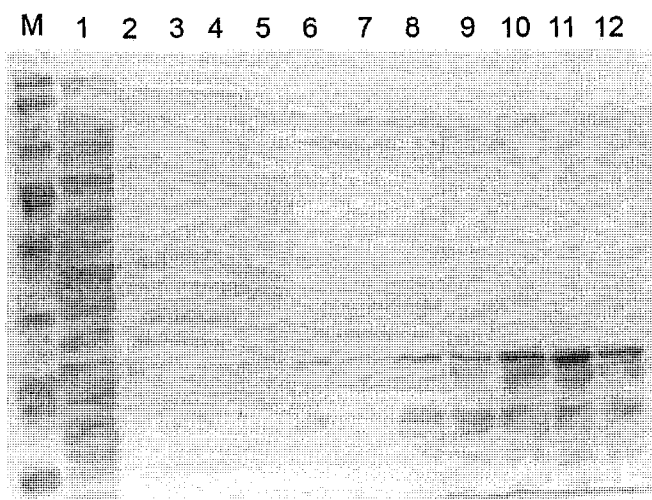
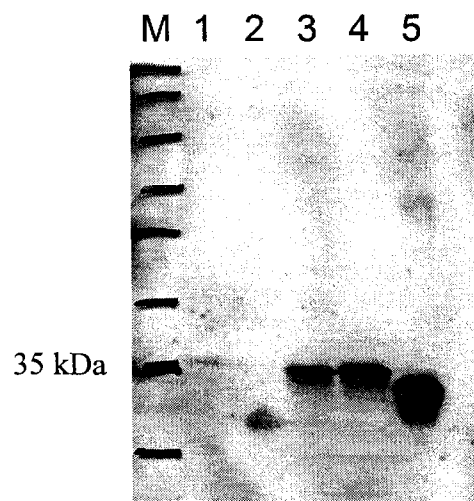
**Figure 4.3. Mean fluorescence intensity (MFI) as a function of concentration of HD37 mAb.** MFI was measured by FACS as described in Chapter 2. **A)** MFI as a function of increasing concentration of HD37 mAb. **B)** Double reciprocal plot of MFI vs. [HD37 mAb] for Lineweaver-Burk analysis of the equilibrium dissociation constant ( $K_D$ ).

3-fold lower than that of the scFv fragment, HD37-CCH ( $K_D \approx 6-9 \times 10^{-9}$  M) (Fig. 4.4).

When the HD37-CCH construct was purified from periplasmic extracts, modest yields of 0.4-0.6 mg/L culture were obtained. The scFv was present in whole cell lysates and periplasmic extracts (Fig. 4.5B) and was enriched in eluate fractions after affinity purification (Fig. 4.5A and B). The purified protein bound to CD19-positive cells (Fig. 4.1B) and was stable in PBS. The purified HD37-CCH scFv was coupled to liposomes resulting in a coupling density of 0.4-0.6 nmol/ $\mu$ mol PL (20-29% coupling efficiency). SIL[HD37-CCH] showed increased binding to Raji cells compared to SL (Fig. 4.6A and B) and the increased binding was abolished when cells were pre-incubated with the whole HD37 mAb in a competition experiment. Thus, binding of SIL[HD37-CCH] was specific to CD19. In another control, a mixture of unconjugated HD37-CCH and SL did not result in an increase in binding compared to SL. Specific binding of SIL[HD37-CCH] at 37 °C (permissive for internalization) and 4 °C (non-permissive for internalization) were also compared (Fig. 4.6C). Increased liposome uptake and binding occurred at 37 °C relative to 4 °C, probably due to recycling of CD19 at 37 °C following receptor-mediated internalization. When binding of SIL[HD37-CCH] to CD19<sup>-</sup> Molt4 control cells was tested, there was no difference between the binding of SIL[HD37-CCH] and SL (Fig. 4.6D). The binding of SIL[HD37-CCH] and SIL[HD37 mAb] to Raji cells was also compared. Taking into consideration that each mAb has two antigen binding sites, the number of available binding sites on SIL[HD37-CCH] and SIL[HD37 mAb] were 0.45 nmol/ $\mu$ mol PL (16  $\mu$ g scFv / $\mu$ mol PL) and 0.32 nmol/ $\mu$ mol PL (25  $\mu$ g mAb / $\mu$ mol PL) respectively. At similar numbers of available binding sites on the surfaces of



**Figure 4.4. Mean fluorescence intensity (MFI) as a function of concentration of HD37-CCH.** MFI was measured by FACS as described in Chapter 2. **A)** MFI as a function of increasing concentration of HD37-CCH. **B)** Double reciprocal plot of MFI vs. [HD37-CCH] for Lineweaver-Burk analysis of the equilibrium dissociation constant ( $K_D$ ).

**A.****B.**

**Figure 4.5. Purification of HD37-CCH after periplasmic extraction.** A) SDS-PAGE gel of purified HD37-CCH after purification using a Ni-NTA column. Lane M, molecular weight markers; Lane 1, unbound fraction; Lane 2-7, wash fractions; lanes 8-12, eluted fractions of scFv. B) Western blot of HD37-CCH fragments, detected using murine anti-His mAb and then GAM-HRP. Lane M; molecular weight markers: Lanes 1 and 2: periplasmic extracts; Lanes 3 and 4: purified HD37-CCH; Lane 5: positive control (poly-His-containing scFv).

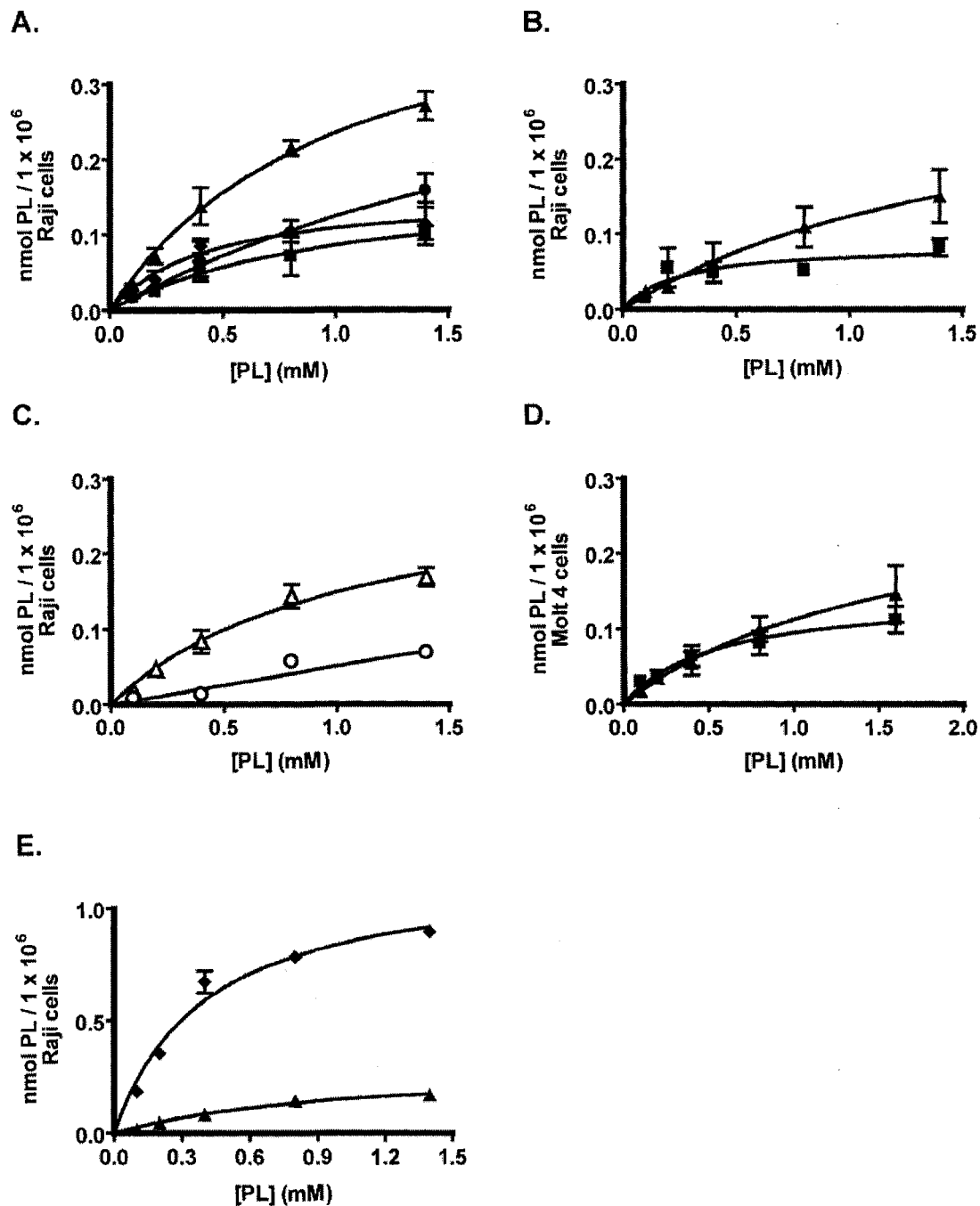


**Figure 4.6. Binding of SIL[HD37-CCH] to Raji Cells.**  $1 \times 10^6$  Raji cells were incubated with increasing PL concentrations of SIL[HD37-CCH] or SL for 1 h. For the competition study, Raji cells were pre-incubated with 100  $\mu$ g of HD37 mAb (7.5- to 120-fold excess) for 15 min. Binding was measured by scintillation counting of the liposomal <sup>3</sup>H-CHE label. **A)** Binding at 37 °C. SIL[HD37-CCH] (▲), SIL[HD37-CCH] + HD37 mAb (●), HD37-CCH + SL (◆), SL (■). **B)** Binding at 4 °C. SIL[HD37-CCH] (▲), SL (■). **C)** Specific binding of SIL[HD37-CCH]. 37 °C (Δ), 4 °C (○). **D)** Binding to Molt4 cells at 37 °C. SIL[HD37-CCH] (▲), SL (■). **E)** Specific binding of SIL[HD37-CCH] and SIL[HD37 mAb] at 37 °C. SIL[HD37-CCH] (▲), SIL[HD37 mAb] (◆).

liposomes, the binding of SIL[HD37 mAb] at 37 °C was significantly better than for the SIL[HD37-CCH] (Fig. 4.6E).

In vitro MTT cytotoxicity study, with a 1 h incubation, demonstrated that SIL-DXR[HD37-CCH] were approximately 11-fold more cytotoxic to Raji cells than untargeted SL-DXR. The concentrations of drugs inhibiting 50% of cell growth ( $IC_{50}$ s) were  $21 \pm 9 \mu\text{M}$ ,  $244 \pm 36 \mu\text{M}$  and  $225 \pm 33 \mu\text{M}$  for SIL-DXR[HD37-CCH], SL-DXR and HD37-CCH + SL-DXR, respectively. The  $IC_{50}$  for the free drug was  $0.7 \pm 0.4 \mu\text{M}$ . There was no toxicity observed when Raji cells were treated with free HD37-CCH at concentrations which were typically found on the surface of SIL-DXR[HD37-CCH].  $IC_{50}$ 's for Molt4 cells treated with SIL-DXR[HD37-CCH], SL-DXR and free DXR were  $235 \pm 71 \mu\text{M}$ ,  $181 \pm 35 \mu\text{M}$ , and  $0.6 \pm 0.1 \mu\text{M}$  respectively.

#### 4.5. Discussion and Conclusions

FMC63 and HD37 effectively bound to the B-lymphoid cell lines, and both mAbs produced a greater than 2 log shift in fluorescence, indicating efficient binding of the mAbs to the CD19 antigen on intact cells. Binding profiles to Raji cells of both antibodies were similar to those obtained with Namalwa cells (not shown). The HD37-CCH scFv also interacted efficiently with Raji cells, producing approximately a 1 log shift in fluorescence intensity. Using the standard radiolabeled mAb assay, the reported equilibrium dissociation constant ( $K_D$ ) for FMC63 mAb is  $2.4 \times 10^{-10}$  M, while the  $K_D$  of HD37 mAb is  $3.3 \times 10^{-9}$  M (212, 242), which are similar to the results that were observed in this study. However, the flow cytometry assay used in this study assumes that the calculation of the  $K_D$  value of the scFv was not affected by the avidity of the anti-His antibody (i.e., the detection antibody) for the scFv.

The HD37-CCH scFv, when coupled to the surface of liposomes, resulted in specific and increase binding of the immunoliposomes into Raji cells. The binding of SIL[HD37-CCH] to Raji cells also resulted in internalization of these liposomes. These results are similar to published studies using the FMC63 mAb and Fab'-conjugated liposomes (61, 62). In these studies, the conjugation of the mAb and Fab' to the surfaces of liposomes led to internalization of the immunoliposomes, recycling of CD19 and higher uptake and binding at 37 °C than at 4 °C. A significant difference in cell-binding was observed when SIL[HD37-CCH] was compared to SIL[HD37 mAb] at similar densities of binding sites on the surface of liposomes. The decrease in uptake and binding of SIL[HD37-CCH] was speculated to be due to a decrease in avidity of the scFv for CD19 in comparison to the mAb. Normally, a decrease in avidity is observed when single chain fragments are compared to their parent mAb. This agrees with the observation of targeted liposomes where avidity of SIL[HD37-CCH] to Raji cells was decreased by approximately 3-fold when compared to SIL[HD37 mAb]. A decrease in avidity could also lead to the decreased binding of SIL[HD37-CCH]. Coupling ligands with single binding sites, e.g., Fab' or scFv, to liposomes will make them multivalent, but the degree to which this will restore avidity will depend on factors such as the ligand concentration and its degree of flexibility and orientation.

The increase in cytotoxicity of SIL-DXR[HD37-CCH] can be attributed to the targeting of the CD19 antigen and internalization of the liposome-drug package. For a 1 h incubation, prior to washing away the liposomes very little leakage of DXR from either the targeted or untargeted formulation of liposomal DXR is expected, since they have leakage half lives in excess of 90 h (85). The current cytotoxicity results with the HD37-

CCH scFv fragment is consistent with previous results, showing that DXR-loaded anti-CD19 mAb and Fab' immunoliposomes were more cytotoxic than SL (62, 63, 104, 204). In addition, the increase in cytotoxicity associated with SIL-DXR[HD37-CCH] was shown to be CD19-mediated. The  $IC_{50}$ s of Raji cells, treated with a mixture of unconjugated SL-DXR + HD37-CCH and SL-DXR, and the  $IC_{50}$ s of Molt4 cells (CD19) treated with either SIL-DXR[HD37-CCH] or SL-DXR, were similar. For this *in vitro* assay, it is not surprising to find that the cytotoxicity of free DXR is higher than that of the slow release liposomal formulations, since free drug will diffuse rapidly into the cells during the 1 h incubation and the free drug concentrations for the free DXR group are considerably higher than those for the liposomal group, where almost no free drug is present at 1 h. This observation is similar to previous findings (61, 62, 104).

In comparison with other DDS, such as drug-conjugated polymers, antibody-targeted liposomal drugs can selectively deliver large payloads of drugs to cancer cells. Small antibody fragments, such as scFv, can reduce the immunogenicity associated with larger fragments of foreign origin. Many groups have demonstrated the potential of using scFv as targeting moieties for liposomal anticancer drugs (91, 138, 217, 243) and at least one formulation of scFv-coupled liposomal doxorubicin is near clinical testing (66). It was found that although isolating scFv from inclusion bodies with subsequent refolding can dramatically increase protein yield, the purified scFv may not refold properly, leading to issues with activity and stability. On the other hand, extraction of the native scFv from the periplasmic space, although producing relatively smaller amounts of protein, resulted, in these experiments, in proteins that are active and are relatively stable. Therefore, it was concluded that this is the method of choice for producing scFv fragments for future

studies in this thesis. After some preliminary experiments with the HD37-C construct, the HD37-CCH was selected for subsequent experiments due to its stability and affinity for the CD19 antigen. When the scFv is conjugated to the surface of liposomes, these HD37-CCH immunoliposomes can specifically bind to CD19-expressing cells and trigger internalization of the liposome package. Initial cytotoxicity studies demonstrated that the doxorubicin-loaded SIL[HD37-CCH] was more cytotoxic than Caelyx<sup>®</sup>, a commercial formulation of untargeted Stealth<sup>®</sup> liposomal doxorubicin. Future experiments will examine the *in vivo* pharmacokinetics properties and therapeutic activity of the SIL[HD37-CCH] in comparison to liposomes targeted with the HD37 mAb and HD37 Fab'.

## Chapter 5

### **Targeted Delivery of Anti-CD19 Liposomal Doxorubicin in B-cell Lymphoma: A Comparison of Whole Monoclonal Antibody, Fab' and Single Chain Fv Fragments**

(This chapter is published. Cheng W. W. and Allen T. M., J. Control Release, 2007 Nov 17, [Epub ahead of print])

## 5. Targeted Delivery of Anti-CD19 Liposomal Doxorubicin in B-cell Lymphoma: A Comparison of Whole Monoclonal Antibody, Fab' and Single Chain Fv Fragments

### 5.1. Abstract

This study compared long-circulating (Stealth<sup>®</sup>) immunoliposomes (SIL) that were targeted against the B-cell antigen CD19, via a whole HD37 monoclonal antibody (HD37 mAb), versus its Fab' fragment (HD37 Fab') or an HD37-c-myc-Cys-His5 single chain Fv fragment (scFv, HD37-CCH) directed against the same epitope. Compared to untargeted liposomes (SL), SIL showed increased binding *in vitro* to CD19-expressing Raji cells and, when loaded with doxorubicin (SIL-DXR), increased cytotoxicity against Raji (CD19<sup>+</sup>), but not Molt4 (CD19<sup>-</sup>) cells. Pharmacokinetics and biodistribution studies using dual-labeled liposomes (lipid and drug) in naïve and Raji-bearing mice showed that SIL-DXR targeted via HD37 Fab' exhibited the same long circulation half-life as SL-DXR. SIL-DXR targeted via HD37-CCH was cleared faster than SL-DXR due to increased liver uptake and binding, which is related to the poly-His and/or the c-myc tags in the scFv construct. SIL-DXR targeted via HD37 mAb was cleared rapidly from circulation due to Fc receptor-mediated uptake and binding in the liver and spleen. All three formulations of SIL-DXR extended the mean survival time of Raji-bearing mice compared to SL-DXR or free DXR. SIL-DXR targeted via HD37 Fab', which had the longest circulation half-life, appeared to be slightly more effective in prolonging survival times than SIL-DXR targeted via either HD37-CCH or HD37 mAb.

## 5.2. Introduction

Conventional anticancer drugs have many adverse effects resulting from non-selective toxicity and distribution of the drug to normal cells. Liposomes were one of the first nanoparticulate drug delivery systems to show increased delivery of small molecule anticancer drugs to solid tumors (244, 245). Drug-loaded liposomes with diameters in the range of 100 nm can accumulate in solid tumors, but not normal tissue, via the enhanced permeability and retention (EPR) effect (43, 44), which occurs when nanoparticles extravasate from the circulation into tumors through gaps in the tumor vasculature endothelium (45). Once there, the liposomes release their contents at a rate that is determined by the physical properties of the liposome and the drug (18). The ability of liposomes to localize in tumors via the EPR effect depends in part on having long circulation half-lives ( $t_{1/2}$  on the order of 24 h or longer), which can be achieved by grafting polyethylene glycol (PEG) to the surface of the liposomes (i.e., Stealth<sup>®</sup> liposomes, SL). A Stealth<sup>®</sup> or PEGylated liposomal formulation of the anticancer drug doxorubicin (DXR), Doxil/Caelyx<sup>®</sup>, which has an increased therapeutic index in various solid tumors such as ovarian cancer relative to the free drug, has been in clinical use for over a decade (48, 246).

Stealth<sup>®</sup> liposomal drugs can be specifically targeted to cancer cells by surface conjugation of one or more of a variety of ligands against tumor antigens that are uniquely expressed or over-expressed on the tumor cells, including whole monoclonal antibodies (mAb) or their fragments, e.g., Fab' or single chain Fv (scFv) (12, 136). Although no immunoliposomes are yet in clinical use, extensive preclinical research activity is taking place in this area.

Previously published studies from this laboratory have shown that treatment with Stealth<sup>®</sup> immunoliposomal doxorubicin (SIL-DXR), targeted via the FMC63 anti-CD19 mAb or its Fab' fragment, resulted in increased survival times in murine models of human B lymphoma relative to free DXR or untargeted Stealth<sup>®</sup> liposomal DXR (SL-DXR) (62). The CD19 antigen is an attractive target for delivery of liposomal anticancer drugs since it is an internalizing antigen exclusive to B cells, and it is expressed in most types of B-lymphoid malignancies (211). Internalization of the antibody-CD19 complex has been shown to be important for delivery of liposomal DXR (104, 212).

At the pre-clinical development stage of antibody-targeted liposomes it is important to have a clear understanding of the advantages and disadvantages of the use of whole mAb vs. Fab' or scFv fragments as targeting ligands. Factors to be considered include the ease of production, yield, ease of purification, stability, affinity and avidity, immunogenicity and pharmacokinetics/biodistribution (PK/BD) (197). Improved circulation half-lives and therapeutic effects have been observed when SIL conjugated with various Fab' were compared to SIL conjugated with the parental whole mAb, since Fab'-targeted liposomes avoid Fc receptor-mediated clearance (62, 92, 137). In this study, these experiments have now been extended to include a comparison with scFv fragments. Using SIL targeted via the anti-CD19 HD37 mAb, compared to its Fab' and scFv constructs, all of which bind to the same epitope on CD19, the current study examined the *in vitro* binding and cytotoxicity, the *in vivo* pharmacokinetics and biodistribution (PK/BD), and therapeutics of all three formulations of anti-CD19 SIL, compared to untargeted liposomes.

### 5.3. Whole Monoclonal Antibody and Fragments of Antibody Used

The HD37 mAb, Fab' and HD37-CCH scFv were used in this study (Chapter 2 for details).

### 5.4. Results

In some initial experiments with the scFv fragment stored at -20 °C, the scFv-targeted liposomes failed to bind to B cells and it was suspected that the fragment was not stable to frozen storage. This was confirmed by FACS (Fig. 5.1A). In an attempt to increase the storage stability, and in the interests of simplifying the preparations of the SIL, immediately after purification of the scFv, it was coupled to Mal- PEG<sub>2000</sub>-DSPE micelles before storage at -20 °C. This resulted in retention of the binding activity of the scFv (Fig. 5.1B), and preparation of SIL[HD37-CCH] from the scFv-conjugated PEG micelles using the post-insertion method (98) showed good binding to B cells. Subsequently, all SIL were prepared using the post-insertion method.

All three formulations of SIL showed increased total (i.e., specific + non-specific) binding with Raji cells compared to SL (Fig 5.2). Figure 5.2 (A to C) shows the specific binding (total minus non-specific) of SIL[HD37-CCH], SIL[HD37 Fab'] and SIL[HD37 mAb] at different surface densities of CD19 binding sites. At the densities tested, binding of SIL[HD37-CCH], SIL[HD37 Fab'] and SIL[HD37 mAb] to Raji cells was not affected by changes in surface density of CD19 binding sites. At similar binding site densities, cell binding of SIL[HD37 Fab'] was similar to SIL[HD37 mAb], but higher than SIL[HD37-CCH] (Fig. 5.2D).

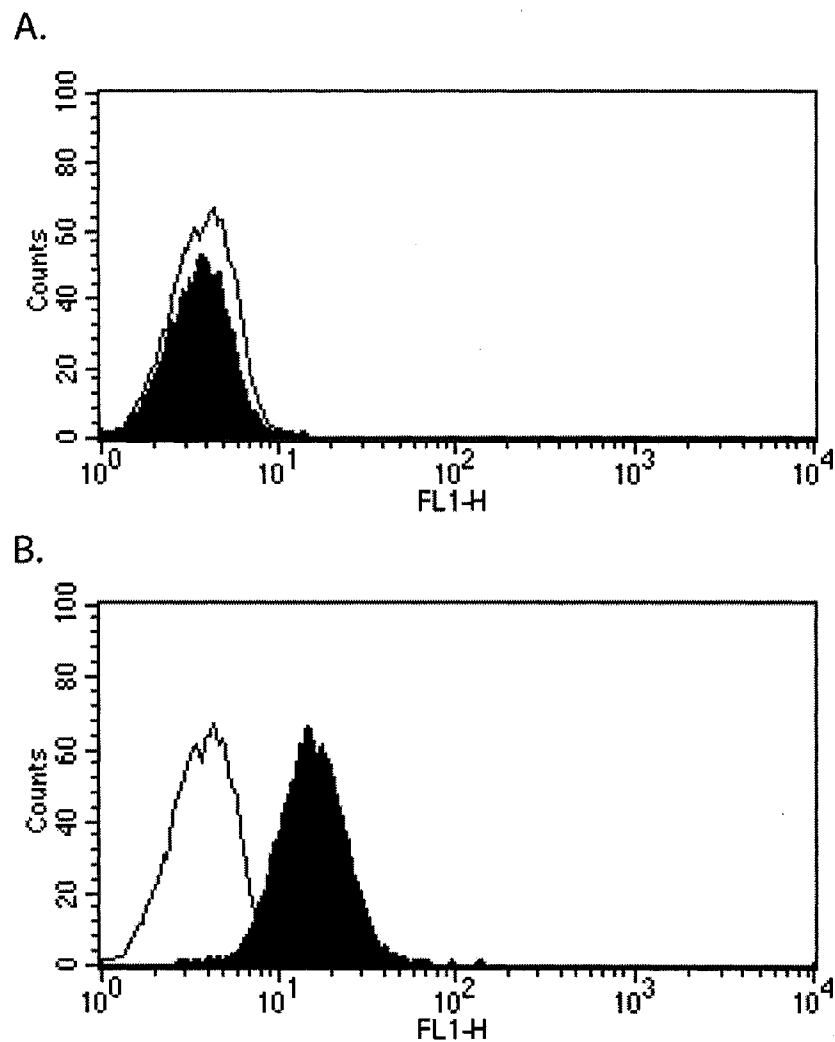


**Figure 5.1. Binding of HD37-CCH and HD37-CCH Mal-PEG<sub>2000</sub>-DSPE micelles to Raji cells.** Free scFv or scFv-conjugated micelles were stored at  $-20^{\circ}\text{C}$  and then incubated with  $1 \times 10^6$  Raji cells for 1 h at  $4^{\circ}\text{C}$ . Binding was analyzed by FACS. **A)** Binding of free HD37-CCH (0.14 nM). HD37-CCH (■); no treatment control (□). **B)** Binding of HD37-CCH Mal-PEG<sub>2000</sub>-DSPE micelles (0.14 nM). HD37-CCH Mal-PEG<sub>2000</sub>-DSPE micelles (■); no treatment control (□). Additional controls, with similar fluorescence to untreated cells, included cells treated with anti-His mAb and cells treated with anti-His mAb plus GAM-FITC.

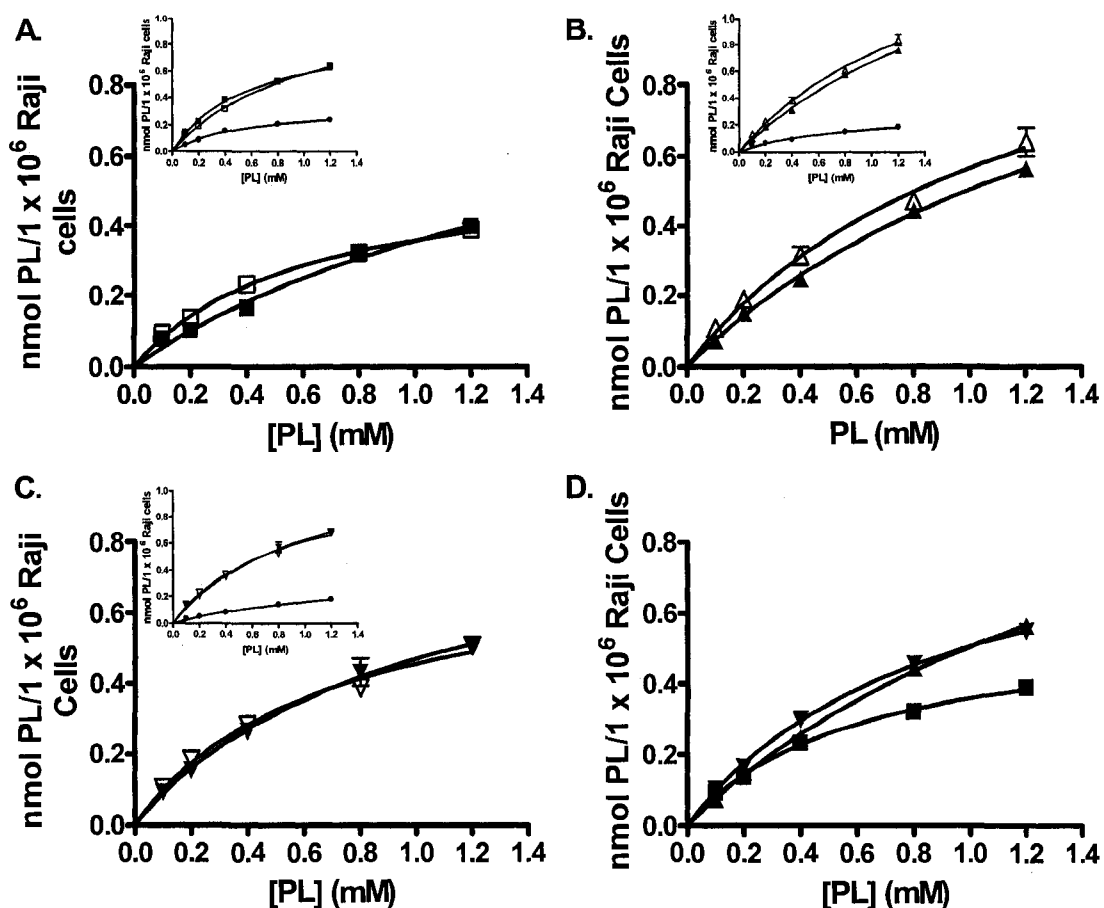


**Figure 5.2. Specific binding of SIL[HD37-CCH], SIL[HD37 Fab'] and SIL[HD37 mAb] to Raji cells.** Immunoliposomes and SL were incubated with  $1 \times 10^6$  Raji cells for 1 h at  $37^\circ\text{C}$ . Specific binding was calculated by subtraction of cell-associated radioactivity counts of SL from SIL. ScFv and Fab' have only one binding site for CD19, while whole mAb has two binding sites. **A)** Specific binding of SIL[HD37-CCH] at 0.35 nmol scFv/ $\mu\text{mol}$  PL (□) or at 0.60 nmol scFv/ $\mu\text{mol}$  PL (■). Inset: total binding of SL (●), or binding of SIL[HD37-CCH] at 0.35 nmol scFv/ $\mu\text{mol}$  PL (□) or at 0.60 nmol scFv/ $\mu\text{mol}$  PL (■). **B)** Specific binding of SIL[HD37 Fab'] at 0.55 nmol Fab'/ $\mu\text{mol}$  PL (▲) or at 0.70 nmol Fab'/ $\mu\text{mol}$  PL (△). Inset: total binding of SL (●), or binding of SIL[HD37 Fab'] at 0.55 nmol Fab'/ $\mu\text{mol}$  PL (▲) or at 0.70 nmol Fab'/ $\mu\text{mol}$  PL (△). **C)** Specific binding of SIL[HD37 mAb] at 0.27 nmol mAb/ $\mu\text{mol}$  PL (0.54 nmol of CD19 binding sites/ $\mu\text{mol}$  PL) (▼) or 0.51 nmol mAb/ $\mu\text{mol}$  PL (1.02 nmol CD19 binding sites/ $\mu\text{mol}$  PL) (▽). Inset: total binding of SL (●) or binding of SIL[HD37 mAb] at 0.27 nmoles mAb/ $\mu\text{mol}$  PL (▼) or 0.51 nmol mAb/ $\mu\text{mol}$  PL (▽). **D)** Comparison of the specific binding of SIL[HD37-CCH], SIL[HD37 Fab'] and SIL[HD37 mAb]. SIL[HD37-CCH] (0.60 nmol scFv/ $\mu\text{mol}$  PL, ■); SIL[HD37 Fab'] (0.55 nmol Fab'/ $\mu\text{mol}$  PL, ▲); SIL[HD37 mAb] (0.28 nmol mAb/ $\mu\text{mol}$  PL, ▼).

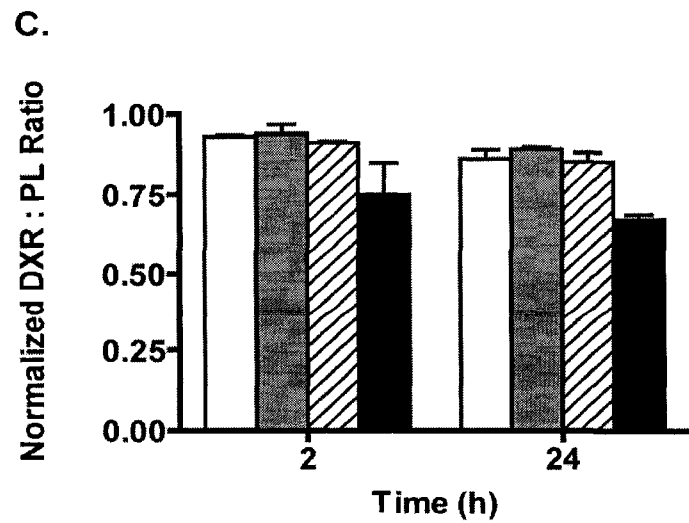
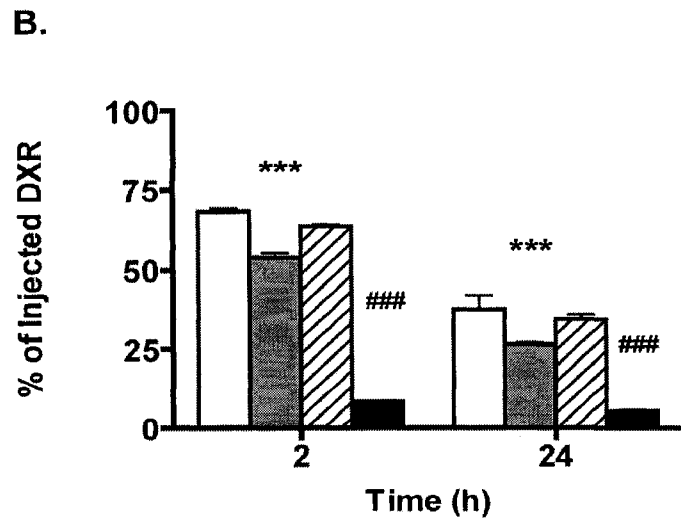
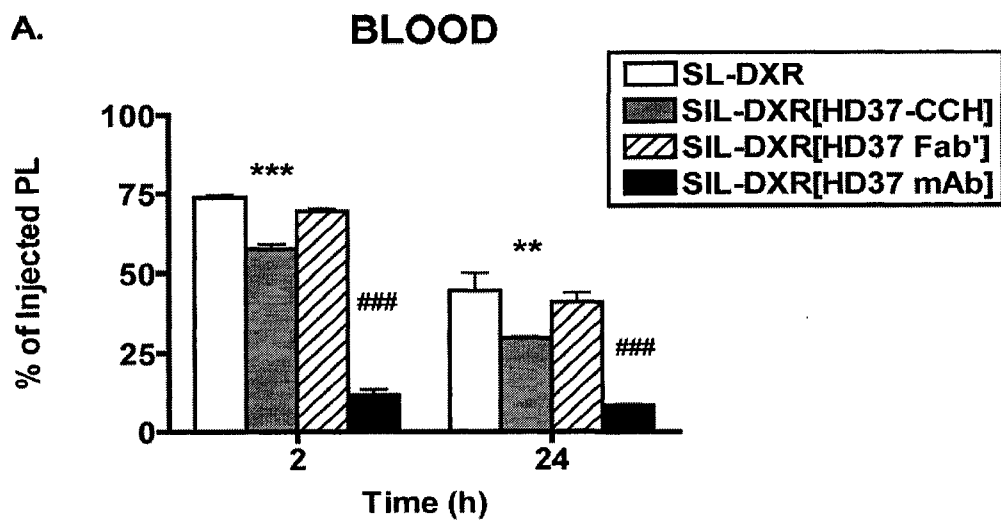
When the SIL were loaded with DXR, all three SIL formulations had similar  $IC_{50}$ s against Raji cells ( $P > 0.05$ ) at surface binding site densities of  $\sim 55$  nmol of CD19-binding sites/ $\mu$ mol of PL, and the  $IC_{50}$ s for the SIL-DXR were significantly lower than that for SL-DXR ( $P < 0.001$ ) (Table 5.1). For CD19-negative Molt4 cells, the SIL-DXR formulations had similar  $IC_{50}$ s to SL-DXR.

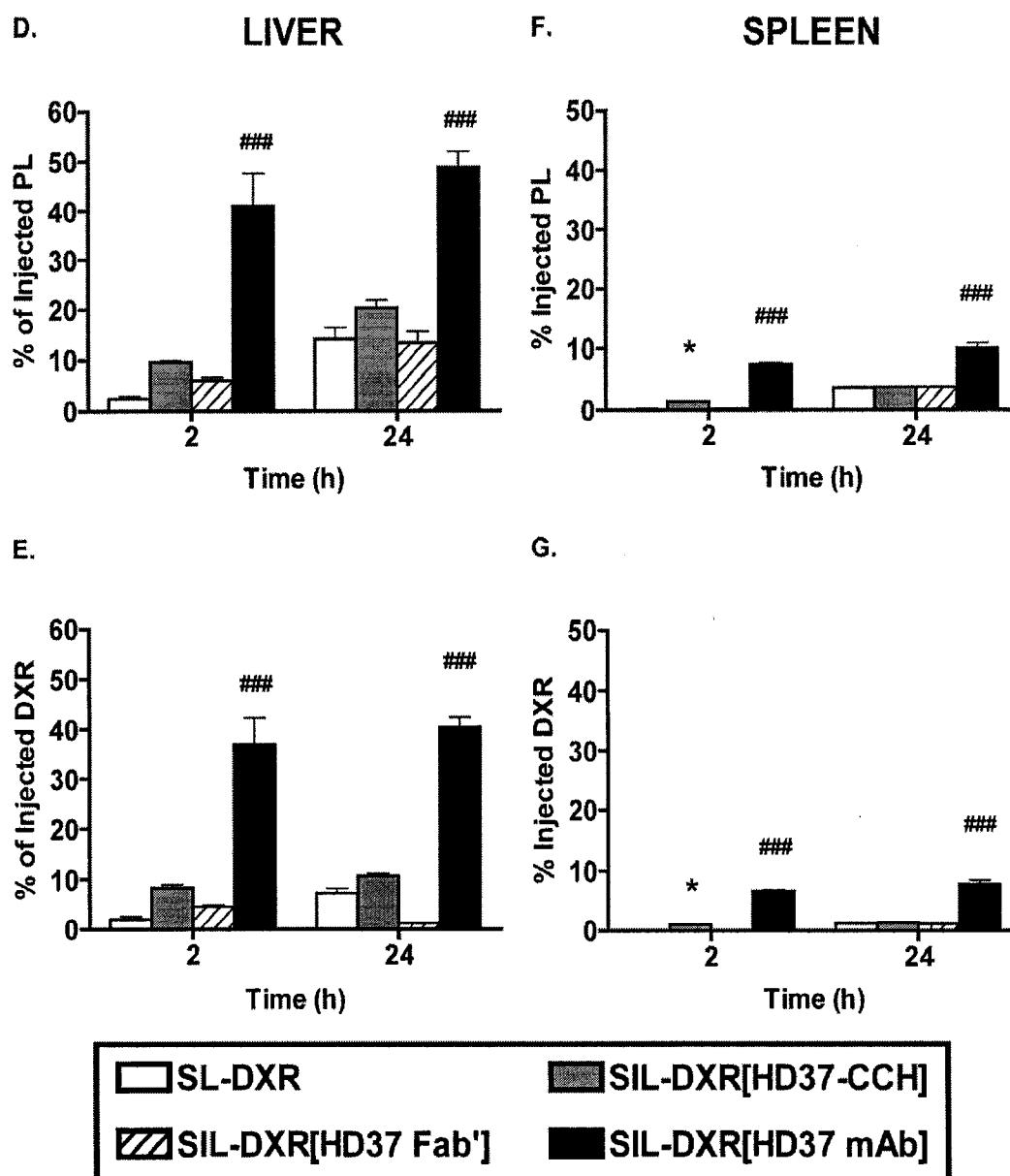
The PK and BD of dual-labeled ( $^3H$ -CHE and  $^{14}C$ -DXR) SL or SIL were first examined in naïve BALB/c mice, where the distribution is not affected by the presence of tumor cells (Fig. 5.3). Blood levels of SL-DXR and SIL-DXR[HD37 Fab'] were similar at 2 and 24 h after liposome injection for drug and lipid, but those of SIL-DXR[HD37-CCH] and SIL-DXR[HD37 mAb] were significantly lower (Fig. 5.3A and B). Since the drug to lipid ratios changed very little, it is concluded that very little leakage of DXR occurred over the 24 hr period for all formulations of liposomal DXR (Fig. 5.3C). In comparison to SL-DXR, there was significantly higher uptake and binding of SIL-DXR[HD37 mAb] in the liver and spleen, which explains its faster clearance from blood (Fig. 5.3D, E, F and G). For SIL-DXR[HD37-CCH] there was slightly higher uptake and binding in the liver and spleen, in comparison to SL-DXR, but this difference was not statistically significant. Uptake of SIL-DXR[HD37 Fab'] by the liver and spleen was similar to SL-DXR. Uptake into lungs, heart and kidneys was low (less than 2% of injected label for all formulations), with slightly higher uptake and binding of SIL-DXR[HD37 mAb] by these tissues compared to SL-DXR.

In Raji-bearing SCID mice, SL-DXR and SIL-DXR[HD37 Fab'] both exhibited log-linear PK with circulation half-lives of 13.8 h and 12.6 h, respectively. Other PK parameters were similar for these two formulations (Fig. 5.4 and Table 5.2).

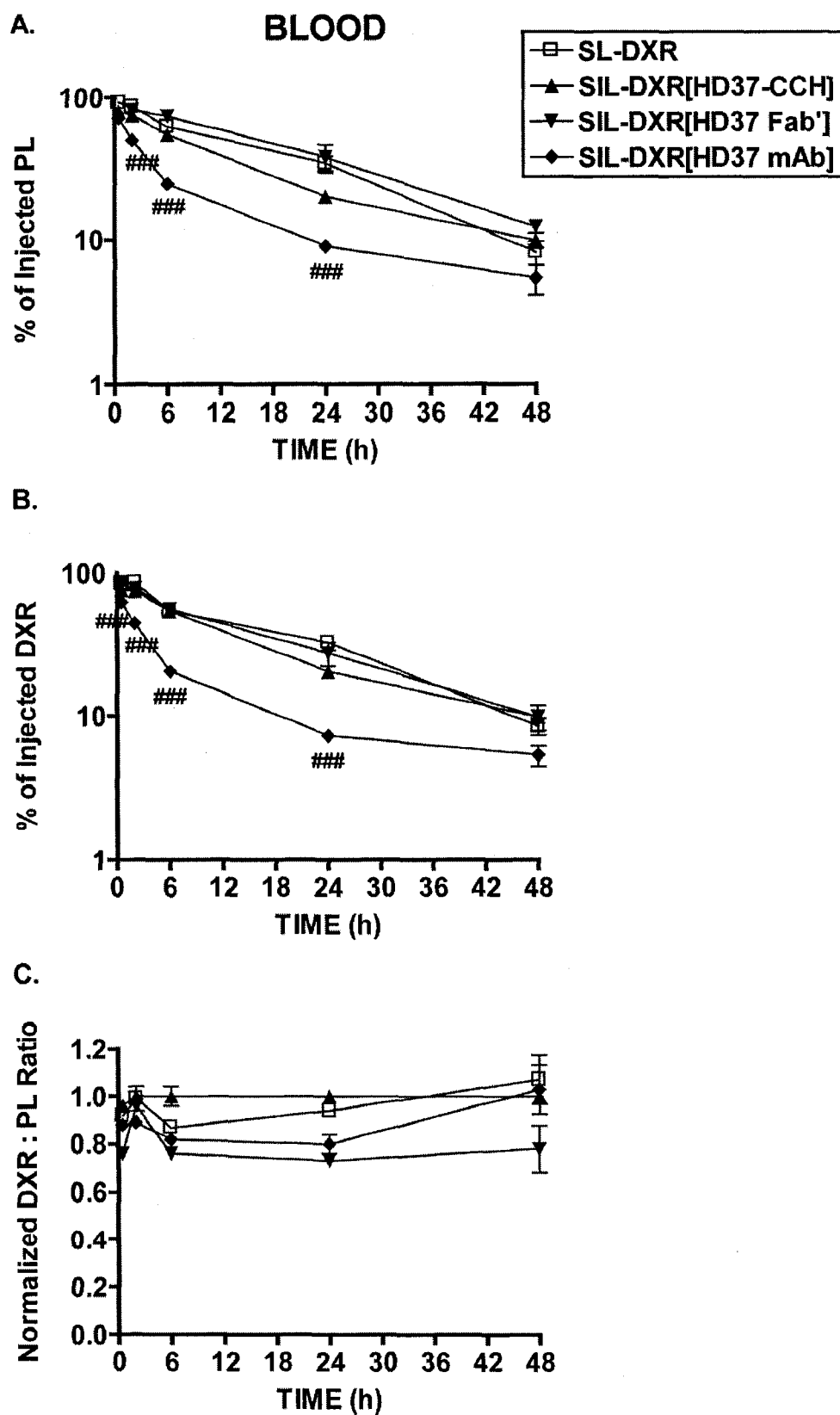
**Table 5.1. Cytotoxicity of free and liposomal DXR against Raji and Molt4 cells (n = 3).**

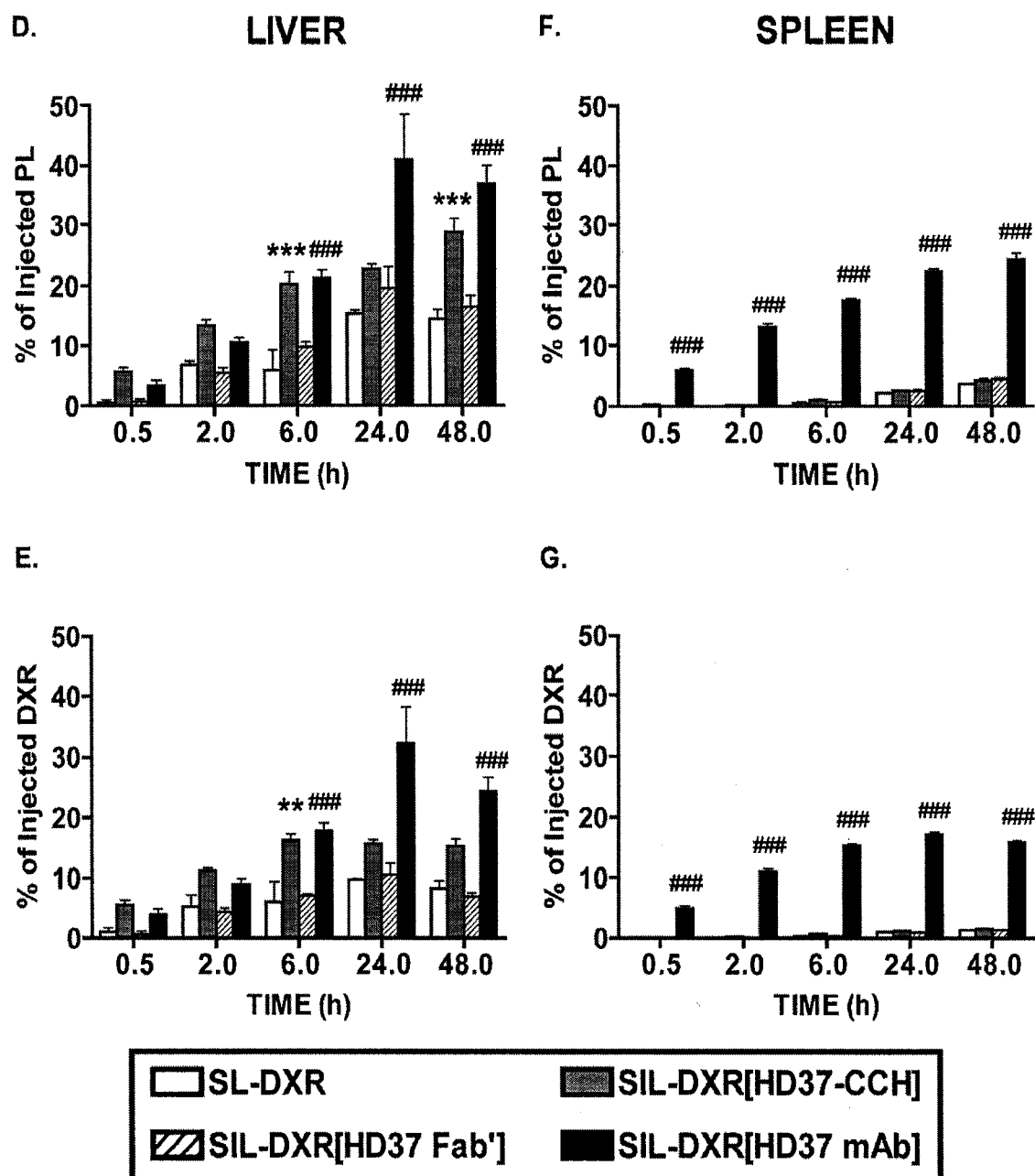
	<b>IC<sub>50</sub> ± S.D. (µM of DXR)</b>	
	<b>Raji</b>	<b>Molt4</b>
<b>Free DXR</b>	0.7 ± 0.4	0.6 ± 0.2
<b>SL-DXR</b>	238.1 ± 46.5	187.2 ± 33.6
<b>SIL-DXR[HD37-CCH]</b>	44.4 ± 6.1	207.3 ± 48.0
<b>SIL-DXR[HD37 Fab']</b>	33.6 ± 6.4	174.1 ± 28.1
<b>SIL-DXR[HD37 mAb]</b>	48.1 ± 11.6	160.5 ± 28.9





**Figure 5.3. Pharmacokinetics and bio-distribution study of SIL-DXR in naïve mice.** BALB/c mice were injected with SL-DXR, SIL-DXR[HD37-CCH] (0.53 nmol scFv/ $\mu$ mol PL), SIL-DXR[HD37 Fab'] (0.45 nmol Fab'/ $\mu$ mol PL), or SIL-DXR[HD37 mAb] (0.34 nmol/ $\mu$ mol PL) at a dose of 3 mg DXR/kg. Liposomes were dual-labelled with  $^3$ H-CHE (lipid) and  $^{14}$ C-DXR (drug). Mice were euthanized at selected time points; organs and blood were collected, processed and the associated radioactivities were measured. Data are presented as the % of injected PL- or DXR-associated radioactivity ( $n = 3 \pm$  S.D.). Panels A, B and C are data collected in blood; D and E, liver; F and G, spleen. For statistical comparison between SIL-DXR[HD37-CCH] and SL, \*  $P < 0.05$ , \*\*  $P < 0.01$ . For statistical comparison between SIL-DXR[HD37 mAb] and SL, #  $P < 0.05$ , ##  $P < 0.01$ , ###  $P < 0.001$ .





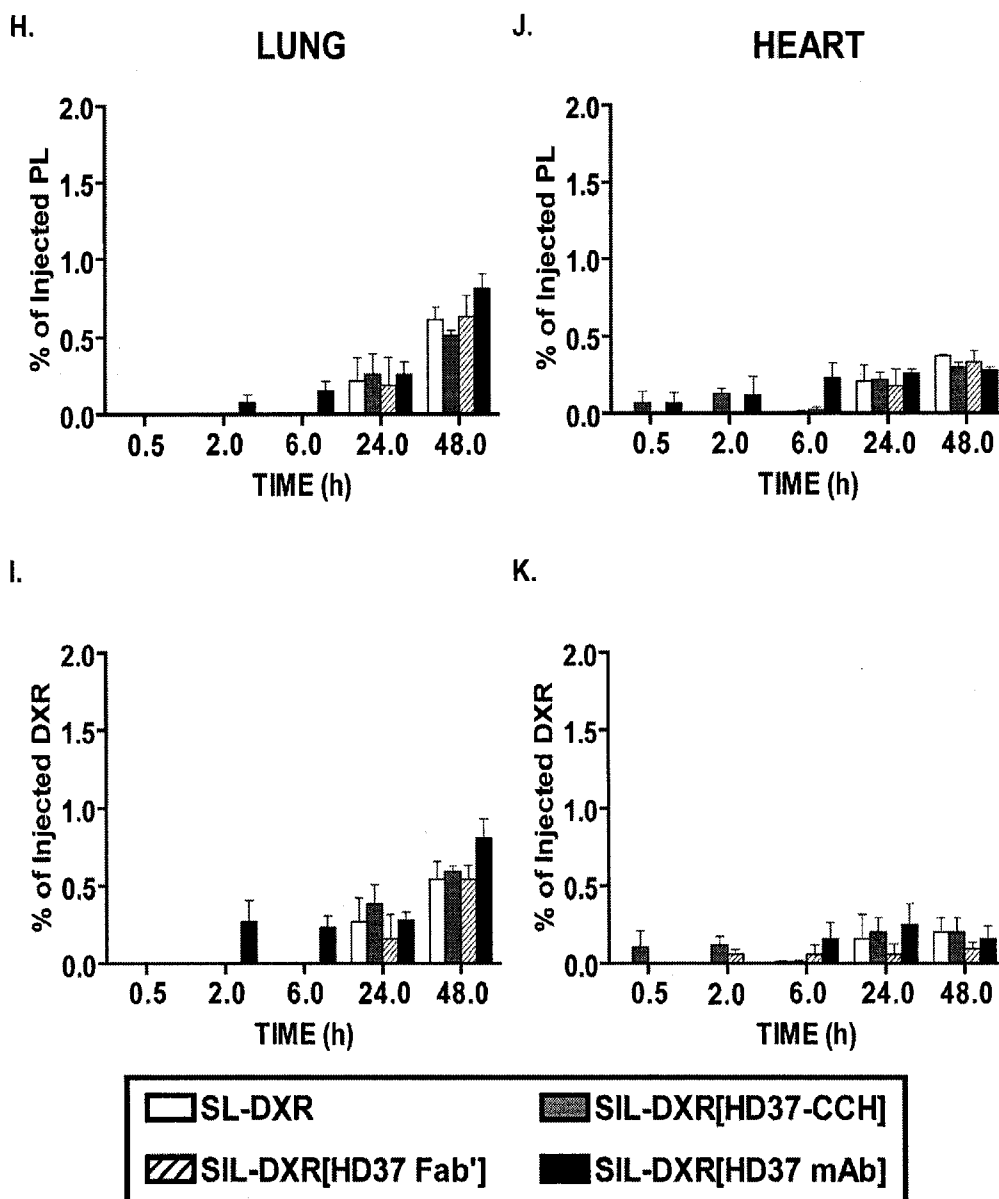


**Figure 5.4. Pharmacokinetics and bio-distribution study of SIL-DXR in Raji-bearing mice.** SCID mice were injected with  $2.5 \times 10^6$  Raji cells and were treated 24 h later with either SL-DXR, SIL-DXR[HD37-CCH] (0.73 nmol scFv/ $\mu$ mol PL), SIL-DXR[HD37 Fab'] (0.45 nmol Fab'/ $\mu$ mol PL), or SIL-DXR[HD37 mAb] (0.34 nmol mAb/ $\mu$ mol PL) at a dose of 3 mg DXR/kg ( $n = 3 \pm$  S.D.). Liposomes were dual-labelled with  $^3$ H-CHE (lipid) and  $^{14}$ C-DXR (drug). Mice were euthanized at selected time points; organs and blood were collected, processed and the associated radioactivities were measured. Data are presented as the % of injected PL- or DXR-associated radioactivity. Panels A, B and C are data collected in blood; D and E, liver; F and G, spleen; H and I, lungs; J and K, heart. For statistical comparison between SIL-DXR[HD37-CCH] and SL, \*  $P < 0.05$ , \*\*  $P < 0.01$ . For statistical comparison between SIL-DXR[HD37 mAb] and SL, #  $P < 0.05$ , ##  $P < 0.01$ , ###  $P < 0.001$ .

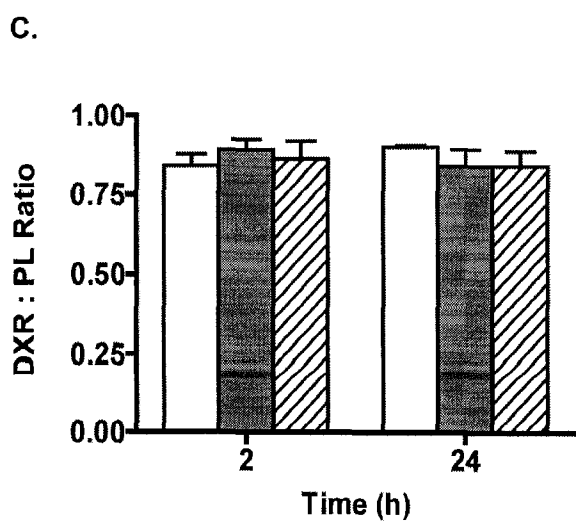
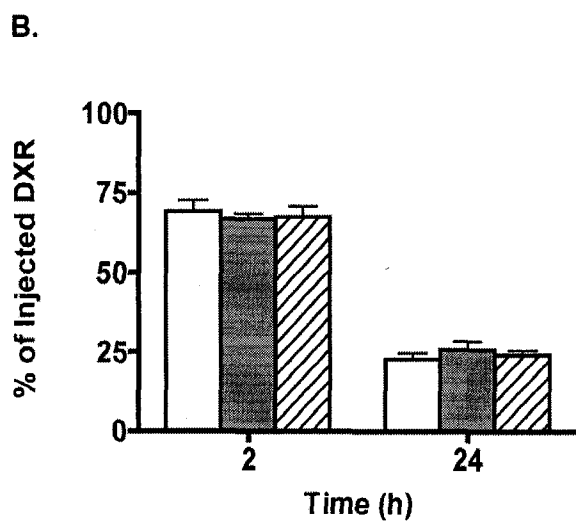
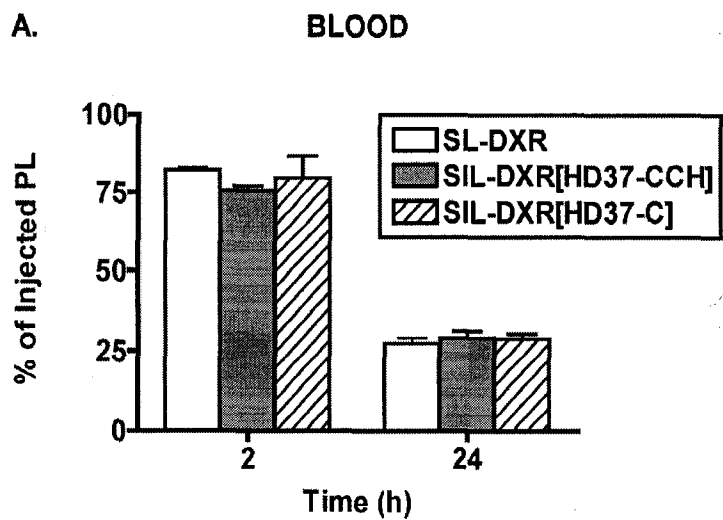
**Table 5.2. Comparison of the pharmacokinetic parameters of targeted and untargeted liposomal DXR in Raji-bearing SCID mice.** Mice were injected with various formulations of liposomal DXR at 3 mg DXR/kg.

<b>Liposome formulation</b>	<b>MRT<sup>a</sup> (h)</b>	<b>AUC<sub>0→∞</sub><sup>b</sup> (μmol•h/mL)</b>	<b>CL<sup>c</sup> (μL/h)</b>	<b>t<sub>1/2α</sub><sup>d</sup> (h)</b>	<b>t<sub>1/2β</sub><sup>e</sup> (h)</b>	<b>Vd<sub>ss</sub><sup>f</sup> (mL)</b>
<b>SL-DXR</b>	19.9	1417.6	0.08	-	13.8	1.7
<b>SIL-DXR [HD37-CCH]</b>	14.2	997.7	0.12	-	9.9	1.7
<b>SIL-DXR [HD37 Fab']</b>	18.1	1291.2	0.10	-	12.6	1.8
<b>SIL-DXR [HD37 mAb]</b>	5.6	292.6	0.41	0.2	4.0	2.3

<sup>a</sup> Mean residence time (MRT); <sup>b</sup> Area under the blood concentration versus time curve (AUC<sub>0→∞</sub>); <sup>c</sup> Clearance (CL), calculated by the formula CL = Dose/ AUC<sub>0→∞</sub>; <sup>d</sup> Half-life of the alpha distribution phase (t<sub>1/2α</sub>); <sup>e</sup> Half-life of the beta elimination phase (t<sub>1/2β</sub>); <sup>f</sup> Volume of distribution at steady state (Vd<sub>ss</sub>).

Slightly faster clearance of SIL-DXR[HD37-CCH] relative to SL-DXR and SIL-DXR[HD37 Fab'] was observed, and the area under the time vs. concentration curve (AUC) was slightly lower for SIL-DXR[HD37-CCH] than for SL-DXR (Table 5.2, 998  $\mu\text{mol}\cdot\text{h}/\text{mL}$  for SIL-DXR[HD37-CCH] vs. 1418  $\mu\text{mol}\cdot\text{h}/\text{mL}$  for SL-DXR). Compared to SL-DXR, uptake and binding of SIL-DXR[HD37-CCH] into liver and spleen was significantly higher at the later time points (Fig. 5.4D, E, F and G), which explains the more rapid clearance of this formulation. Compared to the other formulation (targeted and untargeted), SIL-DXR[HD37 mAb] was cleared rapidly from circulation in a biphasic manner with a rapid  $\alpha$  (distribution) phase and a slower  $\beta$  (elimination) phase (Fig. 5.4A and B). The steeper  $\alpha$  phase appeared to be due to rapid uptake into the liver and spleen, likely Fc receptor-mediated (Fig. 5.4D, E, F and G). The *in vivo*, lipid to drug ratios for all the formulations changed little over 48 h, suggesting that leakage rates of drug from the liposomes were slow, and were not influenced by the presence of surface ligands (Fig. 5.4C). Uptake into the lung and heart was similar for all formulations and was less than 2% of injected counts (Fig 5.4H, I, J and K).

The somewhat elevated liver uptake and binding of SIL-DXR[HD37-CCH] was postulated to be a result of the poly-His and c-myc tags on the HD37-CCH scFv construct. To examine whether the changes in PK were a result of the tags, an *in vivo* PK/BD experiment was performed in Raji-bearing SCID mice, comparing SIL targeted via HD37-CCH vs. SIL targeted via the tagless construct HD37-C (Fig. 5.5). Although no significant differences in blood levels were observed for SIL-DXR[HD37-CCH], SIL-DXR[HD37-C] or SL-DXR (Fig. 5.5A), significantly higher uptake and binding in the liver was observed for SIL[HD37-CCH] compared to SIL[HD37-C] (Fig. 5.5D and F).



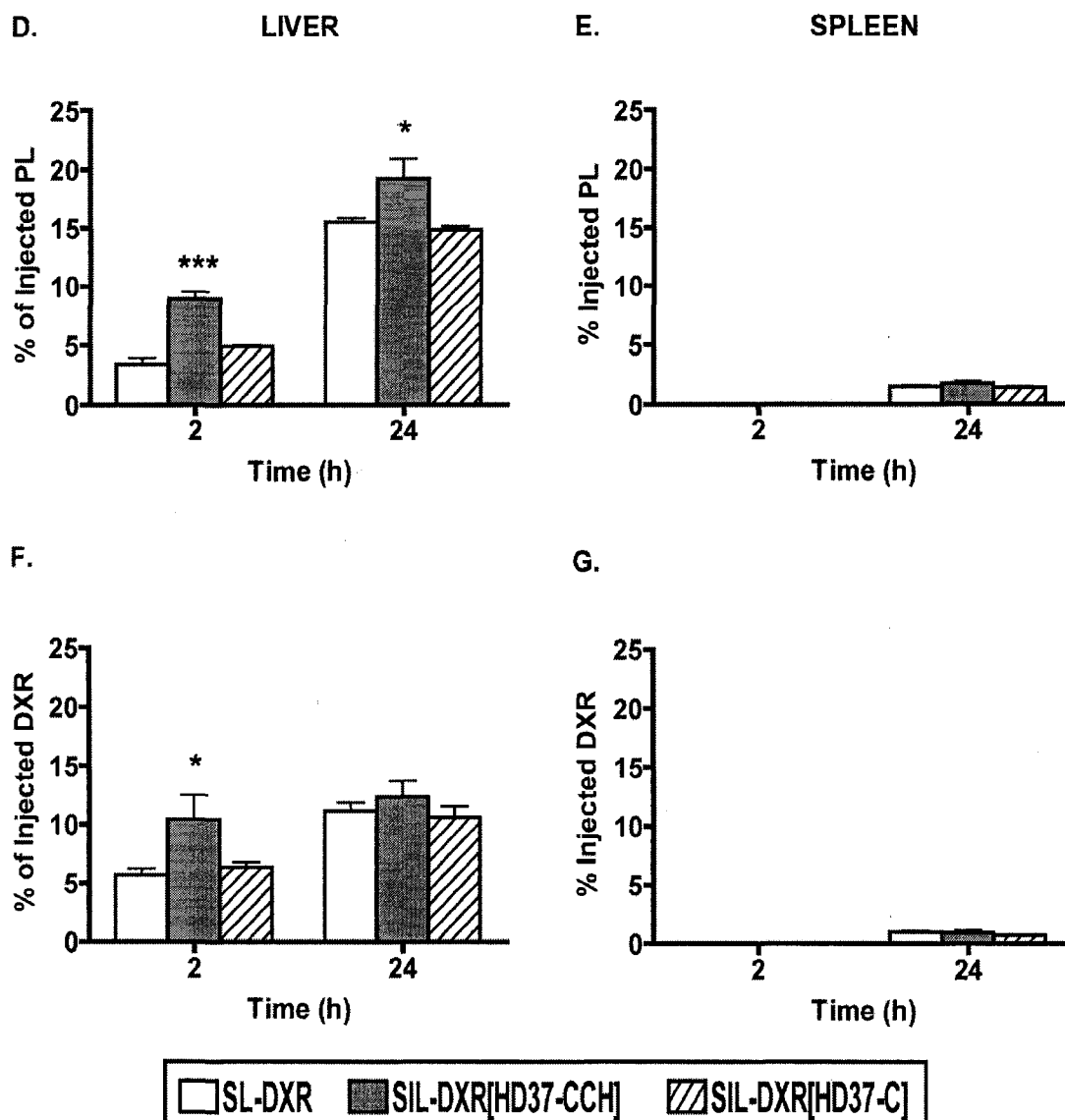


**Figure 5.5. Pharmacokinetics and bio-distribution study of SIL-DXR targeted via tagged or non-tagged scFv constructs.** SCID mice were injected with  $2.5 \times 10^6$  Raji cells and were treated 24 h later with either SL-DXR, SIL-DXR[HD37-CCH] (0.85 nmol scFv /  $\mu\text{mol}$  PL), or SIL-DXR[HD37-C] (0.95 nmol scFv /  $\mu\text{mol}$  PL) at a dose of 3 mg DXR/kg ( $n = 3 \pm \text{S.D.}$ ). Liposomes were dual-labelled with  $^3\text{H}$ -CHE (lipid) and  $^{14}\text{C}$ -DXR (drug). Mice were euthanized at selected time points; organs and blood were collected, processed and the associated radioactivities were measured. Data are presented as the % of injected PL- or DXR-associated radioactivity. Panels A, B and C are data collected in blood; D and E, liver; F and G, spleen. For statistical comparison between SIL-DXR[HD37-CCH] and SL, \*  $P < 0.05$ , \*\*\*  $P < 0.001$ .

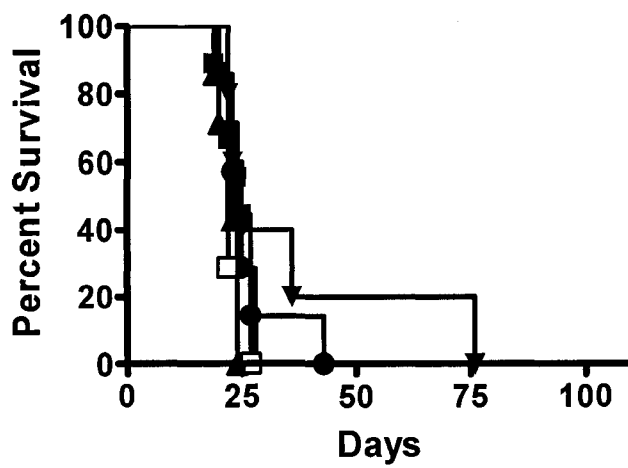
No significant difference was observed for uptake and binding in the spleen (Fig. 5.5E and G).

An *in vivo* survival study was performed in Raji-bearing SCID mice, at the maximum tolerated dose of 3 mg DXR/kg, in order to examine the effects of treatment with different formulations of DXR (Fig. 5.6B). Mean survival times (MST) of Raji-bearing SCID mice, with and without treatment, are summarized in Table 5.3A. The *P* values of various statistical comparisons between each treatment group are summarized in Table 5.3B. The MST of the control (saline) group was  $28.0 \pm 3.3$  days and all liposome treatments significantly increased the survival of mice in comparison to control ( $P < 0.005$ ). The MST of mice treated with free DXR was not significantly different from mice treated with SL-DXR ( $P > 0.05$ ). The MSTs of mice treated with any of the three targeted SIL-DXR formulations were significantly longer compared to mice treated with SL-DXR ( $P < 0.05$ ), with some long term survivors in each group. Survival times of mice treated with SIL-DXR targeted with HD37-CCH, HD37 Fab' or HD37 mAb were not significantly different ( $P > 0.05$ ). However, there were more long term survivors (> 100 days) in the group treated with SIL-DXR[HD37 Fab'] (5 of 7) than in the other two groups of SIL, where only 3 or 7 mice were long term survivors.

## 5.5. Discussion and Conclusions

For the clinical development of immunoliposomal anticancer drugs, it is important to compare different antibody constructs in order to determine the construct that has the most beneficial combination of properties leading to ease of production, while not compromising the therapeutic activity and toxicity profiles. To the best

A.



B.

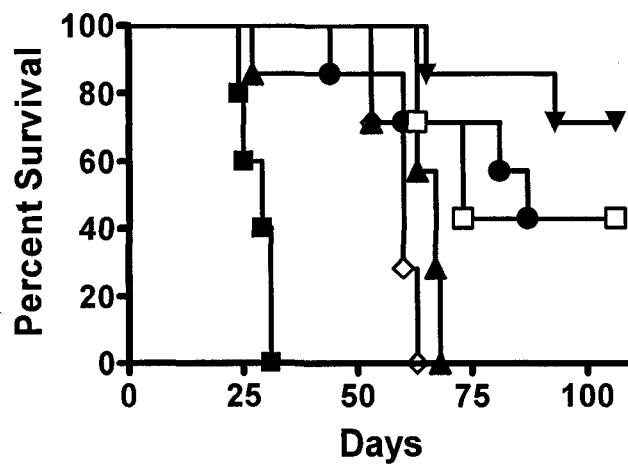


**Figure 5.6. Kaplan-Meier plot for Raji-bearing SCID mice treated with various formulations of DXR.** SCID mice (5 - 7/group) were injected with  $2.5 \times 10^6$  Raji cells (Day 0) and were treated 24 h later with either saline (■), free DXR (◇), SL-DXR (▲), SIL-DXR[HD37-CCH] (●), SIL-DXR[HD37 Fab'] (▼), or SIL-DXR[HD37 mAb] (□), at a dose of **A)** 1 mg DXR/kg or **B)** 3 mg DXR/kg. Mice were monitored daily and were euthanized when hind-leg paralysis developed.

**Table 5.3A. Survival times of SCID mice after tumor cells implantation and DXR treatment.** SCID mice (5 – 7/group) were injected with  $2.5 \times 10^6$  Raji cells (Day 0) and were treated 24 h later with saline, free DXR, SL-DXR, SIL-DXR[HD37-CCH], SIL-DXR[HD37 Fab'], or SIL-DXR[HD37 mAb], at 3 mg DXR/kg. Mice were monitored daily and were euthanized when hind-leg paralysis developed.

<b>Group</b>	<b>Mean Survival Time <math>\pm</math> S.D. (Days)</b>	<b>% Increase in Life Span</b>	<b>Long-term Survivors (&gt; 100 Days)</b>
<b>Saline</b>	28.0 $\pm$ 3.3		0/5
<b>Free DXR</b>	58.9 $\pm$ 4.2	81	0/7
<b>SL-DXR</b>	59.0 $\pm$ 15.1	81	0/7
<b>SIL-DXR[HD37-CCH]</b>	84.3 $\pm$ 24.6	159	3/7
<b>SIL-DXR[HD37 Fab']</b>	98.3 $\pm$ 15.5	202	5/7
<b>SIL-DXR[HD37 mAb]</b>	84.3 $\pm$ 20.7	159	3/7

**Table 5.3B. Statistical comparisons of mean survival times.**

<b>Comparison</b>	<b><i>P</i> value</b>
Saline vs. free DXR	0.0002
Saline vs. SL-DXR	0.0033
Saline vs. SIL-DXR[HD37-CCH]	0.0007
Saline vs. SIL-DXR[HD37 Fab']	0.0002
Saline vs. SIL-DXR[HD37 mAb]	0.0002
Free DXR vs. SL-DXR	0.064
Free DXR vs. SIL-DXR[HD37-CCH]	0.022
Free DXR vs. SIL-DXR[HD37 Fab']	0.0002
Free DXR vs. SIL-DXR[HD37 mAb]	0.002
SL-DXR vs. SIL-DXR[HD37-CCH]	0.028
SL-DXR vs. SIL-DXR[HD37 Fab']	0.003
SL-DXR vs. SIL-DXR[HD37 mAb]	0.015
SIL-DXR[HD37-CCH] vs. SIL-DXR[HD37 Fab']	0.23
SIL-DXR[HD37-CCH] vs. SIL-DXR[HD37 mAb]	1.0
SIL-DXR[HD37 Fab'] vs. SIL-DXR[HD37 mAb]	0.25

knowledge of the authors, this is the first study to compare the PK and therapeutic effects of SIL-DXR targeted by three different antibody constructs with identical binding domains against the same antigen epitope. Other studies have only compared therapeutic activity of scFv-targeted SIL against untargeted SL (106, 138).

ScFv fragments are inherently unstable and various strategies, such as mutagenesis, have been developed for increasing their stability (247). SIL[HD37-CCH] prepared with freshly produced HD37-CCH and coupled using a conventional coupling method has been shown to exhibit affinity for CD19<sup>+</sup> cells (197). However, the relatively low yield of the HD37 scFv, purified from the periplasmic space of *E. coli*, limited its application in research since it required frequent production of fresh scFv. This study demonstrated that the stability and affinity of the HD37-CCH scFv can be preserved, during sub-zero storage, by simply coupling the scFv to Mal-PEG<sub>2000</sub>-DSPE micelles, requiring no re-engineering of the scFv construct and allowing production and storage of larger batches of scFv for later use. It is postulated that the long hydrophilic PEG chains of the Mal-PEG<sub>2000</sub>-DSPE stabilized the scFv during storage and the subsequent thawing. This method of stabilizing scFv may have wider applicability in the preparation of SIL from other unstable scFv fragments against different antigens.

The lower binding of SIL targeted via HD37-CCH scFv to Raji cells in comparison to the Fab'- and mAb-targeted SIL, was not unexpected since it has been shown that recombinant scFv may exhibit decreased affinity compared to the parental Fab' (248, 249). In addition, since the scFv is smaller in size, in comparison to the Fab' or mAb, it may be more easily masked by the PEG layer on liposome surface; steric hindrance by the PEG may interfere with binding of the scFv-targeted liposomes.

This study compared, for the first time, the cytotoxicity, PK and in vivo therapeutics of SIL-DXR targeted via a scFv, in relation to its parental mAb and Fab'. The results showed that SIL-DXR[HD37-CCH] had similar cytotoxicity to Raji cells as SIL-DXR targeted via Fab' or mAb, despite the lower binding affinity observed for the scFv construct. The lack of antibody-mediated toxicity against the CD19<sup>-</sup> Molt4 cells suggests that the increased cytotoxicity against the Raji cells is mediated by the internalizing antigen, CD19, as previously demonstrated for other internalizing ligands (61, 91, 104, 250).

In Raji-bearing SCID mice, the blood levels of SIL-DXR[HD37 mAb] followed a bi-phasic model, where the  $\alpha$  distribution phase was likely due to recognition of the Fc region and uptake into the liver and spleen (62, 137). However, contrary to expectations, the rapid clearance of SIL-DXR[HD37 mAb] did not significantly affect the therapeutic activity of SIL-DXR[HD37 mAb] in comparison to SIL-DXR[HD37 Fab']. SL-DXR and SIL-DXR[HD37 Fab'] (which lacks the Fc region) were long-circulating with log-linear PK, as expected (39, 61, 62). The observation that the blood clearance of SIL-DXR[HD37-CCH] (which also lacks the Fc region) was more rapid than SL-DXR or SIL-DXR[HD37 Fab'] was unexpected. A separate experiment, comparing SIL targeted via the tagged HD37-CCH and the tagless HD37-C, showed that the removal of the poly-His and c-myc tags resulted in decreased uptake and binding of SIL in the liver. However, it is not clear whether the changes are a result of either poly-His or c-myc, or the two tags in combination. The absence of tags may make the scFv constructs more acceptable for clinical uses (66, 67, 234).

In this study, SIL-DXR[HD37 Fab'], which had longer circulation times than either the SIL-DXR[HD37-CCH] or the SIL-DXR[HD37 mAb], resulted in higher numbers of long-term survivors, although the differences did not reach statistical significance. A repeat therapeutic study at a lower dose of DXR (Fig. 5.6A), which did not result in long-term survivors, also could not determine a statistically significant relationship between circulation half-lives and survival times in this model. However, in another B-cell model, Namalwa-bearing SCID mice treated with SIL-DXR targeted via the Fab' of the anti-CD19 FMC63 mAb had longer survival times than those treated with SIL-DXR targeted via the parental mAb, which were cleared more rapidly (62). It is conceivable that long circulation half-lives are less important in haematological models such as these, where the accessibility of the single cells leads to rapid binding of the SIL. In solid tumor models, long circulation half-lives are expected to be of prime importance.

This study has shown that targeting SIL-DXR with HD37-CCH or HD37 Fab' is at least as effective as SIL-DXR targeted with HD37 mAb in spite of significant differences in pharmacokinetics. This suggests that the choice of the targeting construct can be based, in part, on other considerations such as ease of production and purification, suitable levels of stability and reduced immunogenicity. Single chain Fv are expected to be preferred over Fab' and mAb for clinical development of immunoliposomes, due to factors such as the decreased presence of foreign peptides, the lack of the Fc domain and the ease of production. Expression of scFv in bacterial or algal fermentation systems may also be more economical than the production of mAb in cell culture systems. The presence of poly-His and c-myc tags in the scFv construct appears to result in an increase

in liver uptake and binding, and this, along with their potential for causing adverse effects in humans, should be considered in future designs of scFv-targeted SIL.

**Chapter 6**

**General Discussion and Future Directions**

## 6. General Discussion and Future Directions

### 6.1. Discussion

#### 6.1.1. Stability of ScFv Constructs

This thesis presented data on the expression, purification and binding of several constructs of anti-CD19 scFv, which were screened as potential ligands for use in targeting liposomal DXR against malignant B-cells. Of the 7 constructs tested, one construct, HD37-CCH, demonstrated sufficient stability and affinity for CD19 to warrant further pursuit, and this construct was chosen for *in vitro* and *in vivo* comparison studies, with its parental mAb and Fab' fragment.

Various studies, in addition to the results presented in this thesis, have highlighted the fact that *in vitro* stability of scFv fragments is essential for successful targeting *in vivo* (219, 220). The stability of an scFv fragment is especially important for therapeutic applications, including the use of immunoliposomes, because these applications generally require large amounts of the targeting agents, and the stability of a scFv can affect its production yield (251). In addition, scFv may sometimes be subjected to relatively harsh conditions during the coupling procedures used in the production of immunoliposomes and immunoconjugates. Therefore, optimization of stability is an integral part of the developmental process of any scFv-targeted therapeutic.

In this thesis, the targeting of various constructs of anti-CD19 scFv was tested by examining their binding to CD19<sup>+</sup> cells, and their tendency to precipitate above the minimum concentration required for generation of immunoliposomes provided some estimation of their *in vitro* stability. A more accurate assessment of the stability of an

scFv can be measured quantitatively by determining the free energy of folding at equilibrium as a function of increasing concentration of denaturant (e.g., urea or Gu HCl) (247). However, interpretation of results generated from this analysis can be problematic since it requires modelling of the data, and the presence of partially unfolded intermediates can complicate the interpretation of results (221). The stability of scFv can also be measured by stressed incubation, where the scFv is incubated in conditions similar to its intended application (e.g., in serum at 37 °C) (252), followed by evaluation of the remaining activity or the amount of protein aggregation after the incubation (221, 253).

Invariably, most scFv constructs require molecular engineering to improve their stability. Indeed, this thesis showed that most of the scFv constructs tested could benefit from some modifications. Intradomain disulfide bonds at conserved positions within scFvs are associated with their intrinsic stability (247, 254, 255). Many scFv cannot tolerate the loss of these disulfide bonds (256). Only a very few scFv constructs have been shown to fold correctly and retain their activity in the absence of intradomain disulfide bonds (255, 257, 258). Proba et al. demonstrated that, although the stable ABPC48 scFv derived from its wild-type parental mAb is naturally missing a disulfide bond in the V<sub>H</sub> chain, restoration of the disulfide bond by point mutation can increase the stability of the scFv above the unmodified ABPC48 scFv (255).

Examination of the HD37 scFv sequences showed that the V<sub>L</sub> and V<sub>H</sub> chains each contain a pair of Cys residues, suggesting the possibility of disulfide bonds within each domain. However, the differences in stability noted in this thesis between HD37-CHC, HD37-C and HD37-CCH suggest that other elements such as the stability of the V<sub>L</sub> and

$V_H$  domain interface (247), in addition to the intradomain disulfide bonds, may affect the stability of a particular scFv construct. Spontaneous and transient opening of the interface between the  $V_L$  and  $V_H$  chains has been suggested to result in exposure of normally hidden hydrophobic patches, leading to aggregation (252). The introduction of an interdomain disulfide bond (between the  $V_L$  and  $V_H$  chains) (259), and variations in the length and flexibility of the  $V_L$ - $V_H$  linker (260) have been shown to increase interdomain stability by limiting the opening of the  $V_L$ - $V_H$  interface. An alternative approach to increase the stability of an scFv is the CDR-grafting method, which was originally developed for humanization of murine mAb, has also proven to be useful for scFv constructs (219). In this method, the CDR sequence (i.e, the antigen-binding sequence) of an unstable scFv is grafted onto a framework of another scFv construct with proven stability.

All of the above strategies require modifications to the DNA sequence of the scFv constructs. In this thesis, a simple method of conjugating the HD37-CCH to Mal-PEG<sub>2000</sub>-DSPE micelles, was shown to increase the storage stability of the scFv without requiring any modifications to its protein sequence. Although the HD37-CCH was demonstrated to possess superior stability, in comparison to the other constructs tested, conjugation of the HD37-CCH scFv to Mal-PEG-DSPE micelles resulted in preservation of its activity over the unconjugated scFv, after extended storage at sub-zero temperature. This observation allowed for batch production and stockpiling of the HD37-CCH scFv, a significant breakthrough in this project, because storage of the unconjugated HD37-CCH in large quantities was initially impossible since aggregation necessitated the production of fresh scFv for every experiment. It is postulated that other scFv constructs can be

stabilized by conjugation to micelles, allowing for scale-up of their production. In fact, an anti-HER2 scFv fragment that is intended for clinical trials of immunoliposomal anticancer drugs is manufactured and coupled to Mal-PEG-DSPE micelles, and stored as the scFv-Mal-PEG-DSPE conjugate (66, 67).

### **6.1.2. Refolding of ScFv**

In this thesis, the refolding of scFv from denatured inclusion bodies was examined, and it was shown to be more problematic than was anticipated. Various studies have suggested that the folding of scFv is a difficult and complex process, but an increase in the production yield of properly refolded scFv can be achieved through stability engineering as described above (155, 221, 251). If the stability of a scFv construct can be optimized through molecular engineering for proper folding, refolding scFv from inclusion bodies can be a valuable method of producing scFv, since it can dramatically increase the production yield. The accumulation of recombinant proteins in inclusion bodies can account for > 20% of total cellular protein (261-263).

### **6.1.3. Effect of ScFv Tags.**

This was one of the first studies to compare the targeting of liposomes with scFv against results obtained with the parent mAb and Fab' fragment. All targeted formulations of liposomal DXR demonstrated specific cytotoxicity to CD19<sup>+</sup> cells over untargeted liposomal DXR via CD19-mediated mechanisms. Fab'-targeted liposomes were shown to be long circulating, similar to untargeted Stealth<sup>®</sup> liposomes. Liposomes targeted via mAb were cleared more rapidly from the circulation via Fc receptor-mediated uptake and binding into the liver and spleen. For the first time, it was shown

that scFv-targeted liposomes had a shorter circulation time, compared to untargeted Stealth<sup>®</sup> liposomes, and that this was mediated by the presence of molecular tags. Additional evidence can be found in the literature where recent studies have shown that a His-tagged anti-CEA scFv was rapidly taken up by the liver (30–40% of the injected dose) (264). In a separate study by another group, using a tag-free anti-CD45 scFv, the uptake and binding by the liver was much lower at only < 5% of the injected dose (265). Taken together, these results further suggest that the PK/BD of a scFv or scFv conjugate may be influenced by molecular tags within the scFv construct.

#### **6.1.4. Targeting of Immunoliposomes Using MAb, Fab' or ScFv**

The results presented in this thesis showed that an anti-CD19 scFv-targeted immunoliposomal DXR is at least as effective, in an *in vivo* mouse model of human B-cell lymphoma, as immunoliposomal DXR targeted via the parent mAb. Although there was a trend to suggest that immunoliposomal DXR targeted via the Fab' was the most efficacious of the 3 targeted formulations, no statistical significance was observed. In this model, immunoliposomal DXR targeted via the HD37 mAb resulted in improved therapeutic effects similar to the Fab' or scFv; this was unexpected, since the rapid clearance of mAb-targeted liposomes was expected to negatively impact the therapeutic effects of this formulation. These results suggest that, in this haematological model where the target cells are relatively accessible to the immunoliposomes, the differences in PK/BD and their effect on therapeutic activities between targeted formulations may not be as significant as in solid tumor models where an increase in circulation time can lead to greater localization in tumors via passive targeting (42).

Therefore, the choice of targeting agent for the preparation of immunoliposomal drugs may depend on other considerations such as stability, production yields, immunogenicity and toxicity. In this regard, mAb seems to be the least favourable. Despite the fact that immunogenicity can be minimized by the use of chimeric or humanized mAb (140, 266, 267), toxicity to the liver and spleen, resulting from recognition of the Fc domain and uptake and binding of the mAb-targeted immunoliposomal drugs in these organs, is a major concern. Humanized Fab' would appear to be a good targeting agent as it should possess similar stability and affinity as the parental mAb, but its production from humanized mAb with subsequent digestion of the Fc domain would not be a preferred method of manufacture. Production of recombinant humanized Fab' in bacteria or other expression system may be a more acceptable alternative. Single chain Fv are potentially valuable targeting agents, if the scFv fragments are engineered and selected for optimal affinity and stability. However, the mechanism of tag-mediated liver uptake and binding of scFv-targeted liposomes needs to be further studied to minimize potential liver toxicity.

#### **6.1.5. Single Chain Fv in the Clinic as Anticancer Therapy**

Several scFv are currently in different stages of clinical trials for the treatment of various cancers (268, 269). An Anti-CD22 scFv (270) and an anti-mesothelin scFv (271) are conjugated to *Pseudomonas* exotoxin A (PE), while others, such as an anti-CEA scFv (269), are fused to an enzyme and are used in antibody-directed enzyme prodrug therapy (ADEPT) as pretargeting agents. For the scFv-PE fusion protein, each scFv molecule carries a payload of one PE molecule, and a substantial dose of scFv may be needed for effective treatment. The potentially large dose of scFv may lead to a higher frequency of

adverse effects, such as the immunogenic reactions reported by Mayer (269). However, the success of these scFv-targeted therapeutics will pave the way for the clinical acceptance of scFv-targeted immunoliposomal drugs. The benefit of scFv-targeted immunoliposomal drugs, is that a substantially larger payload of drugs can be delivered with a relatively low dose of scFv, thereby minimizing the risk of scFv-associated adverse effects.

#### **6.1.6. Failure to Respond and Resistance to Antibody-targeted Immunoliposomal Drugs.**

The response to immunoliposomal therapy is dependent on the expression of the target antigen. In most cancer cell populations there is a spectrum of antigen expression among cells, with some cells having high expression and others low or no expression of a particular antigen. While antigen expression is usually high and stable in most B cell populations, which are monoclonal in origin, some patient samples contain B cells that lack or have low levels of CD19 expression (272). For anti-CD19 immunoliposomes, obviously, B cells that do not express CD19 or that have low levels of CD19 will be less likely to respond to therapy. The strategy of targeting immunoliposomes to more than one antigen will increase therapeutic success in these cases.

For clinical applications of immunoliposomal drugs, it is crucial to consider that resistance to immunoliposomes may arise. Recent studies have reported resistance to rituximab therapy in some patients following long term rituximab therapy (273, 274). Several mechanisms, including downregulation of CD20 (275) and over-expression of the anti-apoptotic protein Bcl-2 (276), have been proposed. In breast cancers, preclinical studies have postulated that over-expression of the mucin 4 (MUC4) protein on breast

cancer cells as one of the possible mechanisms to trastuzumab resistance by masking HER2/*neu* and induction of steric hinderance to the binding of trastuzumab to HER2/*neu* (277, 278). Therefore, it can be speculated that cells may acquire resistance to anti-CD19 immunoliposomal drugs through various mechanisms. A potential approach to overcoming resistance resulting from downregulation of cell surface antigens is to target immunoliposomal drug against multiple antigens expressed on B cells, such as CD19, CD20 or CD22 (63, 136). Other mechanisms of resistance, such as decreased expression of topoisomerase II, can potentially be combated by treatment with multiple immunoliposomal drugs with different mechanism of actions, for example, immunoliposomal DXR and immunoliposomal VCR.

## **6.2. Future Directions**

### **6.2.1. Combination of Immunoliposomal Drugs**

To date, only a few studies have examined the therapeutic effects of combinations of immunoliposomal drugs (63, 102). In a B-cell lymphoma model, Sapra et al. used immunoliposomal VCR, targeted via a combination of anti-CD19 mAb and anti-CD20 mAb (63). In this study, additive activity was observed for the combination over either anti-CD19- or anti-CD20-immunoliposomal VCR used alone. In a model of neuroblastoma, Pastorino et al. treated mice with liposomal DXR targeted via an anti-GD<sub>2</sub> mAb or Fab', or NGR-peptide in combination (102) and also was able to demonstrate additive activity over either ligand used alone. These studies showed that combining either drugs or antigens can result in increased therapeutic effects over single immunoliposomal treatments. Examination of different combinations of immunoliposomal drugs containing either different drugs and/or different targeting

agents could result in enhanced efficacy. Co-encapsulation of two different anticancer drugs in the same liposome have recently been described (279-282), making it possible to investigate the therapeutic effects of bispecific immunoliposomes co-encapsulating a combination of drugs.

### 6.2.2. Triggered Release Systems

Various triggered release liposomes, including liposomes containing dioleoylphosphatidylethanolamine (DOPE) (283) and liposomes containing fusogenic peptides (284), have been developed for fusion of the liposomal and endosomal membranes after antigen-mediated endocytosis, allowing efficient release of liposomal contents into the cytoplasm. Although DOPE-containing liposomes can enhance drug delivery to cells, *in vivo* results were less than desired since these liposomes had very short circulation times despite the addition of PEG onto the surface of liposomes (285). Recently, DOPE-free liposomes targeted via transferrin and containing a fusogenic peptide (GALA) incorporated on the liposome surface have been shown to efficiently fuse with the endosomal membrane after internalization (286). Because it is known that surface PEG can interfere with liposome fusion (287), these GALA-modified liposomes were classical liposomes that lacked a stabilizing polymer such as PEG on the liposome surface. Therefore, an opportunity exists to examine the effect of long-circulating immunoliposomes containing fusogenic peptides such as GALA or TAT (286, 288) on the liposome surface. To make these liposomes long circulating, they can be modified with PEG molecules that are anchored on the surface of these liposomes via pH-sensitive linkage, which can be cleaved at endosomal pH (289). The PEG molecules would mask the fusogenic peptides at the bilayer interface and prevent unintended membrane fusion

during circulation, but upon binding of the antibodies to their antigens, and antigen-mediated internalization, cleavage of the PEG-liposomes linkers would expose the fusogenic peptides on the liposome surface and allow for fusion with the endosomal membrane.

### **6.2.3. Novel Antibody Constructs: Bispecific Antibodies**

Novel antibody constructs, such as bispecific antibodies, may be useful for targeting liposomal drugs. Bispecific (bs) antibodies can be used as a pretargeting agent for liposomes. In one example, a bsmAb, with an anti-tumor domain and an anti-biotin domain, was injected and allowed to localize in the tumor, prior to the treatment of biotinylated liposomal drug (290). Alternatively, immunoliposomes can be conjugated with bsmAb targeted against a tumor antigen and an antigen on effector cells, for example, CD16 on NK cells (291). Binding of these immunoliposomes to tumor cells would lead to specific delivery of the drug as well as the recruitment of NK cells; this would result in direct cell-mediated cytotoxicity against the tumor cells. Bispecific antibodies can also be used to target liposomal drugs against multiple tumor antigens in order to increase binding to tumor cells; an example would be a bsmAb containing anti-CD19 and CD20. For this application, additional advantages of using bs antibodies over combinations of individual mAb are that: 1) two different Fab' fragments can be generated from a single digestion; and 2) bispecific immunoliposomes can be prepared from a single coupling procedure, in comparison to previous methods which employed a separate digestion and coupling step for each mAb (136).

#### 6.2.4. Innovative Approaches to Production of Antibody Fragments

In addition to improving the intrinsic stability of a scFv construct, proper folding of the scFv during expression, and increasing production yields, are also crucial for successful application of scFv-targeted immunoliposomal drugs in the clinic. Proper folding of the scFv during expression is essential to the activity of the scFv construct. Newer approaches to facilitate proper folding of scFv during expression include the co-expression of the scFv with chaperone proteins (292). The fusion of the scFv construct to naturally occurring *E. coli* proteins (e.g., thioredoxin) also resulted in an increase in properly folded, active scFv (293).

*E. coli* has traditionally been the vector of choice for expression of proteins, but induced expression of proteins such as scFv in large quantities in *E. coli* and the resulting formation of insoluble inclusion bodies can be toxic to the bacteria, resulting in lysis of cells and a decrease in production yield (294). Expression of scFv in algal systems, such as *Chlamydomonas reinhardtii*, is relatively cost effective in comparison to other eukaryotic systems such as mammalian cells (295). In addition, algal systems are quite flexible, as a variety of induction methods can be used, and the culture volume can be up to 500,000 L (295). The major drawback for algal systems is the relatively low yields of target proteins, i.e., 0.5-1% of total cell protein, expressed and secreted into the media.

A carrier protein YebF was recently found to be secreted into the culture media of a lab strain of *E. coli* (296). The investigators then went on to demonstrate that functional YebF-fusion proteins, such as YebF- $\alpha$ -amylase and YebF-alkaline phosphatase, both of which are larger than the typical scFv construct, can be secreted into and accumulate in the culture media. Therefore, fusion of scFv constructs to YebF may

result in an increase in production yield of properly folded protein, since the large volume and oxidative environment of the culture media is less conducive to formation of inclusion bodies than the cytoplasm. An additional advantage to purifying scFv from culture media, compared to purification from the periplasmic space or from inclusion bodies in the cytoplasm, is that there are fewer problems with bacterial contaminants in the culture media than in fractionated cells.

### 6.3. Conclusions

In conclusion, this thesis showed that the *in vitro* stability of a scFv construct is crucial to its success as a targeting agent for immunoliposomes. The refolding of scFv from denatured inclusion bodies, although it can dramatically increase the production yield, proved problematic. Hence this approach may not be suitable for many scFv constructs. In addition, this thesis demonstrated that the storage stability of a scFv construct can be increased by conjugation to PEG-lipid micelles. Results in this thesis showed that targeting of immunoliposomal DXR via an anti-CD19 mAb, Fab', or scFv resulted in an increase in toxicity to CD19<sup>+</sup> cells, which is mediated by the CD19 antigen. This thesis has also provided some evidence that, for haematological malignancies, the choice of antibody constructs for the targeting of immunoliposomes may not be wholly dependent on the PK and binding properties of the individual construct, but may also be dependent on other properties such as stability, production yields, cost, immunogenicity and toxicity. ScFv is potentially a useful targeting agent for immunoliposomal drugs, and results in this thesis should provide some future directions for the development of clinically acceptable immunoliposomal anticancer therapy.

## References

1. Greenlee, R. T., Hill-Harmon, M., Murray, T., and Thun, M. Cancer Statistics, *CA Cancer J. Clin.*, 51: 15-36, 2001.
2. Canadian Cancer Statistics. Toronto: National Cancer Institute of Canada; 2007.
3. Demtri, G. D., von Mehren, M., Blanke, C., *et al.* Efficacy and safety of imatinib mesylate in advanced gastrointestinal stromal tumors, *N. Engl. J. Med.*, 347: 472-480, 2002.
4. Cohen, M. H., Williams, G. A., Sridhara, R., Chen, G., and Pazdur, R. FDA drug approval summary: gefitinib (ZD1839) (Iressa) tablets, *Oncologist*, 8: 303-306, 2003.
5. Herbst, R. S., Prager, D., Hermann, R., *et al.* TRIBUTE: a phase III trial of erlotinib hydrochloride (OSI-774) combined with carboplatin and paclitaxel chemotherapy in advanced non-small-cell lung cancer, *J. Clin. Oncol.*, 23: 5892-5899, 2005.
6. Czuczman, M. S., Grillo-Lopez, A. J., White, C. A., *et al.* Treatment of patients with low-grade B-cell lymphoma with the combination of chimeric anti-CD20 monoclonal antibody and CHOP chemotherapy, *J. Clin. Oncol.*, 17: 268-276, 1999.
7. Coiffier, B., Lepage, E., Briere, J., *et al.* CHOP chemotherapy plus Rituximab compared with CHOP alone in elderly patients with diffuse large B-cell lymphoma, *N. Eng. J. Med.*, 346: 235-242, 2002.
8. Feugier, P., Van Hoof, A., Sebban, C., *et al.* Long-term results of the R-CHOP study in the treatment of elderly patients with diffuse large B-cell lymphoma: a

- study by the Groupe d'Etude des Lymphomes de l'Adulte., *J. Clin. Oncol.*, *23*: 4117-4126, 2005.
9. Feld, R., Sridhar, S. S., Shepherd, F. A., Mackay, J. A., and Evans, W. K. Use of the epidermal growth factor receptor inhibitors gefitinib and erlotinib in the treatment of non-small cell lung cancer: a systematic review, *J. Thorac. Oncol.*, *1*: 367-376, 2006.
  10. Noble, J., Ellis, P. M., Mackay, J. A., and Evans, W. K. Second-line or subsequent systemic therapy for recurrent or progressive non-small cell lung cancer: a systematic review and practice guideline, *J. Thorac. Oncol.*, *1*: 1042-1058, 2006.
  11. Bencardino, K., Manzoni, M., Delfanti, S., Riccardi, A., Danova, M., and Corazza, G. R. Epidermal growth factor receptor tyrosine kinase inhibitors for the treatment of non-small-cell lung cancer: results and open issues, *Intern. Emerg. Med.*, *2*: 3-12, 2007.
  12. Allen, T. M. Ligand-targeted therapeutics in anticancer therapy, *Nat. Rev. Cancer*, *2*: 750-763, 2002.
  13. Kaminski, M. S., Zelenetz, A. D., Press, O. W., *et al.* Pivotal study of iodine I<sup>131</sup> tositumomab for chemotherapy-refractory low-grade or transformed low-grade B-cell non-Hodgkin's lymphomas, *J. Clin. Oncol.*, *19*: 3908-3911, 2001.
  14. Herrera, L., Yarbrough, S., Ghetie, V., Aquino, D. B., and Vitetta, E. S. Treatment of SCID/human B cell precursor ALL with anti-CD19 and anti-CD22 immunotoxins., *Leukemia*, *17*: 334-338, 2003.

15. Trail, P. A., Willner, D., Lasch, S. J., *et al.* Cure of xenografted human carcinomas by BR96-doxorubicin immunoconjugates, *Science*, *261*: 212-215, 1993.
16. Allen, T. M. and Cullis, P. R. Drug delivery systems: entering the mainstream, *Science*, *303*: 1818-1822, 2004.
17. Duncan, R. The dawning era of polymer therapeutics, *Nat. Rev. Drug Discov.*, *2*: 347-360, 2003.
18. Allen, T. M., Cheng, W. W., Hare, J. I., and Laginha, K. M. Pharmacokinetics and pharmacodynamics of lipidic nano-particles in cancer, *Anticancer Agents Med. Chem.*, *6*: 513-523, 2006.
19. Bangham, A. D., Standish, M. M., and Watkins, J. C. Diffusion of univalent ions across the lamellae of swollen phospholipids, *J. Mol. Biol.*, *13*: 238-252, 1965.
20. Adler-Moore, J. AmBisome targeting to fungal infections., *Bone Marrow Transplant.*, *14, Suppl 5*: S3-7, 1994.
21. Batist, G., Ramakrishnan, G., Rao, C. S., *et al.* Reduced cardiotoxicity and preserved antitumor efficacy of liposome-encapsulated doxorubicin and cyclophosphamide compared with conventional doxorubicin and cyclophosphamide in a randomized, multicenter trial of metastatic breast cancer., *J. Clin. Oncol.*, *19*: 1444-1454, 2001.
22. Northfelt, D. W., Dezube, B. J., Thommes, J. A., *et al.* Efficacy of pegylated-liposomal doxorubicin in the treatment of AIDS-related Kaposi's sarcoma after failure of standard chemotherapy, *J. Clin. Oncol.*, *15*: 653-659, 1997.

23. Presant, C. A., Scolaro, M., Kennedy, P., *et al.* Liposomal daunorubicin treatment of HIV-associated Kaposi's sarcoma, *Lancet*, *341*: 1242-1243, 1993.
24. Glantz, M. J., Jaeckle, K. A., Chamberlain, M. C., *et al.* A randomized controlled trial comparing intrathecal sustained-release cytarabine (DepoCyt) to intrathecal methotrexate in patients with neoplastic meningitis from solid tumors., *Clin. Cancer Res.*, *5*: 3394-3402, 1999.
25. Sessa, G. and Weissmann, G. Phospholipid spherules (liposomes) as a model for biological membranes, *J. Lipid Res.*, *9*: 310-318, 1968.
26. Gregoriadis, G. and Ryman, B. E. Liposomes as carriers of enzymes or drugs: a new approach to the treatment of storage diseases., *Biochem. J.*, *124*: 58P, 1971.
27. Gregoriadis, G. Drug entrapment in liposomes, *FEBS Lett.*, *36*: 292, 1973.
28. Lasic, D. D. *Liposomes: from physics to applications*, p.575. Amsterdam: Elsevier Science Publishers B.V.; 1993.
29. Huwyler, J., Wu, D., and Pardridge, W. M. Brain drug delivery of small molecules using immunoliposomes, *Proc. Natl. Acad. Sci. U.S.A.*, *93*: 14164-14169, 1996.
30. Legha, S. S., Benjamin, R. S., Mackay, B., *et al.* Reduction of doxorubicin cardiotoxicity by prolonged continuous intravenous infusion, *Ann. Intern. Med.*, *96*: 133-139, 1982.
31. Doroshow, J. H. Anthracyclines and Antracenediones. *In*: B. A. Chabner and D. L. Longo ('B. A. Chabner and D. L. Longo'('B. A. Chabner and D. L. Longos')). *Cancer chemotherapy & biotherapy: principles and practice*. p.500-537. Philadelphia: Lippincott Williams & Wilkins; 2001.

32. Gabizon, A., Catane, R., Uziely, B., *et al.* Prolonged circulation time and enhanced accumulation in malignant exudates of doxorubicin encapsulated in polyethylene-glycol coated liposomes, *Cancer Res.*, *54*: 987-992, 1994.
33. Cowens, J. W., Creaven, P. J., Greco, W. R., *et al.* Initial clinical (phase I) trial of TLC D-99 (doxorubicin encapsulated in liposomes), *Cancer Res.*, *53*: 2796-2802, 1993.
34. Samuels, B. L., Vogelzang, N. J., Ruane, M., and Simon, M. A. Continuous venous infusion of doxorubicin in advanced sarcomas, *Cancer Treat. Rep.*, *71*: 971-972, 1987.
35. Huan, S., Pazdur, R., Singhakowinta, A., Samal, B., and Vaitkevicius, V. K. Low-dose continuous infusion 5-fluorouracil. Evaluation in advanced breast carcinoma, *Cancer*, *63*: 419-422, 1989.
36. Muggia, F., Hainsworth, J. D., Jeffers, S., *et al.* Phase II study of liposomal doxorubicin in refractory ovarian cancer: antitumor activity and toxicity modification by liposomal encapsulation., *J. Clin. Oncol.*, *15*: 987-993, 1997.
37. Gordon, A. N., Granai, C. O., Rose, P. G., *et al.* Phase II study of liposomal doxorubicin in platinum- and paclitaxel-refractory epithelial ovarian cancer, *J. Clin. Oncol.*, *18*: 3093-3100, 2000.
38. Ranson, M. R., Carmichael, J., O'Byrne, K., Stewart, S., Smith, D., and Howell, A. Treatment of advanced breast cancer with sterically stabilized liposomal doxorubicin: results of a multicenter phase II trial, *J. Clin. Oncol.*, *15*: 3185-3191, 1997.

39. Allen, T. M. and Hansen, C. B. Pharmacokinetics of Stealth versus conventional liposomes: effect of dose, *Biochim. Biophys. Acta*, *1068*: 133-141, 1991.
40. Romberg, B., Metselaar, J. M., deVringer, T., *et al.* Enzymatic degradation of liposome-grafted poly(hydroxyethyl L-glutamine), *Bioconjug. Chem.*, *16*: 767-774, 2005.
41. Romberg, B., Metselaar, J. M., Baranyi, L., *et al.* Poly(amino acid)s: promising enzymatically degradable stealth coatings for liposomes, *Int. J. Pharm.*, *331*: 186-189, 2007.
42. Papahadjopoulos, D., Allen, T. M., Gabizon, A., *et al.* Sterically stabilized liposomes: improvements in pharmacokinetics and antitumor therapeutic efficacy, *Proc. Natl. Acad. Sci. U.S.A.*, *88*: 11460-11464, 1991.
43. Matsumura, Y. and Maeda, H. A new concept for macromolecular therapeutics in cancer chemotherapy; mechanism of tumoritropic accumulation of proteins and the antitumor agent SMANCS, *Cancer Res.*, *46*: 6387-6392, 1986.
44. Seymour, L. W. Passive tumor targeting of soluble macromolecules and drug conjugates, *Crit. Rev. Ther. Drug Carrier Syst.*, *9*: 135-187, 1992.
45. Jain, R. K. Delivery of molecular and cellular medicine to solid tumors., *J. Control. Release*, *53*: 49-67, 1998.
46. Yuan, F., Leunig, M., Huang, S. K., Berk, D. A., Papahadjopoulos, D., and Jain, R. K. Microvascular permeability and interstitial penetration of sterically stabilized (Stealth) liposomes in a human tumor xenograft, *Cancer Res.*, *54*: 3352-3356, 1994.

47. Yuan, F., Dellian, M., Fukumura, D., *et al.* Vascular permeability in a human tumour xenograft: molecular size dependence and cutoff size, *Cancer Res.*, *55*: 3752-3756, 1995.
48. Northfelt, D. W., Martin, F. J., Working, P., *et al.* Doxorubicin encapsulated in liposomes containing surface-bound polyethylene glycol: pharmacokinetics, tumour localization, and safety in patients with AIDS-related Kaposi's sarcoma, *J. Clin. Pharmacol.*, *36*: 55-63, 1996.
49. Gabizon, A., Shiota, R., and Papahadjopoulos, D. Pharmacokinetics and tissue distribution of doxorubicin encapsulated in stable liposomes with long circulation times, *J. Natl. Cancer Inst.*, *81*: 1484-1488, 1989.
50. Gabizon, A. A. Selective tumor localization and improved therapeutic index of anthracyclines encapsulated in long-circulating liposomes, *Cancer Res.*, *52*: 891-896, 1992.
51. Gabizon, A. A., Lyass, O., Berry, G. J., and Wildgust, M. Cardiac safety of pegylated liposomal doxorubicin (Doxil/Caelyx) demonstrated by endomyocardial biopsy in patients with advanced malignancies., *Cancer Invest.*, *22*: 663-669, 2004.
52. Lee, R. J. and Low, P. S. Folate-mediated tumor cell targeting of liposome-entrapped doxorubicin *in vitro*, *Biochim. Biophys. Acta*, *1233*: 134-144, 1995.
53. Gabizon, A., Horowitz, A. T., Goren, D., *et al.* Targeting folate receptor with folate linked to extremities of poly(ethylene glycol)-grafted liposomes: *in vitro* studies, *Bioconjugate Chem.*, *10*: 289-298, 1999.

54. Suzuki, S., Inoue, K., Hongoh, A., Hashimoto, Y., and Yamazoe, Y. Modulation of doxorubicin resistance in a doxorubicin-resistant human leukaemia cell by an immunoliposome targeting transferrin receptor, *Br. J. Cancer*, *76*: 83-89, 1997.
55. Pastorino, F., Brignole, C., Marimpietri, D., *et al.* Vascular damage and anti-angiogenic effects of tumor vessel-targeted liposomal chemotherapy., *Cancer Res.*, *63*: 7400-7409, 2003.
56. Dubey, P. K., Mishra, V., Jain, S., Mahor, S., and Vyas, S. P. Liposomes modified with cyclic RGD peptide for tumor targeting, *J Drug Target.*, *12*: 257-264, 2004.
57. Maruyama, K., Takizawa, T., Yuda, T., Kennel, S. J., Huang, L., and Iwatsuru, M. Targetability of novel immunoliposomes modified with amphipathic poly(ethylene glycol)s conjugated at their distal terminals to monoclonal antibodies, *Biochim. Biophys. Acta*, *1234*: 74-80, 1995.
58. Emanuel, N., Kedar, E., Bolotin, E. M., Smorokinsky, N. I., and Barenholz, Y. Preparation and characterization of doxorubicin-loaded sterically stabilized immunoliposomes, *Pharm. Res.*, *13*: 352-359, 1996.
59. Atobe, K., Ishida, T., Ishida, E., *et al.* In vitro efficacy of a sterically stabilized immunoliposomes targeted to membrane type 1 matrix metalloproteinase (MT1-MMP), *Biol. Pharm. Bull.*, *30*: 972-978, 2007.
60. Ahmad, I. and Allen, T. M. Antibody-mediated specific binding and cytotoxicity of liposome-entrapped doxorubicin to lung cancer cells in vitro, *Cancer Res.*, *52*: 4817-4820, 1992.

61. Lopes de Menezes, D. E., Pilarski, L. M., and Allen, T. M. In vitro and in vivo targeting of immunoliposomal doxorubicin to human B-cell lymphoma, *Cancer Res.*, *58*: 3320-3330, 1998.
62. Sapra, P., Moase, E. H., Ma, J., and Allen, T. M. Improved therapeutic responses in a xenograft model of human B-lymphoma (Namalwa) for liposomal vincristine versus liposomal doxorubicin targeted via anti-CD19 IgG2a or Fab' fragments, *Clin. Cancer Res.*, *10*: 1100-1111, 2004.
63. Sapra, P. and Allen, T. M. Improved outcome when B-cell lymphoma is treated with combinations of immunoliposomal anticancer drugs targeted to both the CD19 and CD20 epitopes, *Clin. Cancer Res.*, *10*: 2530-2537, 2004.
64. Park, J. W., Hong, K., Kirpotin, D. B., *et al.* Anti-HER2 immunoliposomes: Enhanced efficacy attributable to targeted delivery, *Clin. Cancer Res.*, *8*: 1172-1181, 2002.
65. Park, J. W., Hong, K., Carter, P., *et al.* Development of anti-p185<sup>HER2</sup> immunoliposomes for cancer therapy, *Proc. Natl. Acad. Sci. U.S.A.*, *92*: 1327-1331, 1995.
66. Nellis, D. F., Ekstrom, D. L., Kirpotin, D. B., *et al.* Preclinical Manufacture of an Anti-HER2 scFv-PEG-DSPE, Liposome-Inserting conjugate. 1. Gram-Scale Production and Purification, *Biotechnol. Prog.*, *21*: 205-220, 2005.
67. Nellis, D. F., Giardina, S. L., Janini, G. M., *et al.* Preclinical manufacture of anti-HER2 liposome-inserting, scFv-PEG-lipid conjugate. 2. Conjugate micelle identity, purity, stability, and potency analysis, *Biotechnol. Prog.*, *21*: 221-232, 2005.

68. Woodle, M. C. and Papahadjopoulos, D. Liposome preparation and size characterization, *Meth. Enzymol.*, *171*: 193-217, 1989.
69. Szoka, F. and Papahadjopoulos, D. Procedure for preparation of liposomes with large internal aqueous space and high capture by reverse-phase evaporation, *Proc. Natl. Acad. Sci. U.S.A.*, *75*: 4194-4198, 1978.
70. Batzri, S. and Korn, E. D. Single bilayer liposomes prepared without sonication, *Biochim. Biophys. Acta*, *16*: 1015-1019, 1973.
71. Phillipot, J. R. and Liautard, J. P. A very mild method allowing the encapsulation of very high amounts of macromolecules into very large (1000 nm) unilamellar liposomes. *In*: G. Gregoriadis ('G. Gregoriadis'). G. Gregoriadis. Liposome technology: liposome preparation and related techniques. p.81-98. Boca Raton, FL.: CRC Press; 1993.
72. Hope, M. J., Bally, M. B., Mayer, L. D., Janoff, A. S., and Cullis, P. R. Generation of multilamellar and unilamellar phospholipid vesicles, *Chem. Phys. Lipids*, *40*: 89-96, 1986.
73. Mayer, L. D., Hope, M. J., Cullis, P. R., and Janoff, A. S. Solute distributions and trapping efficiencies observed in freeze-thawed multilamellar vesicles, *Biochim. Biophys. Acta*, *817*: 193-196, 1985.
74. Hauser, H. Phospholipid vesicles. *In*: G. Cevc ('G. Cevc'). Phospholipids Handbook. 1993.
75. Huang, C. H. Studies on phosphatidylcholine vesicles: formation and physical characteristics, *Biochemistry*, *8*: 344-352, 1969.

76. Szoka, F., Olson, F., Heath, T., Vail, W., Mayhew, E., and Papahadjopoulos, D. Preparation of unilamellar liposomes of intermediate size (0.1-0.2  $\mu\text{mol}$ ) by a combination of reverse phase evaporation and extrusion through polycarbonate membranes, *Biochim. Biophys. Acta*, *601*: 559-571, 1980.
77. Hope, M. J., Bally, M. B., Webb, G., and Cullis, P. R. Production of large unilamellar vesicles by a rapid extrusion procedure. Characterization of size distribution, trapped volume and ability to maintain a membrane potential., *Biochim. Biophys. Acta*, *812*: 55-65, 1985.
78. Sharma, A. and Straubinger, R. M. Novel taxol formulations, preparation and characterisation of taxol-containing liposomes, *Pharm. Res.*, *11*: 889-896, 1994.
79. Mayer, L. D., Bally, M. B., and Cullis, P. R. Uptake of adriamycin into large unilamellar vesicles in response to a pH gradient, *Biochim. Biophys. Acta*, *857*: 123-126, 1986.
80. Madden, T. D., Harrigan, P. R., Tai, L. C., *et al.* The accumulation of drugs within large unilamellar vesicles exhibiting a proton gradient: a survey, *Chem. Phys. Lipids*, *53*: 37-46, 1990.
81. Haran, G., Cohen, R., Bar, L. K., and Barenholz, Y. Transmembrane ammonium sulfate gradients in liposomes produce efficient and stable entrapment of amphipathic weak bases, *Biochim. Biophys. Acta*, *1151*: 201-215, 1993.
82. Mayer, L. D., Tai, L. C., Bally, M. B., Mitilenes, G. N., Ginsberg, R. S., and Cullis, P. R. Characterization of liposomal systems containing doxorubicin entrapped in response to pH gradients, *Biochim. Biophys. Acta*, *1025*: 143-151, 1990.

83. Bolotin, E. M., Cohen, R., Bar, L. K., Emanuel, S. N., Lasic, D. D., and Barenholz, Y. Ammonium sulphate gradients for efficient and stable remote loading of amphipathic weak bases into liposomes and ligandosomes, *J. Liposome Res.*, *4*: 455-479, 1994.
84. Gabizon, A. A., Barenholz, Y., and Bialer, M. Prolongation of the circulation time of doxorubicin encapsulated in liposomes containing a polyethylene glycol-derivatized phospholipid: pharmacokinetic studies in rodents and dogs, *Pharm. Res.*, *10*: 703-708, 1993.
85. Charrois, G. J. R. and Allen, T. M. Drug release rate influences the pharmacokinetics, biodistribution, therapeutic activity, and toxicity of pegylated liposomal doxorubicin formulations in murine breast cancer, *Biochim. Biophys. Acta*, *1663*: 167-177, 2004.
86. Allen, T. M., Mumbengegwi, D. R., and Charrois, G. J. Anti-CD19-targeted liposomal doxorubicin improves the therapeutic efficacy in murine B-cell lymphoma and ameliorates the toxicity of liposomes with varying drug release rates, *Clin. Cancer Res.*, *11*: 3567-3573, 2005.
87. Johnston, M. J., Semple, S. C., Klimuk, S. K., *et al.* Therapeutically optimized rates of drug release can be achieved by varying the drug-to-lipid ratio in liposomal vincristine formulations, *Biochim. Biophys. Acta*, *1758*: 55-64, 2006.
88. Allen, T. M., Brandeis, E., Hansen, C. B., Kao, G. Y., and Zalipsky, S. A new strategy for attachment of antibodies to sterically stabilized liposomes resulting in efficient targeting to cancer cells, *Biochim. Biophys. Acta*, *1237*: 99-108, 1995.

89. Zalipsky, S. Synthesis of end-group functionalized polyethylene glycol-lipid conjugates for preparation of polymer-grafted liposomes, *Bioconjugate Chem.*, *4*: 296-299, 1993.
90. Kirpotin, D., Park, J. W., Hong, K., *et al.* Sterically stabilized anti-HER2 immunoliposomes: design and targeting to human breast cancer cells *in vitro*, *Biochemistry*, *36*: 66-75, 1997.
91. Mamot, C., Drummond, D. C., Greiser, U., *et al.* Epidermal growth factor receptor (EGFR)-targeted immunoliposomes mediate specific and efficient drug delivery to EGFR- and EGFRvIII-overexpressing tumor cells., *Cancer Res.*, *63*: 3154-3161, 2003.
92. Pastorino, F., Brignole, C., Marimpietri, D., *et al.* Doxorubicin-loaded Fab' fragments of anti-disialoganglioside immunoliposomes selectively inhibit the growth and dissemination of human neuroblastoma in nude mice, *Cancer Res.*, *63*: 86-92, 2003.
93. Loughrey, H., Bally, M. B., and Cullis, P. R. A non-covalent method of attaching antibodies to liposomes, *Biochim. Biophys. Acta*, *901*: 157-160, 1987.
94. Hansen, C. B., Kao, G. Y., Moase, E. H., Zalipsky, S., and Allen, T. M. Attachment of antibodies to sterically stabilized liposomes: evaluation, comparison and optimization of coupling procedures, *Biochim. Biophys. Acta*, *1239*: 133-144, 1995.
95. Pan, X. and Lee, R. J. Construction of anti-EGFR immunoliposomes via folate-folate binding protein affinity, *Int. J. Pharm.*, *336*: 276-283, 2007.

96. Ruger, R., Muller, D., Fahr, A., and Kontermann, R. E. Generation of immunoliposomes using recombinant single-chain Fv fragments bound to Ni-NTA-liposomes, *J. Drug Target.*, *13*: 399-406, 2005.
97. Ruger, R., Muller, D., Fahr, A., and Kontermann, R. E. In vitro characterization of binding and stability of single-chain Fv Ni-NTA-liposomes, *J. Drug Target.*, *14*: 576-582, 2006.
98. Ishida, T., Iden, D. L., and Allen, T. M. A combinatorial approach to producing sterically stabilized (Stealth) immunoliposomal drugs, *FEBS Lett.*, *460*: 129-133, 1999.
99. Iden, D. L. and Allen, T. M. In vitro and in vivo comparison of immunoliposomes made by conventional coupling techniques with those made by a new post-insertion technique, *Biochim. Biophys. Acta*, *1513*: 207-216, 2001.
100. Allen, T. M., Sapra, P., and Moase, E. Use of the post-insertion method for the formation of ligand-coupled liposomes, *Cell. Mol. Biol. Lett.*, *7*: 889-894, 2002.
101. Lundberg, B. B., Griffiths, G., and Hansen, H. J. Cellular association and cytotoxicity of doxorubicin-loaded immunoliposomes targeted via Fab' fragments of an anti-CD74 antibody, *Drug Deliv.*, *14*: 171-175, 2007.
102. Pastorino, F., Brignole, C., Di Paolo, D., *et al.* Targeting liposomal chemotherapy via both tumor cell-specific and tumor vasculature-specific ligands potentiates therapeutic efficacy, *Cancer Res.*, *66*: 10073-10082, 2006.
103. Gazzaniga, S., Bravo, A. I., Guglielmotti, A., *et al.* Targeting tumor-associated macrophages and inhibition of MCP-1 reduce angiogenesis and tumor growth in a human melanoma xenograft, *J. Invest. Dermatol.*, *127*: 2031-2041, 2007.

104. Sapra, P. and Allen, T. M. Internalizing antibodies are necessary for improved therapeutic efficacy of antibody-targeted liposomal drugs, *Cancer Res.*, *62*: 7190-7194, 2002.
105. Kirpotin, D. B., Drummond, D. C., Shao, Y., *et al.* Antibody targeting of long-circulating lipidic nanoparticles does not increase tumor localization but does increase internalization in animal models, *Cancer Res.*, *66*: 6732-6740, 2006.
106. Nielsen, U. B. and Marks, J. D. Internalizing antibodies and targeted cancer therapy: direct selection from phage display libraries, *Pharm. Sci. Technol. Today*, *3*: 282-291, 2000.
107. Hosokawa, S., Tagawa, T., Niki, H., Hirakawa, Y., Nohga, K., and Nagaike, K. Efficacy of immunoliposomes on cancer models in a cell-surface-antigen-density-dependent manner, *Br. J. Cancer*, *89*: 1545-1551, 2003.
108. Neve, R. M., Nielsen, U. B., Kirpotin, D. B., Poul, M. A., Marks, J. D., and Benz, C. C. Biological effects of anti-ErbB2 single chain antibodies selected for internalizing function, *Biochem. Biophys. Res. Commun.*, *280*: 274-279, 2001.
109. Goren, D., Horowitz, A. T., Zalipsky, S., Woodle, M. C., Yarden, Y., and Gabizon, A. Targeting of Stealth liposomes to erB-2 (Her/2) receptor: in vitro and in vivo studies, *Br. J. Cancer*, *74*: 1749-1756, 1996.
110. Park, J. W., Hong, K., Kirpotin, D. B., Meyer, O., Papahadjopoulos, D., and Benz, C. C. Anti-HER2 immunoliposomes for targeted therapy of human tumors, *Cancer Lett.*, *118*: 153-160, 1997.

111. Yarden, Y. Agonistic antibodies stimulate the kinase encoded by the neu protooncogene in living cells but the oncogenic mutant is constitutively active, *Proc. Natl. Acad. Sci. U.S.A.*, *87*: 2569-2573, 1990.
112. Guillemard, V., Nedev, H. N., Berezov, A., Murali, R., and Saragovi, H. U. HER2-mediated internalization of a targeted prodrug cytotoxic conjugate is dependent on the valency of the targeting ligand, *DNA Cell Biol.*, *24*: 350-358, 2005.
113. Paulos, C. M., Reddy, J. A., Leamon, C. P., Turk, M. J., and Low, P. S. Ligand binding and kinetics of folate receptor recycling in vivo: impact on receptor-mediated drug delivery, *Mol. Pharmacol.*, *66*: 1406-1414, 2004.
114. Vose, J. M., Link, B. K., Grossbard, M. L., *et al.* Phase II study of rituximab in combination with CHOP chemotherapy in patients with previously untreated, aggressive non-Hodgkin's lymphoma, *J. Clin. Oncol.*, *19*: 389-397, 2001.
115. Emmanouilides, C., Jazirehi, A. R., and Bonavida, B. Rituximab-mediated sensitization of B-non-Hodgkin's lymphoma (NHL) to cytotoxicity induced by paclitaxel, gemcitabine, and vinorelbine, *Cancer Biother. Radiopharm.*, *17*: 621-630, 2002.
116. Jazirehi, A. R. and Bonavida, B. Cellular and molecular signal transduction pathways modulated by rituximab (rituxan, anti-CD20 mAb) in non-Hodgkin's lymphoma: implications in chemosensitization and therapeutic intervention, *Oncogene*, *24*: 2121-2143, 2005.

117. Sliwkowski, M. X., Lofgren, J. A., Lewis, G. D., Hotaling, T. E., Fendly, B. M., and Fox, J. A. Nonclinical studies addressing the mechanism of action of trastuzumab (Herceptin), *Semin. Oncol.*, 26: 60-70, 1999.
118. Glennie, M. J. and van de Winkel, J. G. Renaissance of cancer therapeutic antibodies, *Drug Discov. Today*, 8: 503-510, 2003.
119. Tempero, M. A., Pour, P. M., Uchida, E., Herlyn, D., and Steplewski, Z. Monoclonal antibody CO17-1A and leukapheresis in immunotherapy of pancreatic cancer, *Hybridoma*, 5 *Suppl 1*: S133-138, 1986.
120. Thorpe, S. J., Turner, C., Heath, A., *et al.* Clonal analysis of a human antimouse antibody (HAMA) response, *Scand. J. Immunol.*, 57: 85-92, 2003.
121. Adams, G. P. and Weiner, L. M. Monoclonal antibody therapy of cancer, *Nat. Biotechnol.*, 23: 1147-1157, 2005.
122. Qu, Z., Griffiths, G. L., Wegener, W. A., *et al.* Development of humanized antibodies as cancer therapeutics, *Methods*, 36: 84-95, 2005.
123. Morrison, S. L., Johnson, M. J., Herzenberg, L. A., and Oi, V. T. Chimeric human antibody molecules: mouse antigen-binding domains with human constant region domains, *Proc. Natl. Acad. Sci. U.S.A.*, 81: 6851-6855, 1984.
124. Jones, P. T., Dear, P. H., Foote, J., Neuberger, M. S., and Winter, G. Replacing the complementarity-determining regions in a human antibody with those from a mouse, *Nature*, 321: 522-525, 1986.
125. Lonberg, N., Taylor, L. D., Harding, F. A., *et al.* Antigen-specific human antibodies from mice comprising four distinct genetic modifications, *Nature*, 368: 856-859, 1994.

126. Shen, G. L., Li, J. L., Ghetie, M. A., *et al.* Evaluation of four CD22 antibodies as ricin A chain-containing immunotoxins for the in vivo therapy of human B-cell leukemias and lymphomas, *Int. J. Cancer*, *42*: 792-797, 1988.
127. Juweid, M., Neumann, R., Paik, C., *et al.* Micropharmacology of monoclonal antibodies in solid tumors: direct experimental evidence for a binding site barrier, *Cancer Res.*, *52*: 5144-5153, 1992.
128. Adams, G. P., Schier, R., McCall, A. M., *et al.* High affinity restricts the localization and tumor penetration of single-chain fv antibody molecules, *Cancer Res.*, *61*: 4750-4755, 2001.
129. Brekke, O. H. and Sandlie, I. Therapeutic antibodies for human diseases at the dawn of the twenty-first century, *Nat. Rev. Cancer*, *2*: 52-62, 2003.
130. Pini, A. and Bracci, L. Phage display of antibody fragments, *Curr. Protein Pept. Sci.*, *1*: 155-169, 2000.
131. Zahnd, C., Amstutz, P., and Pluckthun, A. Ribosome display: selecting and evolving proteins in vitro that specifically bind to a target, *Nat. Methods*, *4*: 269-279, 2007.
132. Nielsen, U. B., Kirpotin, D. B., Pickering, E. M., *et al.* Therapeutic efficacy of anti-ErbB2 immunoliposomes targeted by a phage antibody selected for cellular endocytosis, *Biochim. Biophys. Acta*, *1591*: 109-118, 2002.
133. Willuda, J., Kubetzko, S., Waibel, R., Schubiger, P. A., Zangemeister-Wittke, U., and Pluckthun, A. Tumor targeting of mono-, di-, and tetravalent anti-p185(HER-2) miniantibodies multimerized by self-associating peptides, *J. Biol. Chem.*, *276*: 14385-14392, 2001.

134. Kubetzko, S., Balic, E., Waibel, R., Zangemeister-Wittke, U., and Pluckthun, A. PEGylation and multimerization of the anti-p185HER-2 single chain Fv fragment 4D5: effects on tumor targeting, *J. Biol. Chem.*, *281*: 35186-35201, 2006.
135. Chiu, G. N., Edwards, L. A., Kapanen, A. I., *et al.* Modulation of cancer cell survival pathways using multivalent liposomal therapeutic antibody constructs, *Mol. Cancer Ther.*, *6*: 844-855, 2007.
136. Laginha, K., Mumbengegwi, D., and Allen, T. Liposomes targeted via two different antibodies: assay, B-cell binding and cytotoxicity, *Biochim. Biophys. Acta*, *1711*: 25-32, 2005.
137. Maruyama, K., Takahashi, N., Tagawa, T., Nagaike, K., and Iwatsuru, M. Immunoliposomes bearing polyethyleneglycol-coupled Fab' fragment show prolonged circulation time and high extravasation into targeted solid tumors *in vivo*, *FEBS Lett.*, *413*: 177-180, 1997.
138. Marty, C., Odermatt, B., Schott, H., *et al.* Cytotoxic targeting of F9 teratocarcinoma tumours with anti-ED-B fibronectin scFv antibody modified liposomes, *Br. J. Cancer*, *87*: 106-112, 2002.
139. Kohler, G. and Milstein, C. Continuous cultures of fused cells secreting antibody of predefined specificity, *Nature*, *256*: 495-497, 1975.
140. van Kuik-Romeijn, P., de Groot, N., Hooijberg, E., and de Boer, H. A. Expression of a functional mouse-human chimeric anti-CD19 antibody in the milk of transgenic mice, *Transgenic Res.*, *9*: 155-159, 2000.
141. Andersen, D. C. and Krummen, L. Recombinant protein expression for therapeutic applications, *Curr. Opin. Biotechnol.*, *13*: 117-123, 2002.

142. Roque, A. C., Lowe, C. R., and Taipa, M. A. Antibodies and genetically engineered related molecules: production and purification, *Biotechnol. Prog.*, *20*: 639-654, 2004.
143. Limonta, J., Pedraza, A., Rodriguez, A., *et al.* Production of active anti-CD6 mouse/human chimeric antibodies in the milk of transgenic mice, *Immunotechnology*, *1*: 107-113, 1995.
144. Young, M. W., Meade, H., Curling, J. M., Ziomek, C. A., and Harvey, M. Production of recombinant antibodies in the milk of transgenic animals, *Res. Immunol.*, *149*: 609-610, 1998.
145. Newton, D. L., Pollock, D., DiTullio, P., *et al.* Antitransferrin receptor antibody-RNase fusion protein expressed in the mammary gland of transgenic mice, *J. Immunol. Methods*, *231*: 159-167, 1999.
146. Little, M., Kipriyanov, S. M., Le Gall, F., and Moldenhauer, G. Of mice and men: hybridoma and recombinant antibodies, *Immunol. Today*, *21*: 364-370, 2000.
147. Ma, J. K., Hiatt, A., Hein, M., *et al.* Generation and assembly of secretory antibodies in plants, *Science*, *268*: 716-719, 1995.
148. Fiedler, U. and Conrad, U. High-level production and long-term storage of engineered antibodies in transgenic tobacco seeds, *Biotechnology (N Y)*, *13*: 1090-1093, 1995.
149. Houdebine, L. M. Antibody manufacture in transgenic animals and comparisons with other systems, *Curr. Opin. Biotechnol.*, *13*: 625-629, 2002.
150. Parham, P. On the fragmentation of monoclonal IgG1, IgG2a, and IgG2b from BALB/c mice, *J. Immunol.*, *131*: 2895-2902, 1983.

151. Marty, C., Scheidegger, P., Ballmer-Hofer, K., Klemenz, R., and Schwendener, R. A. Production of functionalized single-chain Fv antibody fragments binding to the ED-B domain of the B-isoform of fibronectin in *Pichia pastoris*, *Protein Expr. Purif.*, *21*: 156-164, 2001.
152. Galeffi, P., Lombardi, A., Pietraforte, I., *et al.* Functional expression of a single-chain antibody to ErbB-2 in plants and cell-free systems, *J. Transl. Med.*, *4*: 39, 2006.
153. Ford, C. F., Suominen, I., and Glatz, C. E. Fusion tails for the recovery and purification of recombinant proteins, *Protein Expr Purif.*, *2*: 95-107, 1991.
154. Einhauer, A. and Jungbauer, A. The FLAG peptide, a versatile fusion tag for the purification of recombinant proteins, *J. Biochem. Biophys. Methods*, *49*: 455-465, 2001.
155. Kipriyanov, S. M., Dubel, S., Breitling, F., Kontermann, R. E., Heymann, S., and Little, M. Bacterial expression and refolding of single-chain Fv fragments with C-terminal cysteines, *Cell Biophys.*, *26*: 187-204, 1995.
156. Tsumoto, K., Shinoki, K., Kondo, H., Uchikawa, M., Juji, T., and Kumagai, I. Highly efficient recovery of functional single-chain Fv fragments from inclusion bodies overexpressed in *Escherichia coli* by controlled introduction of oxidizing reagent--application to a human single-chain Fv fragment, *J. Immunol. Methods*, *219*: 119-129, 1998.
157. Das, D., Kriangkum, J., Nagata, L. P., Fulton, R. E., and Suresh, M. R. Development of a biotin mimic tagged ScFv antibody against western equine

- encephalitis virus: bacterial expression and refolding, *J. Virol. Methods*, *117*: 169-177, 2004.
158. Bessette, P. H., Aslund, F., Beckwith, J., and Georgiou, G. Efficient folding of proteins with multiple disulfide bonds in the *Escherichia coli* cytoplasm, *Proc. Natl. Acad. Sci. U.S.A.*, *96*: 13703-13708, 1999.
159. Lukes, R. J. and Collins, R. D. Immunologic characterization of human malignant lymphomas, *Cancer*, *34*: suppl:1488-1503, 1974.
160. National Cancer Institute sponsored study of classifications of non-Hodgkin's lymphomas: summary and description of a working formulation for clinical usage. The Non-Hodgkin's Lymphoma Pathologic Classification Project, *Cancer*, *49*: 2112-2135, 1982.
161. Harris, N. L., Jaffe, E. S., Stein, H., *et al.* A revised European-American classification of lymphoid neoplasms: a proposal from the International Lymphoma Study Group, *Blood*, *84*: 1361-1392, 1994.
162. Harris, N. L., Jaffe, E. S., Diebold, J., *et al.* The World Health Organization classification of neoplastic diseases of the hematopoietic and lymphoid tissues. Report of the Clinical Advisory Committee meeting, Airlie House, Virginia, November, 1997, *Ann. Oncol.*, *10*: 1419-1432, 1999.
163. Canadian Cancer Statistics. Toronto: National Cancer Institute of Canada; 2006.
164. Skarin, A. T. and Dorfman, D. M. Non-Hodgkin's lymphomas: current classification and management, *CA Cancer J. Clin.*, *47*: 351-372, 1997.
165. Coiffier, B. Monoclonal antibody as therapy for malignant lymphomas, *C. R. Biol.*, *329*: 241-254, 2006.

166. A clinical evaluation of the International Lymphoma Study Group classification of non-Hodgkin's lymphoma. The Non-Hodgkin's Lymphoma Classification Project, *Blood*, 89: 3909-3918, 1997.
167. Galceran, J., Marcos-Gragera, R., Soler, M., *et al.* Cancer incidence in AIDS patients in Catalonia, Spain, *Eur. J. Cancer*, 43: 1085-1091, 2007.
168. Shimakage, M., Sakamoto, H., Harada, S., Sasagawa, T., and Kodama, K. Expression of the Epstein-Barr virus in lymphoproliferative diseases of the lung, *Oncol. Rep.*, 17: 1347-1352, 2007.
169. Busnach, G., Piselli, P., Arbustini, E., *et al.* Immunosuppression and cancer: A comparison of risks in recipients of organ transplants and in HIV-positive individuals, *Transplant Proc.*, 38: 3533-3535, 2006.
170. Rudant, J., Menegaux, F., Leverger, G., *et al.* Family history of cancer in children with acute leukemia, Hodgkin's lymphoma or non-Hodgkin's lymphoma: the ESCALE study (SFCE), *Int. J. Cancer*, 121: 119-126, 2007.
171. Boffetta, P. and de Vocht, F. Occupation and the risk of non-Hodgkin lymphoma, *Cancer Epidemiol. Biomarkers Prev.*, 16: 369-372, 2007.
172. Czuczman, M. S., Weaver, R., Alkuzweny, B., Berlfein, J., and Grillo-Lopez, A. J. Prolonged clinical and molecular remission in patients with low-grade or follicular non-Hodgkin's lymphoma treated with rituximab plus CHOP chemotherapy: 9-year follow-up, *J. Clin. Oncol.*, 22: 4711-4716, 2004.
173. Lenz, G., Dreyling, M., Hoster, E., *et al.* Immunochemotherapy with rituximab and cyclophosphamide, doxorubicin, vincristine, and prednisone significantly improves response and time to treatment failure, but not long-term outcome in

- patients with previously untreated mantle cell lymphoma: results of a prospective randomized trial of the German Low Grade Lymphoma Study Group (GLSG), *J. Clin. Oncol.*, *23*: 1984-1992, 2005.
174. Stamenkovic, I. and Seed, B. CD19, the earliest differentiation antigen of the B cell lineage, bears three extracellular immunoglobulin-like domains and an Epstein-Barr virus-related cytoplasmic tail, *J. Exp. Med.*, *168*: 1205-1210, 1988.
175. Tedder, T. F. and Isaacs, C. M. Isolation of cDNA encoding the CD19 antigen of human and mouse B lymphocytes. A new member of the immunoglobulin superfamily, *J. Immunol.*, *143*: 712-717, 1989.
176. Zhou, L. J., Ord, D. C., Hughes, A. L., and Tedder, T. F. Structure and domain organization of the CD19 antigen of human, mouse, and guinea pig B lymphocytes. Conservation of the extensive cytoplasmic domain, *J. Immunol.*, *147*: 1424-1432, 1991.
177. Uckun, F. M., Jaszcz, W., Ambrus, J. L., *et al.* Detailed studies on expression and function of CD19 surface determinant by using B43 monoclonal antibody and the clinical potential of anti-CD19 immunotoxins, *Blood*, *71*: 13-29, 1988.
178. Tedder, T. F. and Engel, P. CD20: a regulator of cell-cycle progression of B lymphocytes, *Immunol. Today*, *15*: 450-454, 1994.
179. Pezzutto, A., Dorken, B., Rabinovitch, P. S., Ledbetter, J. A., Moldenhauer, G., and Clark, E. A. CD19 monoclonal antibody HD37 inhibits anti-immunoglobulin-induced B cell activation and proliferation, *J. Immunol.*, *138*: 2793-2799, 1987.

180. Fujimoto, M., Poe, J. C., Hasegawa, M., and Tedder, T. F. CD19 amplification of B lymphocyte Ca<sup>2+</sup> responses: a role for Lyn sequestration in extinguishing negative regulation, *J. Biol. Chem.*, *276*: 44820-44827, 2001.
181. Ghetie, M. A., May, R. D., Till, M., *et al.* Evaluation of ricin-A-chain containing immunotoxins directed against CD19 and CD22 antigens on normal and malignant human B cells as potential reagents for in vivo therapy, *Cancer Res.*, *48*: 2610-2617, 1988.
182. Fujimoto, M., Fujimoto, Y., Poe, J. C., *et al.* CD19 regulates Src family protein tyrosine kinase activation in B lymphocytes through processive amplification, *Immunity*, *13*: 47-57, 2000.
183. Matsumoto, A. K., Kopicky-Burd, J., Carter, R. H., Tuveson, D. A., Tedder, T. F., and Fearon, D. T. Intersection of the complement and immune systems: a signal transduction complex of the B lymphocyte-containing complement receptor type 2 and CD19., *J. Exp. Med.*, *173*: 55-64, 1991.
184. Bradbury, L. E., Kansas, G. S., Levy, S., Evans, R. L., and Tedder, T. F. The CD19/CD21 signal transducing complex of human B-lymphocytes includes the target of antiproliferative antibody-1 and leu-13 molecules, *J. Immunol.*, *149*: 2841-2850, 1992.
185. Matsumoto, A. K., Martin, D. R., Carter, R. H., Klickstein, L. B., Ahearn, J. M., and Fearon, D. T. Functional dissection of the CD21/CD19/TAPA-1/Leu-13 complex of B lymphocytes, *J. Exp. Med.*, *178*: 1407-1417, 1993.
186. Carter, R. H. and Fearon, D. T. CD19: lowering the threshold for antigen receptor stimulation of B lymphocytes, *Science*, *256*: 105-107, 1992.

187. Engel, P., Zhou, L. J., Ord, D. C., Sato, S., Koller, B., and Tedder, T. F. Abnormal B lymphocyte development, activation, and differentiation in mice that lack or overexpress the CD19 signal transduction molecule, *Immunity*, 3: 39-50, 1995.
188. Rickert, R. C., Rajewsky, K., and Roes, J. Impairment of T-cell-dependent B-cell responses and B-1 cell development in CD19-deficient mice, *Nature*, 376: 352-355, 1995.
189. Ghetie, M. A., Picker, L. J., Richardson, J. A., Tucker, K., Uhr, J. W., and Vitetta, E. S. Anti-CD19 inhibits the growth of human B-cell tumor lines in vitro and of Daudi cells in SCID mice by inducing cell cycle arrest, *Blood*, 83: 1329-1336, 1994.
190. Waddick, K. G., Chae, H. P., Tuel-Ahlgren, L., *et al.* Engagement of the CD19 receptor on human B-lineage leukemia cells activates LCK tyrosine kinase and facilitates radiation-induced apoptosis, *Radiat. Res.*, 136: 313-319, 1993.
191. Chaouchi, N., Vazquez, A., Galanaud, P., and Leprince, C. B cell antigen receptor-mediated apoptosis. Importance of accessory molecules CD19 and CD22, and of surface IgM cross-linking, *J. Immunol.*, 154: 3096-3104, 1995.
192. Gewirtz, D. A. A critical evaluation of the mechanisms of action proposed for the antitumor effects of the anthracycline antibiotics adriamycin and daunorubicin, *Biochem. Pharmacol.*, 57: 727-741, 1999.
193. Safra, T., Muggia, F., Jeffers, S., *et al.* Pegylated liposomal doxorubicin (Doxil): reduced clinical cardiotoxicity in patients reaching or exceeding cumulative doses of 500 mg/m<sup>2</sup>, *Ann. Oncol.*, 11: 1029-1033, 2000.

194. Lyass, O., Uziely, B., Ben-Yosef, R., *et al.* Correlation of toxicity with pharmacokinetics of pegylated liposomal doxorubicin (Doxil) in metastatic breast carcinoma, *Cancer*, *89*: 1037-1047, 2000.
195. Zola, H., Macardle, P. J., Bradford, T., Weedon, H., Yasui, H., and Kurosawa, Y. Preparation and characterization of a chimeric CD19 monoclonal antibody, *Immunol. Cell Biol.*, *69*: 411-422, 1991.
196. Le Gall, F., Kipriyanov, S. M., Moldenhauer, G., and Little, M. Di-, tri- and tetrameric single chain Fv antibody fragments against human CD19: effect of valency on cell binding, *FEBS Lett.*, *453*: 164-168, 1999.
197. Cheng, W. W., Das, D., Suresh, M., and Allen, T. M. Expression and purification of two anti-CD19 single chain Fv fragments for targeting of liposomes to CD19-expressing cells, *Biochim. Biophys. Acta*, *1768*: 21-29, 2007.
198. Sambrook, J., Fritsch, E. F., and Maniatis, T. *Molecular Cloning: A Laboratory Manual*, New York: Cold Spring Harbor Laboratory Press; 1989.
199. Das, D., Allen, T. M., and Suresh, M. R. Comparative evaluation of two purification methods of anti-CD19-c-myc-His(6)-Cys scFv, *Protein Expr. Purif.*, *39*: 199-208, 2005.
200. Umetsu, M., Tsumoto, K., Hara, M., *et al.* How additives influence the refolding of immunoglobulin-folded proteins in a stepwise dialysis system. Spectroscopic evidence for highly efficient refolding of a single-chain Fv fragment, *J. Biol. Chem.*, *278*: 8979-8987, 2003.

201. Towbin, H., Staehelin, T., and Gordon, J. Electrophoretic transfer of proteins from polyacrylamide gels to nitrocellulose sheets: procedure and some applications, *Proc. Natl. Acad. Sci. U.S.A.*, *76*: 4350-4354, 1979.
202. Pool, G. L., French, M. E., Edwards, R. A., Huang, L., and Lumb, R. H. Use of radiolabelled hexadecyl cholesterol ether as a liposome marker, *Lipids*, *17*: 445-452, 1982.
203. Derksen, J. T., Morselt, H. W., and Scherphof, G. L. Processing of different liposomal markers after *in vitro* uptake of immunoglobulin-coated liposomes by rat liver macrophages, *Biochim. Biophys. Acta*, *931*: 33-40, 1987.
204. Lopes de Menezes, D. E., Kirchmeier, M. J., Gagne, J.-F., Pilarski, L. M., and Allen, T. M. Cellular trafficking and cytotoxicity of anti-CD19-targeted liposomal doxorubicin in B lymphoma cells, *J. Liposome Res.*, *9*: 199-228, 1999.
205. Benedict, C. A., MacKrell, A. J., and Anderson, W. F. Determination of the binding affinity of an anti-CD34 single-chain antibody using a novel, flow cytometry based assay, *J. Immunol. Methods*, *201*: 223-231, 1997.
206. Lopes de Menezes, D. E., Pilarski, L. M., Belch, A. R., and Allen, T. M. Selective targeting of immunoliposomal doxorubicin against human multiple myeloma *in vitro* and *ex vivo*, *Biochim. Biophys. Acta*, *1466*: 205-220, 2000.
207. Allen, T. M., Ahmad, I., Lopes de Menezes, D. E., and Moase, E. H. Immunoliposome-mediated targeting of anti-cancer drugs *in vivo*, *Biochem. Soc. Trans.*, *23*: 1073-1079, 1995.
208. Cattan, A. R. and Douglas, E. The C.B.17 scid mouse strain as a model for human disseminated leukaemia and myeloma *in vivo*, *Leuk. Res.*, *18*: 513-522, 1994.

209. Dubois, V., Dasnois, L., Lebtahi, K., *et al.* CPI-0004Na, a new extracellularly tumor-activated prodrug of doxorubicin: in vivo toxicity, activity, and tissue distribution confirm tumor cell selectivity, *Cancer Res.*, *62*: 2327-2331, 2002.
210. Ghetie, M. A., Richardson, J., Tucker, T., Jones, D., Uhr, J. W., and Vitetta, E. S. Disseminated or localized growth of a human B-cell tumor (Daudi) in SCID mice, *Int. J. Cancer*, *45*: 481-485, 1990.
211. Nadler, L. M., Anderson, K. C., Marti, G., *et al.* B4, a human B lymphocyte-associated antigen expressed on normal, itogen-activated, and malignant B lymphocytes, *J. Immunol.*, *131*: 244-250, 1983.
212. Press, O. W., Farr, A. G., Borroz, K. I., Andersen, S. K., and Martin, P. J. Endocytosis and degradation of monoclonal antibodies targeting human B-cell malignancies, *Cancer Res.*, *49*: 4906-4912, 1989.
213. Herrera, L., Stanciu-Herrera, C., Morgan, C., Ghetie, V., and Vitetta, E. S. Anti-CD19 immunotoxin enhances the activity of chemotherapy in severe combined immunodeficient mice with human pre-B acute lymphoblastic leukemia, *Leuk. Lymphoma*, *47*: 2380-2387, 2006.
214. Stone, M. J., Sausville, E. A., Fay, J. W., *et al.* A phase I study of bolus versus continuous infusion of the anti-CD19 immunotoxin, IgG-HD-37-dgA, in patients with B-cell lymphoma, *Blood*, *88*: 1188-1197, 1996.
215. Vallera, D. A., Todhunter, D. A., Kuroki, D. W., Shu, Y., Sicheneder, A., and Chen, H. A bispecific recombinant immunotoxin, DT2219, targeting human CD19 and CD22 receptors in a mouse xenograft model of B-cell leukemia/lymphoma, *Clin. Cancer Res.*, *11*: 3879-3888, 2005.

216. Schwemmlin, M., Stieglmaier, J., Kellner, C., *et al.* A CD19-specific single-chain immunotoxin mediates potent apoptosis of B-lineage leukemic cells, *Leukemia*, *21*: 1405-1412, 2007.
217. Volkel, T., Holig, P., Merdan, T., Muller, R., and Kontermann, R. E. Targeting of immunoliposomes to endothelial cells using a single-chain Fv fragment directed against human endoglin (CD105), *Biochim. Biophys. Acta*, *1663*: 158-166, 2004.
218. Kipriyanov, S. M., Moldenhauer, G., and Little, M. High level production of soluble single chain antibodies in small-scale *Escherichia coli* cultures, *J. Immunol. Methods*, *200*: 69-77, 1997.
219. Willuda, J., Honegger, A., Waibel, R., *et al.* High thermal stability is essential for tumor targeting of antibody fragments: engineering of a humanized anti-epithelial glycoprotein-2 (epithelial cell adhesion molecule) single-chain Fv fragment, *Cancer Res.*, *59*: 5758-5767, 1999.
220. Worn, A., Auf der Maur, A., Escher, D., Honegger, A., Barberis, A., and Pluckthun, A. Correlation between in vitro stability and in vivo performance of anti-GCN4 intrabodies as cytoplasmic inhibitors, *J. Biol. Chem.*, *275*: 2795-2803, 2000.
221. Worn, A. and Pluckthun, A. Different equilibrium stability behavior of ScFv fragments: identification, classification, and improvement by protein engineering, *Biochemistry*, *38*: 8739-8750, 1999.
222. Pedroso, I., Irun, M. P., Machicado, C., and Sancho, J. Four-state equilibrium unfolding of an scFv antibody fragment, *Biochemistry*, *41*: 9873-9884, 2002.

223. Brockmann, E. C., Cooper, M., Stromsten, N., Vehniainen, M., and Saviranta, P. Selecting for antibody scFv fragments with improved stability using phage display with denaturation under reducing conditions, *J. Immunol. Methods*, *296*: 159-170, 2005.
224. Shusta, E. V., Holler, P. D., Kieke, M. C., Kranz, D. M., and Wittrup, K. D. Directed evolution of a stable scaffold for T-cell receptor engineering, *Nat. Biotechnol.*, *18*: 754-759, 2000.
225. Buchner, J., Pastan, I., and Brinkmann, U. A method for increasing the yield of properly folded recombinant fusion proteins: single-chain immunotoxins from renaturation of bacterial inclusion bodies, *Anal. Biochem.*, *205*: 263-270, 1992.
226. Hoyer M., R. K., Pluckthun A. A kinetic trap is an intrinsic feature in the folding pathway of single-chain Fv fragments, *Biophys. Chem.*, *96*: 273-284, 2002.
227. McLaughlin, P., Grillo-Lopez, A. J., Link, B. K., *et al.* Rituximab chimeric anti-CD20 monoclonal antibody therapy for relapsed indolent lymphoma: half of patients respond to a four-dose treatment program, *J. Clin. Oncol.*, *16*: 2825-2833, 1998.
228. Vogel, C. L., Cobleigh, M. A., Tripathy, D., *et al.* Efficacy and safety of trastuzumab as a single agent in first-line treatment of HER2-overexpressing metastatic breast cancer, *J. Clin. Oncol.*, *20*: 719-726, 2002.
229. Reichert, J. M., Rosensweig, C. J., Faden, L. B., and Dewitz, M. C. Monoclonal antibody successes in the clinic, *Nat. Biotechnol.*, *23*: 1073-1078, 2005.

230. Sievers, E. L., Larson, R. A., Stadtmauer, E. A., *et al.* Efficacy and safety of gemtuzumab ozogamicin in patients with CD33-positive acute myeloid leukemia in first relapse, *J. Clin. Oncol.*, *19*: 3244-3254, 2001.
231. Witzig, T. E., Gordon, L. I., Cabanillas, F., *et al.* Randomized controlled trial of yttrium-90-labeled ibritumomab tiuxetan radioimmunotherapy versus rituximab immunotherapy for patients with relapsed or refractory low-grade, follicular, or transformed B-cell non-Hodgkin's lymphoma, *J. Clin. Oncol.*, *20*: 2453-2463, 2002.
232. Baselga, J., Norton, L., Albanell, J., Kim, Y. M., and Mendelsohn, J. Recombinant humanized anti-HER2 antibody (Herceptin) enhances the antitumor activity of paclitaxel and doxorubicin against HER2/neu overexpressing human breast cancer xenografts, *Cancer Res.*, *58*: 2825-2831, 1998.
233. Klee, G. G. Human anti-mouse antibodies, *Arch. Path. Lab. Med.*, *124*: 921-923, 2000.
234. Holliger, P. and Hudson, P. J. Engineered antibody fragments and the rise of single domains, *Nat. Biotechnol.*, *23*: 1126-1136, 2005.
235. Bhatia, J., Sharma, S. K., Chester, K. A., *et al.* Catalytic activity of an in vivo tumor targeted anti-CEA scFv:carboxypeptidase G2 fusion protein, *Int. J. Cancer*, *85*: 571-577, 2000.
236. Park, Y. S. Tumor-directed targeting of liposomes, *Biosci. Rep.*, *22*: 267-281, 2002.

237. Maeda, H., Wu, J., Sawa, T., Matsumura, Y., and Hori, K. Tumor vascular permeability and the EPR effect in macromolecular therapeutics: a review, *J. Control. Release*, *65*: 271-284, 2000.
238. Drummond, D. C., Hong, K., Park, J. W., Benz, C. C., and Kirpotin, D. B. Liposome targeting to tumors using vitamin and growth factor receptors, *Vitam. Horm.*, *60*: 285-332, 2001.
239. Carter, P. Improving the efficacy of antibody-based cancer therapies, *Nature Rev. Cancer*, *1*: 118-129, 2001.
240. Chan, H. T. C., Hughes, D., French, R. R., *et al.* CD20-induced lymphoma cell death is independent of both caspases and the redistribution into Triton X-100 insoluble membrane rafts, *Cancer Res.*, *63*: 5480-5489, 2003.
241. Luque, R., Brieva, J. A., Moreno, A., *et al.* Normal and clonal B lineage cells can be distinguished by their differential expression of B cell antigens and adhesion molecules in peripheral blood from multiple myeloma (MM) patients--diagnostic and clinical implications, *Clin. Exp. Immunol.*, *112*: 410-418, 1998.
242. Nicholson, I. C., Lenton, K. A., Little, D. J., *et al.* Construction and characterisation of a functional CD19 specific single chain Fv fragment for immunotherapy of B lineage leukemia and lymphoma, *Mol. Immunol.*, *34*: 1157-1165, 1998.
243. Marty, C., Langer-Machova, Z., Sigrist, S., Schott, H., Schwendener, R. A., and Ballmer-Hofer, K. Isolation and characterization of a scFv antibody specific for tumor endothelial marker 1 (TEM1), a new reagent for targeted tumor therapy, *Cancer Lett.*, *235*: 298-308, 2006.

244. Gabizon, A., Goren, D., Fuks, Z., Barenholz, Y., Dagan, A., and Meshorer, A. Enhancement of adriamycin delivery to liver metastatic cells with increased tumoricidal effect using liposomes as drug carriers, *Cancer Res.*, *43*: 4730-4735, 1983.
245. van Hoesel, Q. G. C. M., Steerenberg, P. A., Crommelin, D. J., *et al.* Reduced cardiotoxicity and nephrotoxicity with preservation of antitumor activity of doxorubicin entrapped in stable liposomes in the LOU/M Wsl rat, *Cancer Res.*, *44*: 3698-3705, 1984.
246. Muggia, F. and Hamilton, A. Phase III data on Caelyx in ovarian cancer, *Eur. J. Cancer*, *37*: S15-S18, 2001.
247. Worn, A. and Pluckthun, A. Stability engineering of antibody single-chain Fv fragments, *J. Mol. Biol.*, *305*: 989-1010, 2001.
248. Malby, R. L., Caldwell, J. B., Gruen, L. C., *et al.* Recombinant antineuraminidase single chain antibody: expression, characterization, and crystallization in complex with antigen, *Proteins*, *16*: 57-63, 1993.
249. Schodin, B. A. and Kranz, D. M. Binding affinity and inhibitory properties of a single-chain anti-T cell receptor antibody, *J. Biol. Chem.*, *268*: 25722-25727, 1993.
250. Stephenson, S. M., Low, P. S., and Lee, R. J. Folate receptor-mediated targeting of liposomal drugs to cancer cells, *Meth. Enzymol.*, *387*: 33-50, 2004.
251. Kipriyanov, S. M., Moldenhauer, G., Martin, A. C., Kupriyanova, O. A., and Little, M. Two amino acid mutations in an anti-human CD3 single chain Fv

- antibody fragment that affect the yield on bacterial secretion but not the affinity, *Protein Eng.*, *10*: 445-453, 1997.
252. Reiter, Y., Brinkmann, U., Webber, K. O., Jung, S. H., Lee, B., and Pastan, I. Engineering interchain disulfide bonds into conserved framework regions of Fv fragments: improved biochemical characteristics of recombinant immunotoxins containing disulfide-stabilized Fv, *Protein Eng.*, *7*: 697-704, 1994.
253. Arndt, M. A., Krauss, J., and Rybak, S. M. Antigen binding and stability properties of non-covalently linked anti-CD22 single-chain Fv dimers, *FEBS Lett.*, *578*: 257-261, 2004.
254. Williams, A. F. and Barclay, A. N. The immunoglobulin superfamily--domains for cell surface recognition, *Annu. Rev. Immunol.*, *6*: 381-405, 1988.
255. Proba, K., Honegger, A., and Pluckthun, A. A natural antibody missing a cysteine in VH: consequences for thermodynamic stability and folding, *J. Mol. Biol.*, *265*: 161-172, 1997.
256. Glockshuber, R., Schmidt, T., and Pluckthun, A. The disulfide bonds in antibody variable domains: effects on stability, folding in vitro, and functional expression in *Escherichia coli*, *Biochemistry*, *31*: 1270-1279, 1992.
257. Proba, K., Worn, A., Honegger, A., and Pluckthun, A. Antibody scFv fragments without disulfide bonds made by molecular evolution, *J. Mol. Biol.*, *275*: 245-253, 1998.
258. Worn, A. and Pluckthun, A. An intrinsically stable antibody scFv fragment can tolerate the loss of both disulfide bonds and fold correctly, *FEBS Lett.*, *427*: 357-361, 1998.

259. Reiter, Y., Brinkmann, U., Jung, S. H., Pastan, I., and Lee, B. Disulfide stabilization of antibody Fv: computer predictions and experimental evaluation, *Protein Eng.*, *8*: 1323-1331, 1995.
260. Robinson, C. R. and Sauer, R. T. Optimizing the stability of single-chain proteins by linker length and composition mutagenesis, *Proc. Natl. Acad. Sci. U.S.A.*, *95*: 5929-5934, 1998.
261. Williams, D. C., Van Frank, R. M., Muth, W. L., and Burnett, J. P. Cytoplasmic inclusion bodies in *Escherichia coli* producing biosynthetic human insulin proteins, *Science*, *215*: 687-689, 1982.
262. Guisez, Y., Demolder, J., Mertens, N., *et al.* High-level expression, purification, and renaturation of recombinant murine interleukin-2 from *Escherichia coli*, *Protein Expr. Purif.*, *4*: 240-246, 1993.
263. Seddon, A. P., Hulmes, J. D., Decker, M. M., *et al.* Refolding and characterization of human recombinant heparin-binding neurite-promoting factor, *Protein Expr. Purif.*, *5*: 14-21, 1994.
264. Francis, R. J., Mather, S. J., Chester, K., *et al.* Radiolabelling of glycosylated MFE-23:CPG2 fusion protein (MFECP1) with <sup>99m</sup>Tc for quantitation of tumour antibody-enzyme localisation in antibody-directed enzyme pro-drug therapy (ADEPT), *Eur. J. Nucl. Med. Mol. Imaging*, *31*: 1090-1096, 2004.
265. Lin, Y., Pagel, J. M., Axworthy, D., Pantelias, A., Hedin, N., and Press, O. W. A genetically engineered anti-CD45 single-chain antibody-streptavidin fusion protein for pretargeted radioimmunotherapy of hematologic malignancies, *Cancer Res.*, *66*: 3884-3892, 2006.

266. Roguska, M. A., Pedersen, J. T., Keddy, C. A., *et al.* Humanization of murine monoclonal antibodies through variable domain resurfacing, *Proc. Natl. Acad. Sci. U.S.A.*, *91*: 969-973, 1994.
267. Roguska, M. A., Pedersen, J. T., Henry, A. H., *et al.* A comparison of two murine monoclonal antibodies humanized by CDR-grafting and variable domain resurfacing, *Protein Eng.*, *9*: 895-904, 1996.
268. Wu, A. M. and Senter, P. D. Arming antibodies: prospects and challenges for immunoconjugates, *Nat. Biotechnol.*, *23*: 1137-1146, 2005.
269. Mayer, A., Francis, R. J., Sharma, S. K., *et al.* A phase I study of single administration of antibody-directed enzyme prodrug therapy with the recombinant anti-carcinoembryonic antigen antibody-enzyme fusion protein MFECP1 and a bis-iodo phenol mustard prodrug, *Clin. Cancer Res.*, *12*: 6509-6516, 2006.
270. Bang, S., Nagata, S., Onda, M., Kreitman, R. J., and Pastan, I. HA22 (R490A) is a recombinant immunotoxin with increased antitumor activity without an increase in animal toxicity, *Clin. Cancer Res.*, *11*: 1545-1550, 2005.
271. Filpula, D., Yang, K., Basu, A., *et al.* Releasable PEGylation of mesothelin targeted immunotoxin SS1P achieves single dosage complete regression of a human carcinoma in mice, *Bioconjug. Chem.*, *18*: 773-784, 2007.
272. Laane, E., Tani, E., Bjorklund, E., *et al.* Flow cytometric immunophenotyping including Bcl-2 detection on fine needle aspirates in the diagnosis of reactive lymphadenopathy and non-Hodgkin's lymphoma, *Cytometry B. Clin. Cytom.*, *64*: 34-42, 2005.

273. Maloney, D. G., Smith, B., and Rose, A. Rituximab: mechanism of action and resistance, *Semin. Oncol.*, *29*: 2-9, 2002.
274. Smith, M. R. Rituximab (monoclonal anti-CD20 antibody): mechanisms of action and resistance, *Oncogene*, *22*: 7359-73568, 2003.
275. Jilani, I., O'Brien, S., Manshuri, T., *et al.* Transient down-modulation of CD20 by rituximab in patients with chronic lymphocytic leukemia, *Blood*, *102*: 3514-3520, 2003.
276. Wobser, M., Voigt, H., Eggert, A. O., *et al.* Bcl-2 expression in rituximab refractory cutaneous B-cell lymphoma, *Br. J. Cancer*, *96*: 1540-1543, 2007.
277. Price-Schiavi, S. A., Jepson, S., Li, P., *et al.* Rat Muc4 (sialomucin complex) reduces binding of anti-ErbB2 antibodies to tumor cell surfaces, a potential mechanism for herceptin resistance, *Int. J. Cancer*, *99*: 783-791, 2002.
278. Nagy, P., Friedlander, E., Tanner, M., *et al.* Decreased accessibility and lack of activation of ErbB2 in JIMT-1, a herceptin-resistant, MUC4-expressing breast cancer cell line, *Cancer Res.*, *65*: 473-482, 2005.
279. Fenske, D. B., Wong, K. F., Maurer, E., *et al.* Ionophore-mediated uptake of ciprofloxacin and vincristine into large unilamellar vesicles exhibiting transmembrane ion gradients, *Biochim. Biophys. Acta*, *1414*: 188-204, 1998.
280. Abraham, S. A., McKenzie, C., Masin, D., *et al.* In vitro and in vivo characterization of doxorubicin and vincristine coencapsulated within liposomes through use of transition metal ion complexation and pH gradient loading, *Clin. Cancer Res.*, *10*: 728-738, 2004.

281. Tardi, P. G., Gallagher, R. C., Johnstone, S., *et al.* Coencapsulation of irinotecan and floxuridine into low cholesterol-containing liposomes that coordinate drug release in vivo, *Biochim. Biophys. Acta*, *1768*: 678-687, 2007.
282. Mayer, L. D., Harasym, T. O., Tardi, P. G., *et al.* Ratiometric dosing of anticancer drug combinations: controlling drug ratios after systemic administration regulates therapeutic activity in tumor-bearing mice, *Mol. Cancer Ther.*, *5*: 1854-1863, 2006.
283. Caplen, N. J., Kinrade, E., Sorgi, F., *et al.* In vitro liposome mediated DNA transfection of epithelial cell lines using the cationic liposome Dc Chol/Dope, *Gene Ther.*, *2*: 603-613, 1995.
284. de Lima, M. C., Simoes, S., Pires, P., Gaspar, R., Slepushkin, V., and Duzgunes, N. Gene delivery mediated by cationic liposomes: from biophysical aspects to enhancement of transfection, *Mol. Membr. Biol.*, *16*: 103-109, 1999.
285. Ishida, T., Kirchmeier, M. J., Moase, E. H., Zalipsky, S., and Allen, T. M. Targeted delivery and triggered release of liposomal doxorubicin enhances cytotoxicity against human B lymphoma cells, *Biochim. Biophys. Acta*, *1515*: 144-158, 2001.
286. Kakudo, T., Chaki, S., Futaki, S., *et al.* Transferrin-modified liposomes equipped with a pH-sensitive fusogenic peptide: an artificial viral-like delivery system, *Biochemistry*, *43*: 5618-5628, 2004.
287. Kirpotin, D., Hong, K., Mullah, N., Papahadjopoulos, D., and Zalipsky, S. Liposomes with detachable polymer coating: destabilization and fusion of

- dioleoylphosphatidylethanolamine vesicles triggered by cleavage of surface-grafted poly(ethylene glycol), *FEBS Lett.*, 388: 115-118, 1996.
288. Torchilin, V. P., Rammohan, R., Weissig, V., and Levchenko, T. S. TAT peptide on the surface of liposomes affords their efficient intracellular delivery even at low temperature and in the presence of metabolic inhibitors, *Proc. Natl. Acad. Sci. U.S.A.*, 98: 8786-8791, 2001.
289. Zhang, J. X., Zalipsky, S., Mullah, N., Pechar, M., and Allen, T. M. Pharmacological attributes of dioleoylphosphatidylethanolamine/cholesterylhemisuccinate liposomes containing different types of cleavable lipopolymers, *Pharmacol. Res.*, 49: 185-198, 2004.
290. Cao, Y. and Suresh, M. R. Bispecific mAb aided liposomal drug delivery, *J. Drug Target.*, 8: 257-266, 2000.
291. Bruenke, J., Fischer, B., Barbin, K., *et al.* A recombinant bispecific single-chain Fv antibody against HLA class II and FcγRIII (CD16) triggers effective lysis of lymphoma cells, *Br. J. Haematol.*, 125: 167-179, 2004.
292. Hu, X., O'Hara, L., White, S., Magner, E., Kane, M., and Wall, J. G. Optimisation of production of a domoic acid-binding scFv antibody fragment in *Escherichia coli* using molecular chaperones and functional immobilisation on a mesoporous silicate support, *Protein Expr. Purif.*, 52: 194-201, 2007.
293. Jurado, P., de Lorenzo, V., and Fernandez, L. A. Thioredoxin fusions increase folding of single chain Fv antibodies in the cytoplasm of *Escherichia coli*: evidence that chaperone activity is the prime effect of thioredoxin, *J. Mol. Biol.*, 357: 49-61, 2006.

294. Wall, J. G. and Pluckthun, A. The hierarchy of mutations influencing the folding of antibody domains in *Escherichia coli*, *Protein Eng.*, *12*: 605-611, 1999.
295. Franklin, S. E. and Mayfield, S. P. Prospects for molecular farming in the green alga *Chlamydomonas*, *Curr. Opin. Plant Biol.*, *7*: 159-165, 2004.
296. Zhang, G., Brokx, S., and Weiner, J. H. Extracellular accumulation of recombinant proteins fused to the carrier protein YebF in *Escherichia coli*, *Nat. Biotechnol.*, *24*: 100-104, 2006.